SIMULTANEOUS ACTIVE/PASSIVE CONTROL OF EXTENSIONAL AND FLEXURAL POWER FLOWS IN INFINITE THIN BEAMS

by

Florence L. Deneufve

Thesis submitted to the Faculty of the

Virginia Polytechnic Institute and State University

in partial fulfillment of the requirements for the degree of

Master of Science

in

Mechanical Engineering

APPROVED:

Dr. Chris R. Fuller, Chairman

Dr. Ricardo A. Burdisso

Dr. Catherine R. J. Guigou

July, 1996

Blacksburg, Virginia

Keywords: Active/Passive Control, Vibration Control, Smart Structures

c. 2

LD
5655
V855
1995
D464
c.2

SIMULTANEOUS ACTIVE/PASSIVE CONTROL OF EXTENSIONAL AND FLEXURAL POWER FLOWS IN INFINITE THIN BEAMS

by

Florence L. Deneufve

Committee Chairman: Chris R. Fuller

Mechanical Engineering

(ABSTRACT)

Passive control techniques to minimize structural vibrations are limited with respect to the amount of attenuation obtained especially in the low frequency region but do not require adding any power. Active control methods are effective for reducing structural vibrations, especially at low frequencies, but may require significant control effort. Thus, passive and active control methods have complementary frequency ranges of application. This research consists of combining active and passive control techniques to simultaneously attenuate extensional and flexural power flows in infinite thin beams and determine the advantages and disadvantages of such a combination. An analytical model is developed for an infinite beam with a passive insert of high damping placed at some distance from a point force excitation (passive approach). The passive control of vibrations results in a reduction of both extensional and flexural power flows downstream of the passive material discontinuity. The simultaneous active control of extensional and flexural waves, using two co-located independent piezoceramic actuators bonded to the surface of the beam, is theoretically studied. The active control model shows that the use of two independent piezoceramic actuators allows complete cancellation of the total power flow (sum of the extensional and flexural power flows) downstream of the actuators. The combination of passive and active control methods for three different configurations (actuators located upstream of, downstream of, and on the passive insert) is investigated and complete control of the total power flow is again achieved. The results demonstrate

that in the case of the actuators bonded to the passive material discontinuity, the active/passive combination has great potential for reducing the control effort required for the active controller. Finally, an approximation of the influence of heavy fluid flanking paths on the optimal active/passive system is developed by simulation of these flanking paths using axial and torsional springs. This last study shows that both axial and torsional springs will result in modification of the control effort required by the actuators if their respective stiffness is greater than the equivalent stiffness of the section in parallel with the springs.

Acknowledgements

First I would like to express my appreciation to my advisor, Dr. Chris Fuller, for giving me the opportunity to learn about the active control field, for his guidance, and for allowing me to study abroad.

I would also like to acknowledge Dr. Ricardo Burdisso for his assistance and suggestions during my research.

I am thankful to my friend Catherine Guigou for her precious help and advice in some problems I had to face; and the many others for their assistance: Steve Booth, Bertrand Brevart, Jamie Carneal, Sandy Gentry, Gary Gibbs, John Heilmann, Julien Maillard, Brian Mankhen, Hector Rodriguez, Dawn Williams.

I am grateful to my friend Jerome for his guidance and support during my adaptation in the United-States and for the memorable moments spent together.

I give my appreciation to Mme Nicole Jaffrin and Dr. Robert Mahan, coordinators of the exchange program between Virginia Polytechnic Institute and the Université de Technologie de Compiègne, for giving me the opportunity to study in a foreign country and discover another culture.

Finally, I would like to express special thanks to my family, especially my Mom and Dad, my brothers Frédéric and Stéphane and their wives, for their support throughout my studies and their interest in my success.

Table Of Contents

Chapter 1

Introduction 1

1.1 Passive Control Approaches 1

1.2 Active Noise Control (ANC) 3

1.3 Active Structural Acoustic Control (ASAC) 4

1.4 Active Vibration Control (AVC) 5

1.5 Previous Active/Passive Work 7

1.6 Piezoelectric Actuator Models 9

1.7 Overview and Objectives of Thesis 12

Chapter 2

Theoretical Developments of System Components 16

2.1 Assumptions 16

2.2 Extensional and Flexural Equations of Motion of Thin beams 17

2.2.1 Extensional Equation of Motion 17

2.2.2 Flexural Equation of Motion 21

2.3 Derivation of Extensional and Flexural Power Flows in Thin Beams 23

2.3.1 Finite Section of Beam 25

2.3.2 Semi-infinite Section of Beam 27

2.4 Extensional and Flexural Responses of an Infinite Thin Beam to a Point Force Excitation 28

2.4.1 Point Force Excitation 28
2.4.2 Extensional and Flexural Responses 30
2.5 Asymmetric Piezoelectric Actuator Model 31
2.5.1 Asymmetric Piezoelectric Excitation 32
2.5.2 Extensional Equation of Motion 36
2.5.3 Flexural Equation of Motion 37
2.5.4 Extension to Two Co-located Independent Piezoelectric Actuators 40

Chapter 3
Analysis of the Control System Behavior 42
3.1 Passive Control System 42
3.1.1 Passive Control System for Extensional Motion 44
3.1.2 Passive Control System for Bending Motion 46
3.2 Active Control System 48
3.2.1 Optimal Control of Extensional and Flexural Power Flows in Infinite Beams 48
3.2.2 Active Control System for Extensional Motion 50
3.2.3 Active Control System for Bending Motion 52
3.2.4 Optimal Applied Voltages for the Minimum of the Cost Function 52
3.3 Active/Passive Control Systems (Hybrid Active Control Systems) . . 55
3.3.1 Configuration 1 55
3.3.2 Configuration 2 56
3.3.3 Configuration 3 58

Chapter 4
Results of the Control System Behavior Analysis 60

4.1 Characteristic Properties of the Control Systems 60
4.2 Passive Approach Results 64
4.3 Active Control Results 73
4.4 Active/Passive Control Results 78
4.4.1 Configuration 1 78
4.4.2 Configuration 2 84
4.4.3 Configuration 3 90
4.5 Actuator Power Transfer and Impedance Matching 93
4.6 Summary 101

Chapter 5
Simulation of Vibration Flanking Paths 103
5.1 Introduction 103
5.2 Association of Flanking Paths with the Active and Passive Systems 109
5.2.1 Description of the Active and Passive Systems with Flanking 109
5.2.2 Influence of Flanking Paths on the Active Control Results . 110
5.2.3 Influence of Flanking Paths on the Passive Approach Results 113
5.3 Association of Flanking Paths with the Active/Passive System Configuration 1 116
5.3.1 Description of the Active/Passive System Configuration 1 with Flanking 116
5.3.2 Influence of Flanking Paths on the Active/Passive Control Results 117
5.4 Summary 119

Chapter 6

Conclusions and Recommendations 122

Bibliography 126

Appendix A

Infinite Beam Response to a Point Force Excitation 133

A.1 Extensional Response to a Point Force 133

A.2 Flexural Response to a Point Force 135

Appendix B

Matrices For Control System Analysis 137

B.1 Passive Control System 138

B.2 Active Control System 140

B.3 Active/Passive Control System Configuration 1 142

Appendix C

Derivation of the Minimum of the Cost Function 147

Vita 151

List of Figures

Figure 1.1 General schematic of the different systems studied. 15
Figure 2.1 Free-body diagram of an element of beam in extension. 18
Figure 2.2 Extensional waves propagating in finite and semi-infinite sections of beams. 20
Figure 2.3 Free-body diagram of an element of beam in flexure. 22
Figure 2.4 Flexural waves propagating in finite and semi-infinite sections of beams. 24
Figure 2.5 Decomposition of a point force excitation at an angle. 29
Figure 2.6 Strain distribution for 1-D asymmetric piezoelectric actuator. 33
Figure 2.7 Extensional loading condition induced by a single piezoelectric actuator. 38
Figure 2.8 Flexural loading condition induced by a single piezoelectric actuator. 39
Figure 2.9 Infinite beam excited by two co-located independent piezoelectric patches. 41
Figure 3.1 Schematic of the passive control system for extensional and flexural excitations. 43
Figure 3.2 Schematic of the active control system for extensional and flexural excitations. 51
Figure 3.3 Schematic of the active/passive control system configuration 1. . . . 57
Figure 3.4 Schematic of the active/passive control system configurations 2 and 3.59
Figure 4.1 Extensional and flexural power flows P_e^d (·····) and P_f^d (——)

before treatment. 62
Figure 4.2 Extensional and flexural power flow reductions as functions of the frequency and the length of the passive hard rubber insert. 67
Figure 4.3 Extensional and flexural power flow reductions using a passive hard rubber insert. 69
Figure 4.4 Magnitudes of (a) the extensional and (b) the flexural displacements for f=600 Hz. 70
Figure 4.5 Magnitudes of (a) the extensional and (b) the flexural displacements for f=600 Hz. 74
Figure 4.6 (a) Control effort V_{eff} and (b) magnitudes of the control voltages v_e (——) and v_f (·····) obtained for active control. 77
Figure 4.7 Magnitudes of (a) the extensional and (b) the flexural displacements for f=600 Hz. 79
Figure 4.8 Comparison of the control effort V_{eff} for active control (·····) and active/passive control configuration 1 (——). 82
Figure 4.9 Comparison of the control voltages (a) v_e and (b) v_f for active control (·····) and active/passive control configuration 1 (——). 83
Figure 4.10 Magnitudes of (a) the extensional and (b) the flexural displacements for f=600 Hz. 85
Figure 4.11 Comparison of the control effort V_{eff} for active control (·····) and active/passive control configuration 2 (——). 88
Figure 4.12 Comparison of the control voltages (a) v_e and (b) v_f for active control (·····) and active/passive control configuration 2 (——). 89
Figure 4.13 Magnitudes of (a) the extensional and (b) the flexural displacements for f=600 Hz. 91
Figure 4.14 Comparison of the control effort V_{eff} for active control (·····) and active/passive control configuration 3 (——). 94
Figure 4.15 Comparison of the control voltages (a) v_e and (b) v_f for active

control (·····) and active/passive control configuration 3 (——). 95
Figure 4.16 Comparison of (a) the extensional and (b) the flexural power flows induced by two PZTs on a steel beam (——) and a rubber beam (·····). . . 97
Figure 4.17 Comparison of the PZTs impedance (——), the steel beam impedance (- - -) and the rubber beam impedance (·····) for the beam in (a) extension and (b) flexure. 100
Figure 5.1 Simulation of vibration flanking paths using axial and torsional springs. 105
Figure 5.2 Schematic of the active and passive systems associated with flanking paths. 107
Figure 5.3 Schematic of the active/passive control system configuration 1 associated with flanking paths. 108
Figure 5.4 Control effort V_{eff} for active control without flanking (·····) and with flanking (——). 111
Figure 5.5 Control voltages (a), (b) v_e and (c), (d) v_f for active control without flanking (·····) and with flanking (——). 112
Figure 5.6 (a), (b) extensional and (c), (d) flexural power flow reductions for passive system without flanking (·····) and with flanking (——). 115
Figure 5.7 Control effort V_{eff} for active/passive control configuration 1 without flanking (·····) and with flanking (——). 118
Figure 5.8 Control voltages (a), (b) v_e and (c), (d) v_f for active/passive control configuration 1 without flanking (·····) and with flanking (——). 120

List of Tables

Table 4.1 Mechanical properties and dimensions of the infinite steel beam. . . 63
Table 4.2 Mechanical properties and dimensions of the passive rubber insert. 65
Table 4.3 Mechanical properties and dimensions of the piezoelectric actuator (PZT G-1195). 66
Table 4.4 Extensional and flexural power flows in each section before and after passive approach for f=600 Hz. 71
Table 4.5 Extensional and flexural power flows in each section before control and after active control for f=600 Hz. 75
Table 4.6 Extensional and flexural power flows in each section before control and after active/passive control configuration 1 for f=600 Hz. 80
Table 4.7 Extensional and flexural power flows in each section before control and after active/passive control configuration 2 for f=600 Hz. 86
Table 4.8 Extensional and flexural power flows in each section before control and after active/passive control configuration 3 for f=600 Hz. 92
Table 5.1 Equivalent spring constants of the different sections of beam in parallel with the axial and torsional springs. 106

Chapter 1
Introduction

Technology has advanced considerably lately, making our lives easier in some ways but introducing also many problems such as those due to the high level of noise in our every day environment. People are living in crowded cities, close to highways or airports where noise problems needed to be solved. Even in factories and offices significant noise can be found. These problems resulting in a degradation of quality of life and communication are at the origin of a recent interest in noise control studies.

The vibration of structures (ducts, plates, beams ...) and the resulting noise radiation are related to each other by a cause-effect phenomenon. Many mechanical structures are equipped with beams as the primary elements of support. These beams can be subjected to forces which produce structure-borne vibrational waves propagating along them. It is then essential to control these unwanted vibrations (and the resulting noise) in order to guaranty the reliability and acceptance of these systems. Two kinds of control approaches are possible, passive control approaches and active control techniques.

1.1 Passive Control Approaches

Passive control techniques are the traditional methods of reducing structural vibrations and radiated noise. Passive noise control methods can be grouped into two main approaches: building an enclosure around the vibrating source, and structurally modifying the original system by adding mass, stiffness or damping. Passive controllers

are thus mainly based on absorption and reflection of waves. Some examples of passive control methods corresponding to the first approach consist of barriers, mufflers, enclosures and wrappings and are relatively well established techniques. Noise barriers are placed between the noise source and the observation points but do not completely cover the source nor the observer. Barriers can be walls, fences or buildings which reflect most of the unwanted noise [1]. Mufflers, also called silencers are used to control the noise created by air/gas flows and the noise propagating in ducts. Two kinds of mufflers exist: dissipative mufflers which reduce noise by the presence of sound-absorbing materials and reactive mufflers which attenuate noise by the creation of destructive interferences inside the expansion chamber [2]. Enclosures and wrappings consist of completely covering the noise source (e.g. machine, duct, pipe) to reduce the noise outside of this surface. Most enclosures and wrappings are multilayer structures made of a heavy exterior layer and a porous sound-absorbing material layer towards the inside. The difference between enclosures and wrappings is the fact that in enclosures the sound-absorbing layer does not touch the vibrating structure while in wrappings the sound-absorbing material is completely in contact with the vibrating system [2].

The second passive control approach includes vibration isolation using mass-spring systems and the addition of passive damping using viscoelastic materials. Many studies have been done on elastic porous materials such as foams to investigate their use as passive absorbers. Recently, Kang et al. [3] studied the acoustical behavior of foam layers for different mounting conditions. They showed that the acoustical properties of polyimide foam layers depend on the backing boundary conditions as well as on the orientation of the layer cut. Another method of passively controlling structure-borne vibrations is to introduce dimensions or material changes in the vibrating structure (impedance changes). The addition of damping through a passive material discontinuity of high loss factor can considerably attenuate vibration amplitudes. Cremer et al. [4] developed a model of an infinite beam with a viscoelastic interlayer of finite length.

Their study consisted of a concrete infinite beam with a 3 cm cork interlayer and attenuation in extensional and flexural wave amplitudes was demonstrated. A similar model will be used for the passive control approach considered in this research.

Effective passive control techniques usually imply a significant mass increase, to some extent, and do not give satisfactory results at low frequencies. The ineffectiveness of this method at low frequencies results from the fact that at these frequencies the wavelength is large compared to the thickness of a usual vibration absorber.

1.2 Active Noise Control (ANC)

The concept of active noise control or anti-sound methods consist of generating an acoustic wave of same magnitude but 180° out-of-phase with the unwanted noise. The idea of using anti-noise to cancel noise is based on the principle of superposition. Superposition of coherent acoustic waves produces either constructive or destructive interference. The cancellation of sound by destructive interference between elementary fields is the basis of active noise control principle and has been explained by Huygens [5]. In ANC, destructive interference is created by generation of an "anti-noise" sound field with secondary acoustic sources (such as loudspeakers), resulting in attenuation or elimination of the primary undesired sound field.

The starting point of active noise control was in Germany in 1936 with Paul Lueg [6] who showed the pressure attenuation due to a simple sound wave propagating in a 1-D duct using a loudspeaker as the cancellation source. Later, Olson and May [7] published a description of an "electronic sound absorber" and Conover [8,9] developed an active controller for reducing the noise radiated by power transformers. These early projects all used a manually adjusted analogous electronic system to optimize the control, and these

studies were not further developed since practical applications were unsuccessful.

The interest in ANC decreased in the late fifties until the late sixties, when a new interest was born due to the many improvements in computers and high speed digital signal processing. Because of a new interest in ANC, numerous authors such as Warnaka [10] and Ffowcs-Williams [11] explicitly defined the concept of ANC. Jessel and Mangiante [12] theoretically developed an approach using active absorption for noise reduction in air ducts. Also, Swinbanks [13] gave a method for attenuating propagating waves in ducts with actively operated acoustic sources mounted on the duct walls. In the eighties, the beginning of industrial applications for ANC appeared with, for instance, Chaplin [14] who proved that many industrial noise and vibration problems could be solved using active control techniques. Since then, the field of ANC has been expanding due to the profound advances in technology and digital signal processors, allowing practical implementations. Active control techniques require efficient and precise signal processing as the magnitude and phase of the unwanted wave must be known with high precision to greatly reduce the noise. Active control is very effective at low frequencies, where passive control is not. An important characteristic of ANC is that the sound radiated from a structure can be reduced without modifying the noise source. ANC can often require large control sources or effort to cancel the primary noise field, especially at low frequencies, and can then be impractical for achieving global noise attenuation.

1.3 Active Structural Acoustic Control (ASAC)

A relatively new concept for active noise control was introduced by Fuller in 1987 [15] known as Active Structural Acoustic Control (ASAC). Fuller demonstrated that farfield acoustic radiation could be reduced by modifying the response of a radiating structure by the application of inputs directly into the structure, instead of using acoustic

sources in the sound field. The principle of active structural acoustic control is thus to control sound radiation from structures by modifying structural vibrations. ASAC involves the addition of secondary control inputs such as forces applied directly to the structure vibrating due to the excitation of a primary disturbance.

In 1987, Fuller and Jones [16,17] investigated the control of the acoustic field radiated from an elastic cylinder submitted to vibrational or acoustical excitations. They demonstrated that a reduction of the sound field inside the closed cylinder could be obtained applying a harmonic point force as the control source on the cylinder wall. Later on, a study performed by Hansen et al. [18] consisted of comparing the results obtained with ANC and ASAC for the control of the radiated sound of a rectangular plate excited by harmonic forces. This work showed that ASAC was a more effective technique for reducing the radiated sound and pointed out some disadvantages in using acoustic control sources. With ANC, the number and size of the control sources are considerably increased compared to the control sources used with ASAC.

1.4 Active Vibration Control (AVC)

Cremer et al. [4] showed in 1973 that vibrations could travel in structures in the form of extensional, flexural and torsional waves and couple to a fluid to radiate sound. The method of AVC has been developed using both the modal and the wave approach. The modal approach consists of reducing the total modal vibrational energy in the finite beam at some frequencies [19]. A system vibrating under on-resonance harmonic disturbance excitation (i.e. disturbance frequency corresponds to a natural mode) has a structural response dominated by that mode. In this case, the dominating mode can be controlled efficiently using only one control actuator. A system vibrating off-resonance has a structural response dominated by many modes, and effective control of these modes

requires one control actuator per mode. Thus, for structures excited off-resonance, the modal approach becomes very complex to implement [19,20]. The wave approach consists of minimizing a cost function downstream of the control point. The cost function is chosen to represent exactly the quantity to minimize, as for instance the energy leaving the structure, the motion of the structure or the noise radiated by the structure. The wave approach in structures was mentioned by Mace [21] as a representation of the vibrations in a beam using propagating and decaying waves. Von Flotow [22,23] also used a wave approach in order to control travelling waves in large spacecraft structures.

Many authors investigated the wave control approach considering the minimization of the power flow (i.e. the travelling energy) and the main structures of interest were beams (finite, semi-infinite or infinite). In 1987, Redman-White et al. [24] investigated an active system to experimentally control the flexural power flow in an infinite beam. They concluded that two actuators were required to cancel the power flow intensity in the farfield of the beam having the error sensors co-located with the actuators. Also, the power flow approach has been studied by Gonidou and Fuller [25] who demonstrated that active forces applied to beam-like structures could attenuate the flexural power flow. With their configuration, only one actuator and controller were necessary to control the total energy travelling downstream of the control point.

In all of the power flow approaches mentioned above, active control of vibrations was accomplished considering that only flexural waves were travelling along the beam. As mentioned earlier, three wave forms known as extensional, flexural and torsional can propagate vibrational energy. Also, when a wave form reaches a discontinuity point (i.e. impedance discontinuity at force input location or boundary), wave conversion can happen between these three wave forms due to their inherent coupling [4]. In consequence, all wave forms should be considered in vibrating structures with structural junctions in order to have a realistic representation of structure-borne vibrations. Recently, Gibbs [26]

investigated the active control of extensional and flexural power flows in thin beams and performed experiments. Thus, many previous studies have been concerned with active control of structural vibrations due to flexural waves, but very little work has been done on active control of all the wave forms present in the vibrating structure.

Another topic of interest involved the active control of vibrational energy due to the presence of discontinuities (structural joints) in the vibrating structure. In 1989, Miller et al. [27] studied the optimal control of power flow at structural junctions. Their cost function to be minimized incorporated the steady state power flow and minimum control efficiency. Also, Gibbs [26] investigated, in the case of thin beams, the influence of a blocking mass on the active control of extensional and flexural power flows.

1.5 Previous Active/Passive Work

Recently, the interest in structural noise absorption using both passive and active control techniques has increased considerably, revealing many advantages of the combination. The application in this thesis is an example of the many ways of combining active and passive control methods. Essentially two main types of active/passive control systems exist: adaptive/passive techniques and active/passive hybrid techniques [28]. The adaptive/passive systems are mainly passive mechanisms whose performance is optimized by adaptations or changes of the passive system properties. The hybrid active/passive systems combine both active and passive elements in either series or parallel. The passive system usually applies the primary control action, while the active system is used to reinforce the action of the passive system or to overcome its limitations [28].

An example of an adaptive/passive system is a tuned vibration absorber, which may come in many different types but always implement a second-order resonant

response to a host system's excitation. Some advantages of tuned vibration absorbers are their simplicity and lack of power consumption, while their disadvantages include the difficulty in obtaining an accurate tune. Adaptive tuned absorbers are able to change their parameters in order to adjust their tuning. Adaptive tuned absorbers have been used in aircraft applications in order to limit fuselage response to engine and propeller excitations [29]. Another application is tuned vibration isolation, such as the vibration isolator invented by Halwes and Simmons [30]. Other adaptive/passive methods include Electro-rheological fluids (ER fluids). ER fluids consist of colloidal suspensions which undergo significant modifications of their mechanical properties when an external electric field is applied upon the fluid. When ER fluids are embedded within electrically conductive solids, creating ER fluid actuators, the global properties of the structural materials can then be controlled [31]. Choi et al. experimentally studied the ability of an embedded ER fluid actuator to control the chaotic behavior of a smart beam. They showed that the chaotic behavior of some structures used in engineering could be reduced by introducing ER fluid actuators in these structures [32]. Finally, a Passive Constrained Layer Damping (PCLD) is an adaptive/passive system composed of a viscoelastic damping layer with a constraining layer of structural material (such as aluminum) on top. Constrained damping layers result in shear strains much greater than those obtained with unconstrained damping layers. Consequently, constrained damping layers are able to dissipate higher vibrational energies and achieve larger damping ratios than unconstrained damping layers [4].

The use of active/passive hybrid systems started with an experimental work by Guicking et al. in 1984 [33]. In their system, the passive absorber consisted of a porous plate placed in an impedance tube at a small distance from the open end of the tube, and the active controller was a control speaker located at the end. They showed that for one of the plates tested, nearly all of the acoustic energy was absorbed over the frequency range 100-600 Hz. Later, Lafleur et al. [34] investigated a single and double layer of piezoelectric composite of piezorubber in order to eliminate reflected and transmitted

sound in a fluid-filled tube. They demonstrated that with the single layer of piezorubber only transmission or reflection of sound could be cancelled, while with the double layer transmission and reflection of sound could be simultaneously eliminated. Another example of an active/passive hybrid is the Active Constrained Layer Damping (ACLD), which consists of a viscoelastic damping layer sandwiched between two piezoelectric layers. When the ACLD is bonded to a vibrating structure, the piezoelectric layer which is directly bonded to the structure acts as the sensor, while the top piezoelectric layer acts as the actuator. The ACLD is thus a conventional PCLD combined with efficient active control methods to control the strain of the constrained layer, resulting in control of the dissipated energy. This ACLD treatment has been used to effectively damp out the vibrations of large flexible structures such as aircraft cabins and car interiors [35]. Recently, Beyene and Burdisso [36] studied an active/passive system made of a layer of absorbing material separated from an active wall by an airspace. Their purpose was to match the impedances of the back surface of the absorbing layer and the air by displacement of the active wall, resulting in minimization of the reflected wave within the airspace. They obtained both experimentally and numerically high absorption coefficients over the frequency range 100-2000 Hz. Also, an experimental work on the potential of adaptive foams as radiation and reflection controllers was introduced by Fuller et al. [37]. A polyvinylidene fluoride (PVDF) actuator was located inside a partially reticulated polyurethane foam forming an adaptive foam. They demonstrated the ability of adaptive foams in controlling low frequency sound and experimentally obtained, for a vibrating piston, 20 dB of attenuation for the farfield sound pressure level.

1.6 Piezoelectric Actuator Models

In the past years, much research has been focused on the development and implementation of smart materials such as structures excited by piezoelectric actuators.

Smart materials can be defined as materials able to detect environmental conditions by sensing changes (sensor function), transfer the information (processor function) and response with an adequate action (actuator function) [38].

In 1981, Forward et al. [39] showed that actuation strain could be induced by piezoelectric materials, and piezoelectricity is now the most common method used to induce strain actuation. Piezoelectric actuators can be bonded to or embedded in a vibrating structure to form a "smart structure" without adding significant mass to the original system. When excited by an electric charge, piezoelectric actuators create a surface strain resulting from the expansion and contraction of the actuator. Since this process is reciprocal, piezoelectric actuators can also be used as sensors and generate a complex charge when submitted to a force or pressure.

In order to predict the structural deformation induced by the piezoelectric actuator, it is necessary to determine the piezoelectric actuation strain. Many models have been created to characterize the interaction between induced strain actuators and induced forces or moments on the host structures. These models can be grouped into three categories:

1. Simple models such as the uniform strain model developed by Crawley and de Luis [40], assuming only uniform extensional strain in the actuator and correct only for surface bonded actuators.

2. More complex models applicable to both bonded and embedded cases, such as the consistent plate model [41], the Bernouilli-Euler model and the model developed by Dimitriadis et al. [42]. The Bernouilli-Euler model includes extensional and flexural strains in the actuator and is the 1-D version of the consistent plate model. The Dimitriadis et al. model is an extension of the 1-D analysis of Crawley and de Luis to excitation of thin plates by rectangular 2-D piezoceramic patches.

3. Complex and accurate models considering transverse shear effects, such as the linear shear stress model by Lin and Rogers [43].

Piezoelectric actuators, in particular piezoceramics, have been used as actuators in many applications on plates and beams. Dimitriadis et al. [42] studied the excitation of a simply supported plate using two co-located 2-D piezoelectric elements bonded on each side of the plate and having the same signal but 180° out-of-phase (pure bending case). They showed that in the case of pure bending, the piezoceramics were creating line moments acting around the periphery of the actuators. They also demonstrated analytically that piezoceramic actuators bonded to the surface of the structure could excite selected modes of vibration. Liang and Rogers [44] established that the actuator stress field for a distributed actuator is undisturbed by the free edge up to about four actuator thicknesses from its periphery. Pure bending is thus obtained with two co-located 180° out-of-phase piezoelectric elements with sizes relatively large compared to their thickness.

Concerning excitation and control of vibrations in beams using piezoceramic actuators, many studies were pursued by Crawley and de Luis. In 1987, they developed an expression for the static and dynamic response of a cantilevered beam excited by two co-located piezoelectric elements and verified this model experimentally. An important result by Crawley and de Luis [40] was that the induced moments generated by the piezoceramic patches could be considered to be located at the ends of the actuators, in the case of a very thin bonding layer. Also, Fanson and Chen [45] demonstrated the potential of using piezoelectric actuators as distributed vibration actuators on beams, controlling several modes at the same time. They also demonstrated that driving the actuators with the same complex voltage but 180° out-of-phase (i.e. anti-symmetric excitation) resulted into two equal and opposite induced moments in the beam, located at the ends of the actuators, the result of which was extended to a 2-D system by Dimitriadis et al. [42]. Crawley and Anderson [46] completed the results obtained by Crawley and de Luis, and Fanson and Chen by developing models that predict the extension, the bending and the shear deformation induced by piezoelectric actuators. They established that two co-located actuators driven in-phase with the same amplitude of voltage (symmetric

excitation) result in a forcing function equivalent to two equal and opposite in-plane forces located at the ends of the actuators. Thus, two co-located piezoelectric elements bonded on each side of a thin beam create pure extensional motion if driven in-phase and pure flexural motion if driven 180° out-of-phase.

Most of the works mentioned earlier have been interested in excitation and control of vibrations in finite beams and plates from a modal point of view. Recently, the interest in controlling structure-borne vibrations in extended structures such as long thin beams resulted in considering the vibrational response in terms of waves instead of modes. Indeed, Miller et al. [27] showed that the transmission of vibrational energy in long beams was dominated by a wave propagation phenomenon, which justifies finding the system response due to the actuators from a wave approach. For instance, Fuller et al. [47] demonstrated that a single asymmetric piezoelectric element bonded on the surface of a thin beam simultaneously excites extensional and flexural waves. Then, they experimentally showed that two co-located independent actuators bonded on each side of the beam can create any wanted combination of extensional and flexural vibrations.

1.7 Overview and Objectives of Thesis

The objective of this work is to study a system combining passive and active control techniques. As mentioned earlier, passive control methods such as those using vibration absorbing materials are mainly effective at high frequencies. Active control systems, on the contrary, are more effective at low frequencies. Also, the passive properties can be chosen to optimize the active input forces via impedance matching. This explains why a new interest of engineers is to develop systems integrating both control techniques in order to take advantage of the complementary frequency ranges of application and achieve vibration control over a wide frequency range. The active/passive

combination developed in this thesis is also expected to result in lower control effort than with the purely active system. The control effort is associated with the amount of energy required by the controller. Thus, this thesis is a theoretical study of the potential of combining passive and active control techniques in order to reduce extensional and flexural vibrations in infinite thin beams. The object is to minimize the total power flow (i.e. extensional and flexural power flow) in the farfield of the infinite beam.

In this work, the passive absorber is implemented as a hard rubber insert located between two semi-infinite beam sections in steel. The passive absorber consists of two attenuation mechanisms: induced reflections due to an impedance mismatch at the interfaces and absorption due to the high damping coefficient of the passive material. The active control is implemented using two co-located independently driven piezoelectric actuators bonded on each side of the beam at three different locations (before, after and on the passive insert). Figure 1.1 shows a general layout of the different systems examined, i.e. the purely active system, the purely passive system, and the three configurations of the active/passive system. The disturbance or primary field at the origin of extensional and flexural vibrations is a point force excitation applied at an angle to the neutral axis of the beam. The secondary field corresponds to the control forces and control moments induced by the piezoelectric actuators. For a single frequency, the extensional and flexural responses of the beam subject to a point force is expressed in terms of waves. The properties of the passive absorbers are studied by calculating the power flow reduction downstream of the passive insert, in the case of the purely passive system. For the purely active system, the cost function corresponding to the total farfield power flow is analytically expressed in terms of the primary and secondary fields. The cost function is chosen to represent exactly the quantity to be minimized. The minimum of the cost function, for which optimal control is achieved, is determined analytically as well as the amplitudes of the associated control sources. For the different active/passive control systems, the amplitudes of the control sources are numerically estimated in order

to have once again optimal control of the total farfield power flow.

A last complementary study involves examining the influence of vibration flanking paths on the purely passive and purely active systems and the optimal active/passive system. In the presence of flanking paths, noise or vibrations transmit through paths different from the direct expected path [1]. In this research, the flanking paths are parallel to the direct path through the beam and are simulated using torsional and linear springs. This last study better illustrates practical cases which usually consist of complex beams, and where the vibrating structure is most likely to exchange energy with the surrounding environment (such as a surrounding heavy fluid for instance).

The main goal is then to study the possible advantages of such hybrid active/passive systems and conclude which of the three configurations of Figure 1.1 results in the lowest control effort over the frequency range 1-1000 Hz. The theoretical background necessary to the understanding of this work is developed in Chapter 2. Chapter 3 contains the description of the different control systems studied, i.e. the purely passive system, the purely active system and the active/passive system for the three configurations. The numerical results obtained for each control system are discussed and compared in Chapter 4. Chapter 5 describes the approximation of the influence of flanking paths on the control performances. Finally, conclusions are drawn and some recommendations for future work are mentioned.

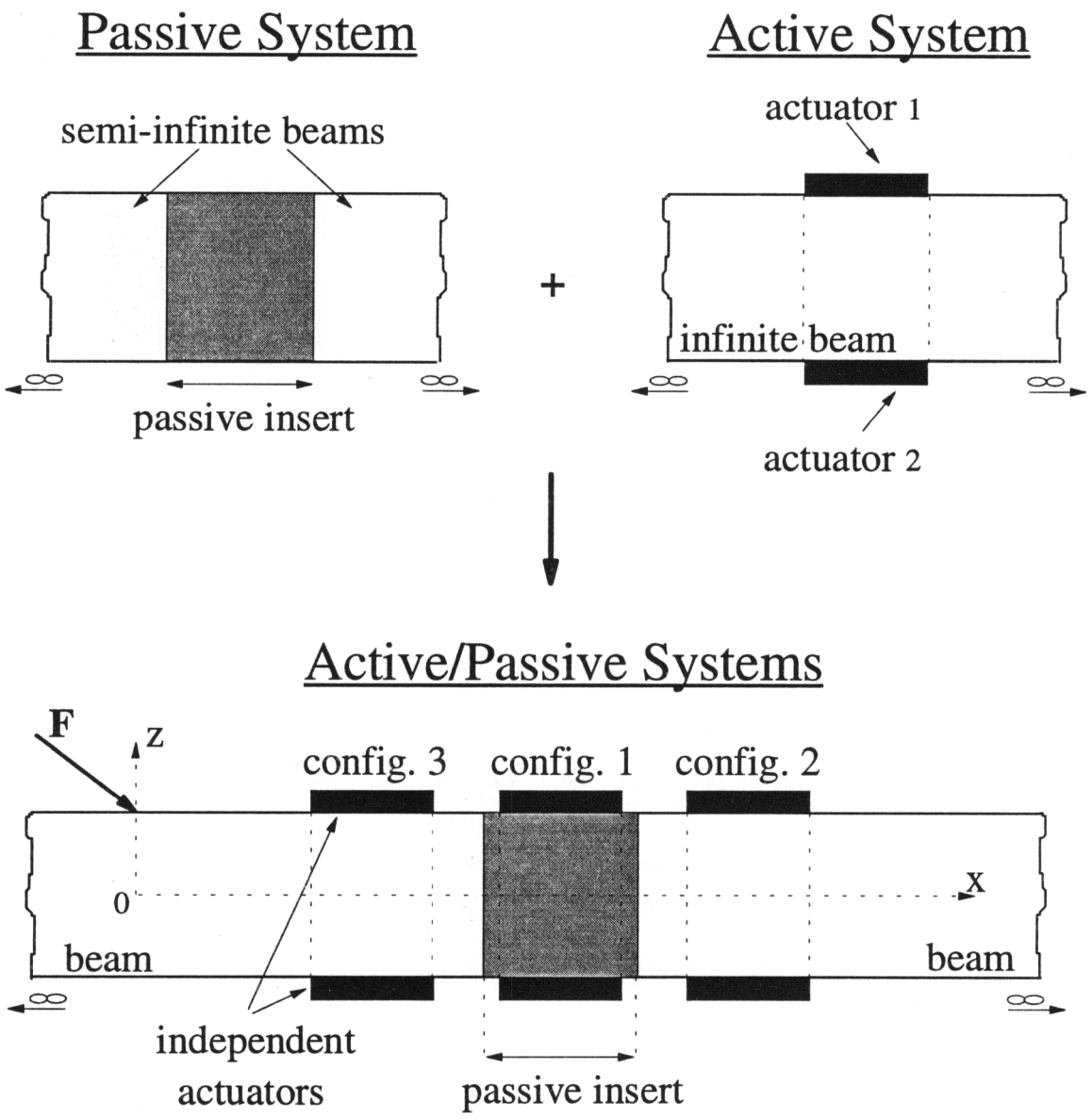

Figure 1.1 General schematic of the different systems studied.

Chapter 2
Theoretical Developments of System Components

2.1 Assumptions

Since the main purpose of this work is to simultaneously control the extensional and flexural energy transmission (total power flow) in infinite thin beams, it is essential to properly excite the structure (i.e. induce these two types of motions). Also, it is necessary to make sure that the vibrations being controlled are the only ones present in the structure. In this analysis, the beam is assumed to follow the Bernouilli-Euler theory of bending or the thin beam theory [4]. The solutions developed throughout this work are thus valid under the following assumptions:

- The loads act either parallel or normal to the surface and the resulting displacements are assumed uniform in the horizontal and vertical section of the beam.
- The in-plane and out-of-plane deformations are small compared to the beam thickness.
- The extensional and flexural motions are considered uncoupled outside of the point forces or line moments areas.
- The shear deformations are ignored in planes perpendicular to the middle surface of the beam (the Kirchhoff hypothesis).
- The rotational inertia is not taken into consideration.
- The neutral axis is assumed to remain unstrained.

- The cross-sectional area is considered to stay constant and normal to the neutral axis.
- The passive insert is assumed to be stiff enough to verify the previous assumptions.

The equation of motion derived for thin beams allows the rotary inertia and transverse shear terms of the Timoshenko equation to be neglected [4]. This permits us to consider extensional and flexural motions uncoupled outside of the discontinuity points. Thus, the previous assumptions are verified only for thin beams. The thin beam assumption is valid for vibrations where the bending wavelength is over six times greater than the thickness of the beam [4]. For the real systems considered in Chapter 4, both the beam and the passive insert will be shown to verify the thin beam condition.

2.2 Extensional and Flexural Equations of Motion of Thin beams

Most of the following derivations have been based upon fundamental vibration theories developed by Cremer et al. [4], Meirovitch [48], Junger and Feit [49], and Fahy [50]. The solutions of the equations of motion will be given in terms of propagating and decaying waves since only the wave approach is studied. The derivations related to extensional and flexural motions will be treated separately since, as mentioned above, these two motions can be assumed uncoupled in thin beams.

2.2.1 Extensional Equation of Motion

The elementary theory of thin beams considers the beam long and slender, and assumes it supports only one-dimensional axial stress (see Figure 2.1).

The quasi-longitudinal equation of motion of thin beams for extensional vibrations is expressed by:

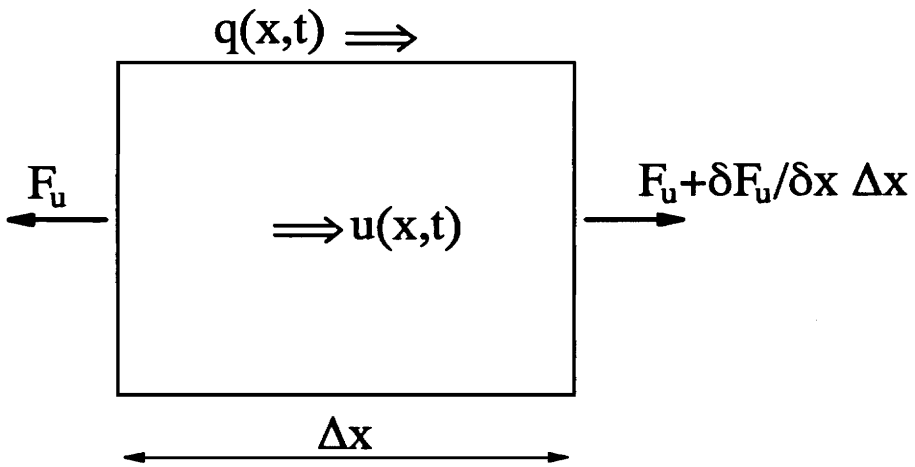

Figure 2.1 Free-body diagram of an element of beam in extension.

$$\frac{\partial^2 u(x,t)}{\partial x^2} - \frac{\rho(1-\nu^2)}{E}\frac{\partial^2 u(x,t)}{\partial t^2} = 0 \qquad (2.1)$$

where E is the Young's modulus of the beam material, ρ is the density, ν is the Poisson ratio, S is the beam cross sectional area, and u(x,t) is the total longitudinal displacement in the x direction. This equation is valid for frequencies of excitation where the extensional wavelength is much larger than the beam cross section, which is consistent with the thin beam assumption.

Assuming a time dependence of the type $e^{i\omega t}$ and harmonic motion of the form $u(x,t) = U(x)\, e^{i\omega t}$, where ω is the angular frequency, equation (2.1) can be rewritten as:

$$\frac{d^2U(x)}{dx^2} + k_e^2 U(x) = 0 \qquad (2.2)$$

where k_e is the extensional wavenumber defined as:

$$k_e = \omega\sqrt{\frac{\rho(1-\nu^2)}{E}} \qquad (2.3)$$

Let q(x,t) be the externally applied body force per unit length as shown in Figure 2.1 representing an element of beam submitted to extensional loads. In presence of an external load, equation (2.2) becomes:

$$\frac{d^2U(x)}{dx^2} + k_e^2 U(x) = -\frac{1-\nu^2}{ES}\, q(x) \qquad (2.4)$$

The in-plane equation of motion is solved using the wave approach with positive waves propagating from left to right. In a region of the beam between two interfaces in x_1 and x_2 (i.e. finite beam section) due to induced forces/moments or material changes, the extensional displacement response can be expressed as follows (see Figure 2.2 (a)):

(a) Extensional waves in a finite section of beam

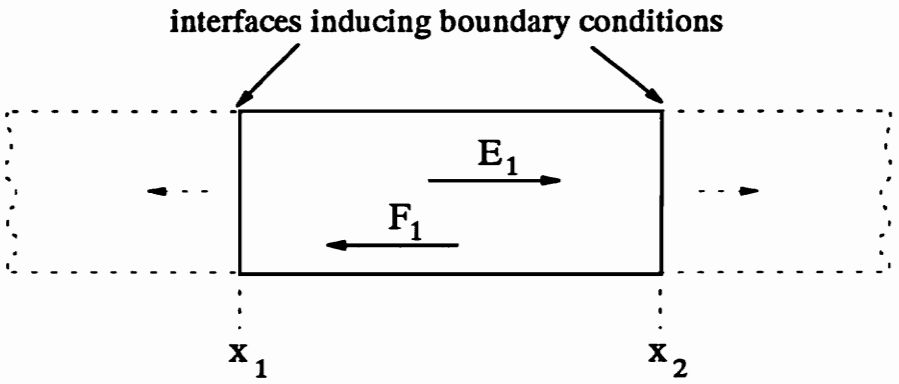

(b) Extensional waves in a semi-infinite section of beam

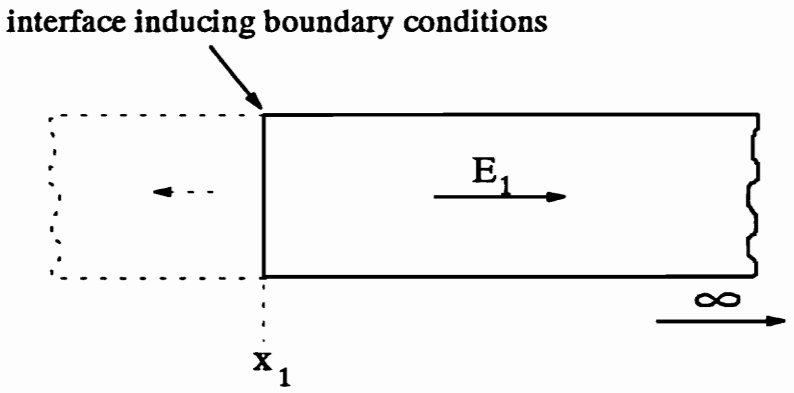

Figure 2.2 Extensional waves propagating in finite and semi-infinite sections of beams.

$$u(x,t) = U(x)\, e^{i\omega t} = (E_1 e^{-ik_e(x-x_1)} + F_1 e^{ik_e(x-x_2)})\, e^{i\omega t} \tag{2.5}$$

where E_1 is the complex coefficient of the positive (right) travelling extensional wave, and F_1 is the complex coefficient of the negative (left) travelling wave. A section of beam bounded by an interface on the left and infinite on the right (i.e. semi-infinite beam section) will have no negative propagating wave, and the coefficient F_1 must equal zero (see Figure 2.2 (b)).

2.2.2 Flexural Equation of Motion

Of all the various types of waves, flexural waves are the most important in terms of structure-borne vibrations. The Bernouilli-Euler beam model assumes that only bending moment M and shear force F_w resultants act at each section. It also assumes that the deflection of the center line is small and only transverse. This theory considers the presence of a transverse shear force but neglects any deformation due to it.

Figure 2.3 shows the free-body diagram of a beam element of length Δx submitted to an external force per unit length q(x,t). The x-axis lies along the neutral axis of the beam, and the z-axis, direction of the flexural displacement, goes through the thickness of the beam. The homogeneous flexural equation of motion of a thin beam is given as:

$$EI\frac{\partial^4 w(x,t)}{\partial x^4} + \rho S\frac{\partial^2 w(x,t)}{\partial t^2} = q(x,t) \tag{2.6}$$

where I is the area moment of inertia, and w(x,t) is the total out-of-plane displacement. Assuming harmonic motion of the form $w(x,t) = W(x)\, e^{i\omega t}$, equation (2.6) becomes:

$$\frac{d^4 W(x)}{dx^4} - k_f^4 W(x) = \frac{q(x)}{EI} \tag{2.7}$$

where k_f is the flexural wavenumber defined as:

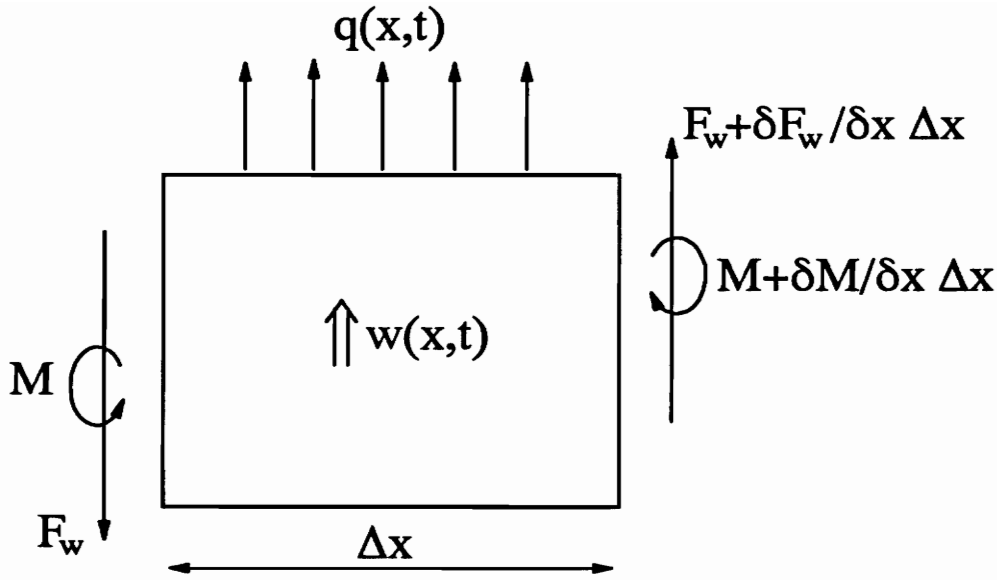

Figure 2.3 Free-body diagram of an element of beam in flexure.

$$k_f = \sqrt[4]{\frac{\rho S}{EI}\omega^2} \tag{2.8}$$

The flexural equation of motion is solved using the wave approach. In a finite section of beam between x_1 and x_2, the flexural displacement response can be written as composed of four waves (see Figure 2.4 (a)):

$$w(x,t) = W(x)e^{i\omega t} = (A_1 e^{-ik_f(x-x_1)} + B_1 e^{ik_f(x-x_2)} + C_1 e^{-k_f(x-x_1)} + D_1 e^{k_f(x-x_2)})e^{i\omega t} \tag{2.9}$$

with A_1 and B_1 the complex coefficients of the positive and negative travelling flexural waves respectively, and C_1 and D_1 the complex coefficients of the positive and negative evanescent or decaying waves respectively. Each interface creates a reflected and a transmitted travelling wave, but also a positive and a negative nearfield whose amplitudes are high near the interface and decay as the wave travels away from the interface. For a semi-infinite section of beam, the negative propagating wave and negative nearfield do not exist, and the coefficients B_1 and D_1 equal zero (see Figure 2.4 (b)).

2.3 Derivation of Extensional and Flexural Power Flows in Thin Beams

The following calculation has been based upon equations presented by Cremer et al. [4]. The derivations will be developed for the case of a finite section of beam and the results for the extensional and flexural power flows will be extended to the case of a semi-infinite section of beam. For the beam considered, the x-axis lies along the neutral axis of the beam, the z-axis goes through the thickness of the beam which is the direction of the transverse displacement, and the y-axis is perpendicular both to the axis of the beam and to the transverse displacement.

(a) Flexural waves in a finite section of beam

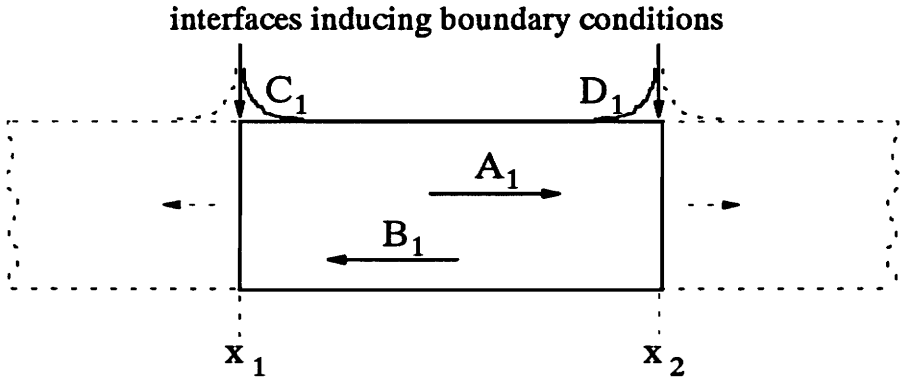

(b) Flexural waves in a semi-infinite section of beam

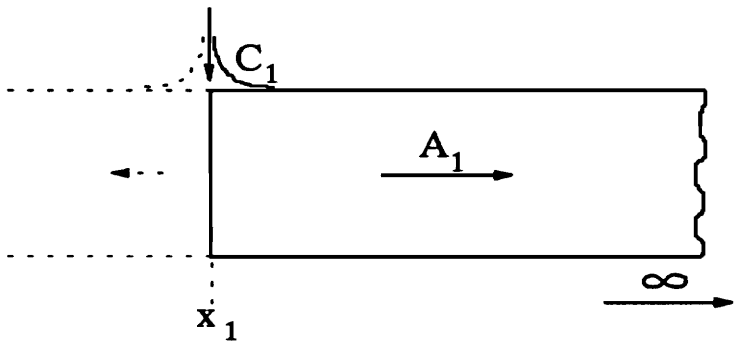

Figure 2.4 Flexural waves propagating in finite and semi-infinite sections of beams.

2.3.1 Finite Section of Beam

The total response for extensional excitation of a finite section of beam is given in equation (2.5) as a positive and negative travelling wave of respective complex amplitudes E_1 and F_1 (see Figure 2.2 (a)). The power flow in the positive x-direction due to extensional excitation is determined by the following relation [4]:

$$P_e(\omega) = \frac{1}{2} \mathrm{Re}(F_u . v_u^*) \tag{2.10}$$

where F_u is the in-plane force acting on the entire cross-sectional area S of the beam and v_u is the in-plane velocity defined by:

$$F_u(x,t) = -SE\frac{\partial u(x,t)}{\partial x} = -iSEk_e(-E_1 e^{-ik_e(x-x_1)} + F_1 e^{ik_e(x-x_2)}) e^{i\omega t} \tag{2.11}$$

$$v_u(x,t) = \frac{\partial u(x,t)}{\partial t} = i\omega (E_1 e^{-ik_e(x-x_1)} + F_1 e^{ik_e(x-x_2)}) e^{i\omega t} \tag{2.12}$$

By substituting equations (2.11) and (2.12) into equation (2.10) and simplifying, the extensional power flow in a finite section of beam is found to be:

$$P_e(\omega) = \frac{ESk_e\omega}{2}(|E_1|^2 - |F_1|^2) \tag{2.13}$$

This power flow has two parts, one resulting from the incident wave of amplitude E_1 and the other resulting from the reflected wave of amplitude F_1. Thus, the net extensional power flow in a finite section of beam consists of the contribution of the incident wave minus the contribution of the reflected wave.

As seen in equation (2.9) , the flexural excitation of a finite beam section results in a total response composed of four waves: a positive and negative travelling wave and

a positive and negative nearfield (see Figure 2.4 (a)). Then, the power flow in the x-direction resulting from flexural excitation is determined by the following relation [4]:

$$P_f(\omega) = \frac{1}{2} \mathrm{Re}(F_w . v_w^* + M . \Theta_w^*) \tag{2.14}$$

where F_w the shear force transmitted across the section, v_w the normal velocity, M the bending moment about the y-axis, and Θ_w the angular velocity about the y-axis are:

$$v_w = \frac{\partial w(x,t)}{\partial t} \tag{2.15}$$

$$\Theta_w = \frac{\partial^2 w(x,t)}{\partial t \partial x} \tag{2.16}$$

$$M = -EI \frac{\partial^2 w(x,t)}{\partial x^2} \tag{2.17}$$

$$F_w = EI \frac{\partial^3 w(x,t)}{\partial x^3} \tag{2.18}$$

By replacing these four equations into equation (2.14) and simplifying, the final expression for the flexural power flow in a finite section of beam is found to be:

$$P_f(\omega) = EI k_f^3 \omega(|A_1|^2 - |B_1|^2 - 2\, e^{k_f(x_1 - x_2)}\, \mathrm{Im}(C_1 D_1^*)) \tag{2.19}$$

The net flexural power flow consists of three terms. The first and second ones are proportional to the incident and reflected travelling wave amplitudes and correspond to the positive and negative energy flows respectively. The third term is proportional to the imaginary part of the complex product of the positive and negative nearfield coefficients. Also, this last term is function of the length of the finite section through the exponential term. This third term corresponds to the nearfield interaction, which is independent of

x and constant at a given frequency. This is associated with the fact that equation (2.19) represents the net power flow, which gives a net value at any x location within the section. Although, the nearfield contribution to the net flexural power flow will vary with the distance between the two interfaces, and this is contained into the term $e^{k_f(x_1-x_2)}$ which decays with frequency but always stays between 1 and 0. Thus, if the opposite nearfields originate at interfaces that are close together (for instance 10 cm apart), the exponential term is close to 1 at all frequencies. Also, if the opposite nearfields originate at interfaces that are far apart (for instance 1 m apart), then the exponential term is zero at all frequencies, and the nearfields does not contribute to the net power flow. It is now necessary to study the other component of the nearfield interaction, which is the imaginary term. Note that when the coefficients C_1 and D_1 are in-phase or 180° out-of-phase, the imaginary term is equal to zero and the power flow is not affected by the nearfields. On the contrary, when the coefficients C_1 and D_1 are 90° out-of-phase, the imaginary term is found to be maximum.

2.3.2 Semi-infinite Section of Beam

The purpose of this research is to cancel the total power flow in the farfield of an infinite beam, i.e. downstream of the discontinuity points due to the control locations. The section of beam downstream of the interfaces is a semi-infinite section of beam, for which the corresponding extensional and flexural power flows are given here.

The extensional displacement downstream of the interfaces of an infinite thin beam is a function of only the positive travelling wave of amplitude E_1, since no wave is reflected from infinity (see Figure 2.2 (b)). The extensional power flow in a semi-infinite section of beam is obtained from equation (2.13) as follows:

$$P_e(\omega) = \frac{ESk_e\omega}{2} |E_1|^2 \quad (2.20)$$

Similarly, the flexural displacement downstream of the interfaces of an infinite thin beam is a function of only the positive travelling and decaying waves of respective amplitudes A_1 and C_1. Again, no wave is reflected from infinity and propagating in the negative direction (see Figure 2.4 (b)). According to equation (2.19), the flexural power flow in a semi-infinite beam section has no nearfield interaction or reflected wave term:

$$P_f(\omega) = EIk_f^3\omega |A_1|^2 \quad (2.21)$$

2.4 Extensional and Flexural Responses of an Infinite Thin Beam to a Point Force Excitation

2.4.1 Point Force Excitation

The responses to minimize in this work are the extensional and flexural power flows induced by a point force excitation of a long thin beam. In order to simultaneously excite both motions, a point force F located on the top of the beam at an angle θ with the neutral axis is applied at the origin (see Figure 2.5). The point force F is decomposed into an in-plane force of amplitude F_e and a normal force of amplitude F_f expressed by:

$$F_e = F\cos(\theta) \quad (2.22)$$

$$F_f = F\sin(\theta) \quad (2.23)$$

Varying the value of θ allows variation of the relative amplitude of the resultant

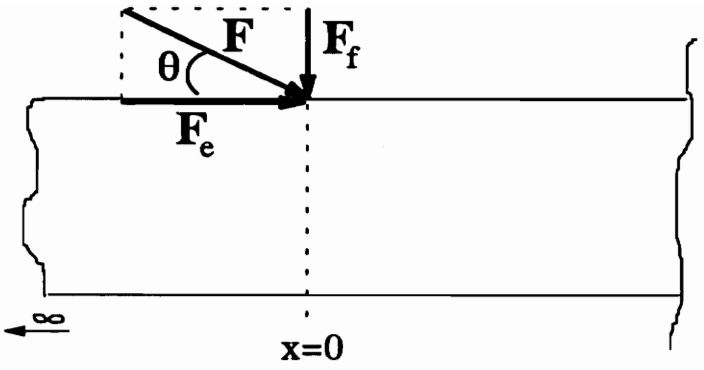

Figure 2.5 Decomposition of a point force excitation at an angle.

extensional and flexural disturbances, which are simultaneously excited. Thus, the normal component of the force is considered to drive the flexural waves while the in-plane component drives the extensional waves [51]. Outside of the point force excitation, extensional and flexural waves are assumed to travel uncoupled, which is a reasonable assumption for a thin beam characterized by a width to thickness ratio of at least ten [26].

2.4.2 Extensional and Flexural Responses

Considering harmonic motion (i.e. $u(x,t) = U(x)\, e^{i\omega t}$), according to equation (2.4) the extensional equation of motion resulting from an in-plane force of amplitude F_e is:

$$\frac{d^2U_d(x)}{dx^2} + k_e^2 U_d(x) = \frac{F_e(1-\nu^2)}{ES}\delta(x) \tag{2.24}$$

where $U_d(x)$ is the spatial component of the extensional displacement due to the disturbance, and $\delta(x)$ is the Dirac function. The solution of equation (2.24) for $x>0$ gives the total extensional displacement, due to an in-plane point force F_e in $x=0$ (extensional disturbance), expressed as follows (see derivation in Appendix A.1):

$$u_d(x,t) = \frac{iF_e(1-\nu^2)}{2ESk_e} e^{-ik_e x} e^{i\omega t} \tag{2.25}$$

This solution consists of a single positive travelling wave. The extensional power flow induced by the in-plane force is obtained below by substituting equation (2.25) into equation (2.10):

$$P_e^d = \frac{\omega(1-\nu^2)^2 |F_e|^2}{8ESk_e} \tag{2.26}$$

where the subscript or superscript d refer to the disturbance.

The flexural equation of motion resulting from a normal point force of amplitude F_f is found considering harmonic motion (i.e. $w(x,t) = W(x)\, e^{i\omega t}$), and expressed as:

$$\frac{d^4 W_d(x)}{dx^4} - k_f^4 W_d(x) = \frac{F_f}{EI}\delta(x) \qquad (2.27)$$

where $W_d(x)$ is the spatial component of the flexural displacement response to the normal disturbance. The solution of equation (2.27) for $x>0$ results in the flexural displacement due to the normal force F_f in $x=0$, and is found to be (see derivation in Appendix A.2):

$$w_d(x,t) = \frac{iF_f}{4EIk_f^3}(-e^{-ik_f x} + ie^{-k_f x})e^{i\omega t} \qquad (2.28)$$

The flexural response to the point force is thus composed of first a positive travelling wave, and second a positive decaying wave. The flexural power flow associated with the normal point force is obtained below by substituting equation (2.28) into equation (2.14):

$$P_f^d = \frac{\omega |F_f|^2}{16EIk_f^3} \qquad (2.29)$$

2.5 Asymmetric Piezoelectric Actuator Model

The purpose of this section is to use the asymmetric model (single sided actuator model) to predict a wave response for the more complicated structure/actuator system considered in this thesis (i.e. two co-located independent actuators). Using the wave approach, an analytical model is presented for the excitation of an infinite thin beam by a single piezoelectric actuator bonded to the surface of the beam. Similar calculations were previously derived by Gibbs and the reader can refer to his work if desired [26]. As mentioned earlier, a single piezoelectric element mounted on a beam simultaneously

excites both extensional and flexural motion [47]. The relative amplitudes of these two motions are functions of the beam/actuator configuration and characteristics. The strain field under the piezoelectric actuator is thus the sum of the two wave components (by the superposition principle) which are coupled by the actuator. When the two waves leave the PZT location they are considered uncoupled in the beam. The following analysis is based upon early work by Crawley and de Luis [40] and Chaudhry and Rogers [52].

2.5.1 Asymmetric Piezoelectric Excitation

The asymmetric piezoelectric actuator is assumed to be infinite in the x-direction, and of thickness T_a in the z-direction. The beam is also infinite in the x-direction and of thickness 2h. The following derivation, based on the Bernouilli-Euler model, is approximated using a static approach valid for a thin actuator compared to the beam.

The principle of piezoelectric material is to strain in all directions when submitted to an applied voltage. The strain distribution for one perfectly bonded asymmetric piezoelectric actuator is shown in Figure 2.6. In this study, a complex voltage $v = V e^{i\phi}$ is applied to the electrodes of the actuator. Piezoelectric actuators are usually mounted such that the direction 1 is oriented along the x-direction of Figure 2.6, direction 2 lies along the y-direction (perpendicular to the plane of Figure 2.6), and direction 3 which is the direction of polarization is along the z-direction of Figure 2.6 [53]. An actuator excited by an applied voltage along its polarization direction 3 will develop a strain applied to the beam, in direction 1 through the coefficient d_{31} and in direction 2 through the coefficient d_{32}. The coefficients d_{31} and d_{32} are the strain sensitivity of the material in directions 1 and 2 respectively. The strain in the y-direction (function of d_{32}) will be neglected since the beam is considerably stiff in that direction. The excitation of an unconstrained piezoelectric element by an applied voltage v results in a strain ε_a in direction 1 expressed by:

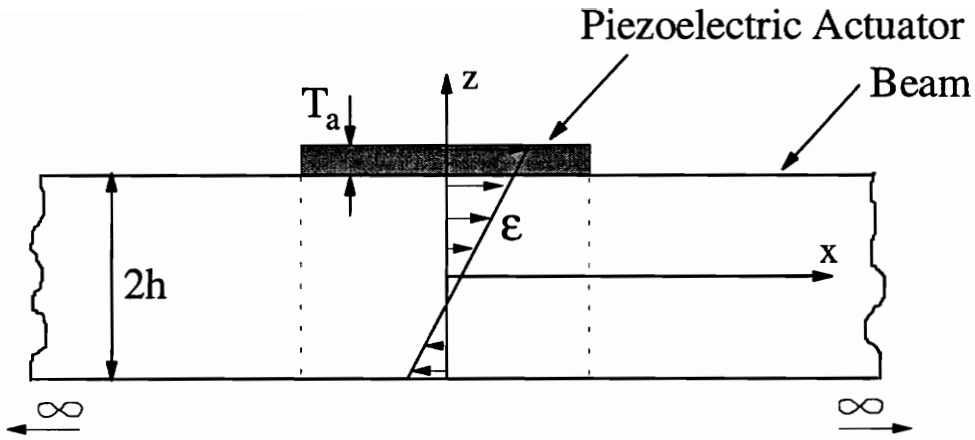

Figure 2.6 Strain distribution for 1-D asymmetric piezoelectric actuator.

$$\varepsilon_a = \frac{d_{31} v}{T_a} \tag{2.30}$$

where the subscript a indicates a characteristic of the actuator.

Since the excitation by a single piezoelectric element bonded to the surface of a beam results in an asymmetric strain distribution $\varepsilon(z)$ shown in Figure 2.6, the beam is thus bending and stretching. According to the Kirchhoff hypothesis of plate theory [54], for which shear strains in planes perpendicular to the middle surface of the beam are neglected, the strain distribution $\varepsilon(z)$ is considered linear and expressed as:

$$\varepsilon(z) = cz + \varepsilon_0 \tag{2.31}$$

where ε_0 is the value of ε at $z=0$ and c is the slope. This strain distribution is then the summation of a uniform strain distribution ε_0 corresponding to the longitudinal displacement and an anti-symmetric strain distribution about the center associated with the bending motion. Hooke's law and the strain distribution expressed in equation (2.31) are combined in order to determine the stress distribution σ within the beam as:

$$\sigma(z) = E(cz + \varepsilon_0) \tag{2.32}$$

where E is the Young's modulus of the beam material to which the actuator is bonded. Also, the stress distribution $\sigma_a(z)$ developed within the actuator is defined as:

$$\sigma_a(z) = E_a(cz + \varepsilon_0 - \varepsilon_a) \tag{2.33}$$

where E_a is the Young's modulus of the actuator material.

Then, force equilibrium in the x-direction and moment equilibrium about the center of the beam are applied, resulting in two equations which are integrated and solved for the parameters ε_0 and c [26]:

$$\varepsilon_0 = K^e \varepsilon_a \tag{2.34}$$

where K^e is the extensional material-geometric constant defined as:

$$K^e = \frac{E_a T_a (8Eh^3 + E_a T_a^3)}{16E^2h^4 + E_a^2 T_a^4 + 8EE_a(4h^3 T_a + 3h^2 T_a^2 + hT_a^3)} \tag{2.35}$$

where h is the half-thickness of the beam. The slope c is expressed as:

$$c = K^f \varepsilon_a \tag{2.36}$$

where K^f is the flexural material-geometric constant specified by:

$$K^f = \frac{12EE_a hT_a(2h + T_a)}{16E^2h^4 + E_a^2 T_a^4 + 8EE_a(4h^3 T_a + 3h^2 T_a^2 + hT_a^3)} \tag{2.37}$$

As mentioned before, the extensional and flexural motions can be considered uncoupled and the purpose here is to separate the extensional and flexural components of the strain distribution. The uniform strain distribution across the beam section created by a single actuator of infinite length and inducing in-plane motion is given by:

$$\varepsilon(x) = \varepsilon_0 = K^e \varepsilon_a \tag{2.38}$$

Resulting from the out-of-plane component of the asymmetric strain distribution, the induced moment distribution in the beam for a piezoelectric element of infinite extent is defined as:

$$m(x) = EIc = EIK^f \varepsilon_a \tag{2.39}$$

where EI is the flexural stiffness in the beam section under the actuator.

Now the excitation of an infinite thin beam by a single piezoelectric actuator of

finite extent is studied. The induced uniform strain distribution is modified in order to act only beneath the actuator location, i.e. for $0 < x < L_a$, which is written as [26]:

$$\varepsilon(x) = K^e \varepsilon_a [H(x) - H(x - L_a)] \tag{2.40}$$

where H(x) is the unit step function at x=0 and $H(x-L_a)$ is the unit step function at $x=L_a$. The finiteness of the actuator is introduced by setting the stress equal to zero at the actuator ends and the induced moment distribution between x=0 and $x=L_a$ is equal to:

$$m(x) = EIK^f \varepsilon_a [H(x) - H(x - L_a)] \tag{2.41}$$

These results follow the assumption made by Liang and Rogers [44] that for distributed actuators of length much greater than thickness, edge effects on the stress distribution can be neglected. The assumed strain distribution of Figure 2.6 is then reasonable.

2.5.2 Extensional Equation of Motion

Referring to Section 2.2, the equation of motion for extensional vibrations excited by an asymmetric piezoelectric actuator of finite length is given as:

$$\frac{d^2U(x)}{dx^2} + k_e^2 U(x) = \frac{d\varepsilon(x)}{dx} \tag{2.42}$$

where ε(x) is the actuator induced in-plane strain distribution. The value of ε(x) obtained in equation (2.42) is substituted in equation (2.44) to obtain the following extensional equation of motion for an infinite thin beam excited by a single piezoelectric element:

$$\frac{d^2U(x)}{dx^2} + k_e^2 U(x) = K^e \varepsilon_a [\delta(x) - \delta(x - L_a)] \tag{2.43}$$

where the Dirac functions δ correspond to line forces in the x-direction. Thus, the in-plane component of the asymmetric piezoelectric element of finite length acts as two equal and opposite in-plane forces (δ functions) located at the ends of the actuator in x=0

and $x=L_a$ (see Figure 2.7). The complex value of this in-plane force F_0 is equal to:

$$F_0 = ES\varepsilon_0 = \frac{ESK^e d_{31}}{T_a} v \tag{2.44}$$

It is then possible to change the amplitude and phase of the induced forces F_0 by modifying the phase and amplitude of the applied complex voltage v.

2.5.3 Flexural Equation of Motion

According to Section 2.2, the equation of motion for flexural waves excited by an asymmetric piezoelectric actuator is given as:

$$EI\frac{d^4W(x)}{dx^4} - \omega^2 \rho S W(x) = \frac{d^2 m(x)}{dx^2} \tag{2.45}$$

where m(x) is the flexural moment induced by the actuator. Again, this equation is obtained considering the rotary inertia and the transverse shear terms of the Timoshenko equation of motion to be negligible, which is the case for a thin beam. The value of m(x) given in equation (2.43) is replaced into equation (2.47) to obtain the final equation of motion of an infinite thin beam for flexural excitation by a single piezoelectric patch:

$$EI\frac{d^4W(x)}{dx^4} - \omega^2 \rho S W(x) = EIK^f \varepsilon_a [\delta'(x) - \delta'(x-L_a)] \tag{2.46}$$

where δ' functions (derivatives of the Delta function) correspond to external moments. Equation (2.48) shows that the out-of-plane component of the asymmetric piezoelectric element of finite length acts as two equal and opposite line moments at the ends of the actuator. The complex value of this line moment M_0 is also proportional to the applied complex voltage v (see Figure 2.8):

$$M_0 = \frac{EIK^f d_{31}}{T_a} v \tag{2.47}$$

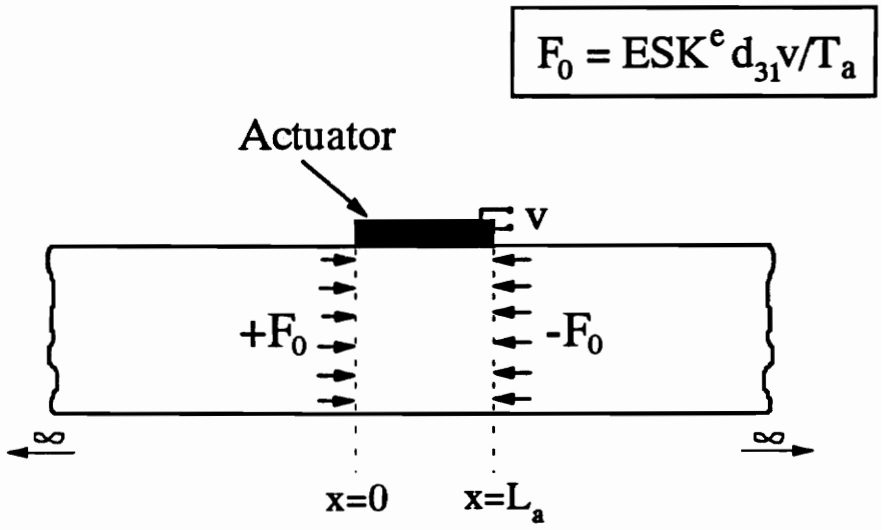

Figure 2.7 Extensional loading condition induced by a single piezoelectric actuator.

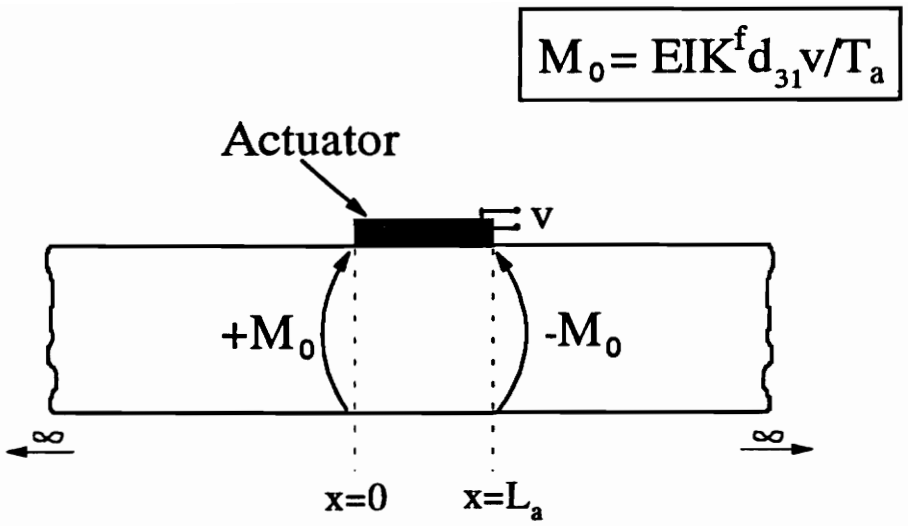

Figure 2.8 Flexural loading condition induced by a single piezoelectric actuator.

2.5.4 Extension to Two Co-located Independent Piezoelectric Actuators

The main purpose of this research is to simultaneously control extensional and flexural power flows. This requires to precisely induce extensional and flexural motions using actuators. A system with two co-located independent PZTs is now presented, based upon the work by Gibbs [26]. The upper PZT is driven by a complex voltage v_1, and the lower PZT by a complex voltage v_2 (see Figure 2.9). The stress induced by the two independent actuators can again be considered equivalent to two equal and opposite forces for extensional excitation and two equal and opposite moments for flexural excitation. Then, the relative magnitude of the induced extensional and flexural waves is precisely determined by the varying relative magnitude and phase of the two complex voltages.

The expressions for the induced forces and moments have to be modified to take into account the two complex voltages v_1 and v_2. Equations (2.44) and (2.47) are then rewritten by superposing the actions of each independent asymmetric piezoelectric patch:

$$F_0 = \frac{ESK^e d_{31}}{T_a}(v_1+v_2) = \frac{ESK^e d_{31}}{T_a} v_e \qquad (2.48)$$

$$M_0 = \frac{EIK^f d_{31}}{T_a}(v_1-v_2) = \frac{EIK^f d_{31}}{T_a} v_f \qquad (2.49)$$

Two new variables v_e and v_f are introduced in equations (2.48) and (2.49). The variable v_e is the complex voltage required to minimize the farfield extensional power flow. Similarly, the variable v_f is the complex voltage applied to minimize the farfield flexural power flow. The voltage v_e is the sum of v_1 and v_2 since purely extensional motion corresponds to voltages in-phase. Also, v_f is the difference of v_1 and v_2 since purely flexural motion is associated with voltages out-of-phase. Throughout this thesis, v_1 and v_2 will be called the applied voltages, and v_e and v_f will be termed the control voltages.

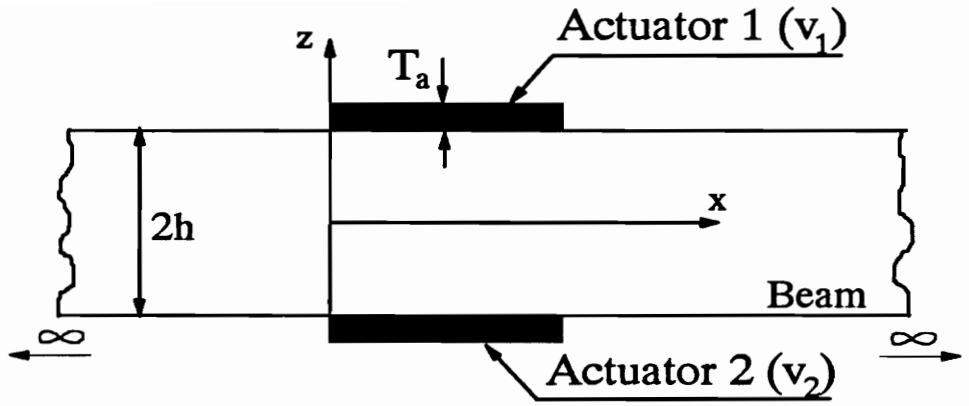

Figure 2.9 Infinite beam excited by two co-located independent piezoelectric patches.

Chapter 3
Analysis of the Control System Behavior

For all the control systems to be studied here, the beam is assumed thin and infinite. As detailed in section 2.4.1, the point force excitation is located on the top surface of the beam at x=0 and makes an angle θ with the horizontal plane (see Figure 2.5). The angle θ will be chosen considering that the beam is much stiffer in extension than flexure, in order to induce approximately equal amounts of extensional and flexural power flows. To have the extensional uncontrolled power flow and the flexural uncontrolled power flow about the same, the in-plane force F_e must be larger than the out-of-plane force F_f, i.e. the angle θ has to be quite small.

3.1 Passive Control System

The passive control in this analytical model is introduced by a passive material insert of length L, positioned within an infinite thin beam as shown in Figure 3.1. An attenuation of the vibrations or energy loss occurs in the passive insert because of two attenuation mechanisms: induced reflections due to the presence of impedance changes at the interfaces, and absorption due to a high damping coefficient of the passive insert material. The viscoelastic insert is characterized by a high loss factor η_p (damping coefficient) compared to that of the infinite beam material, which is neglected in this analysis. The damping phenomena of the passive insert is introduced through a modification of the real modulus of elasticity E_p, which corresponds to hysteretic

(a) Extensional Excitation

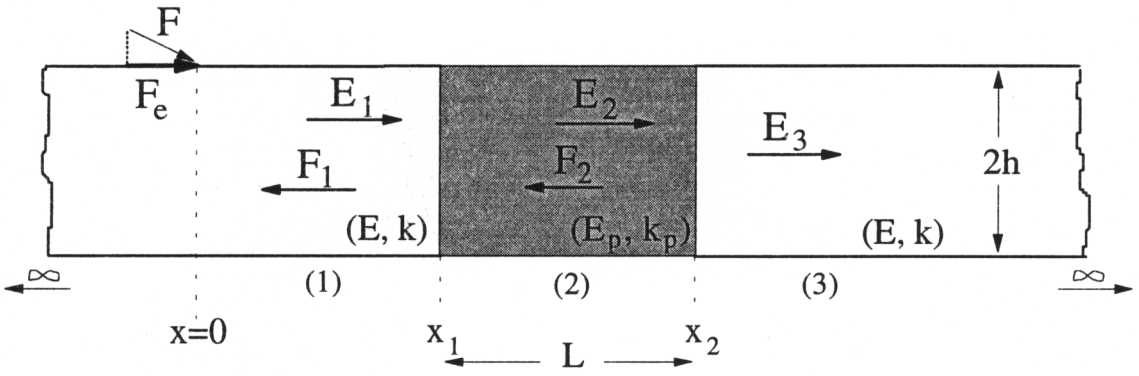

(b) Flexural Excitation

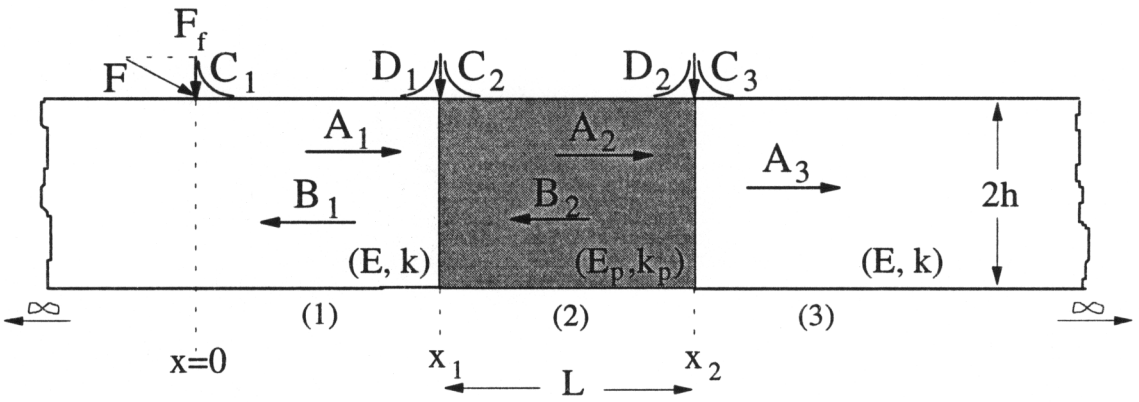

Figure 3.1 Schematic of the passive control system for extensional and flexural excitations.

damping. The modulus of elasticity, $\hat{E}_p$, considered for the passive material is a complex number, which takes into account the internal damping through the loss factor η_p [55,56]:

$$\hat{E}_p = E_p(1 + i\eta_p) \tag{3.1}$$

where the subscript p refers to the passive insert. Note that the hysteretic model of damping is only valid for harmonic motion, i.e. for single frequency analysis. The reason is that for a non harmonic excitation of the structure, the hysteretic damping results in a non-causal response [57,58]. To demonstrate the effectiveness of the viscoelastic insert as a passive absorber, the extensional and flexural power flow reductions will be studied.

3.1.1 Passive Control System for Extensional Motion

The influence of the passive material insert on the propagation of extensional waves is first examined. The passive control system with extensional excitation is represented in Figure 3.1(a). The infinite beam studied for the purely passive approach is composed of three sections (1), (2) and (3). Section (2) corresponds to the passive insert of complex Young modulus $\hat{E}_p$ and extensional wavenumber k_e^p defined as:

$$k_e^p = \omega \sqrt{\frac{\rho_p(1-\nu_p^2)}{\hat{E}_p}} \tag{3.2}$$

where the superscript p refers to the passive insert. The positive propagating waves (coefficients E_i) and negative propagating waves (coefficients F_i) are shown on Figure 3.1 for each section of the beam. The extensional displacements u_1, u_2 and u_3 in each section and the associated extensional power flows are defined below:

$0 < x < x_1$:

$$u_1(x,t) = (E_1 e^{-ik_e x} + F_1 e^{ik_e(x-x_1)})\, e^{i\omega t} \tag{3.3}$$

$$P_{e_1} = \frac{ESk_e\omega}{2}(|E_1|^2 - |F_1|^2) \tag{3.4}$$

$x_1 < x < x_2$:

$$u_2(x,t) = (E_2 e^{-ik_e^P(x-x_1)} + F_2 e^{ik_e^P(x-x_2)}) e^{i\omega t} \tag{3.5}$$

$$P_{e_2} = \frac{\hat{E}_p S k_e^P \omega}{2}(|E_2|^2 - |F_2|^2) \tag{3.6}$$

$x > x_2$:

$$u_3(x,t) = E_3 e^{-ik_e(x-x_2)} e^{i\omega t} \tag{3.7}$$

$$P_{e_3} = \frac{ESk_e\omega}{2}|E_3|^2 \tag{3.8}$$

where E_1 is the complex coefficient of the incident extensional wave due to the disturbance (see equation (2.25)) and defined by:

$$E_1 = \frac{iF_e(1-\nu^2)}{2ESk_e} \tag{3.9}$$

The coefficients F_1, E_2, F_2, and F_3, are the four unknowns of the system determined after applying the extensional boundary conditions at the interfaces in x_1 and x_2. The boundary conditions for extensional waves are the following [59]:

(a) continuity of in-plane velocity $v_u(x,t)$,

(b) continuity of in-plane force $F_u(x,t)$,

where $F_u(x,t)$ and $v_u(x,t)$ are defined in equations (2.11) and (2.12) respectively. The application of the boundary conditions results in a four by four matrix (see Appendix B.1) solved numerically for the four unknowns. The associated extensional power flow reduction, T_e, due to the insert is given as the ratio of the untreated power flow to the farfield power flow after treatment. The untreated extensional power flow is the power flow induced by the extensional disturbance alone as expressed in equation (2.26).

$$T_e(dB) = 10 \times Log_{10}\left(\frac{|P_e^d|}{|P_{e_3}|}\right) \tag{3.10}$$

3.1.2 Passive Control System for Bending Motion

The effect of the passive insert on the propagation of flexural waves created by a normal force of amplitude F_f is studied. The passive system in bending is shown in Figure 3.1(b), and the flexural wavenumber k_f^P for the passive material is given by:

$$k_f^P = \sqrt[4]{\frac{\rho_p S}{\hat{E}_p I}\omega^2} \tag{3.11}$$

In the case of flexural motion, decaying waves are created at the interfaces (x=0, x_1 and x_2) as shown in Figure 3.1(b). The flexural displacements w_1, w_2 and w_3 and the associated flexural power flows present in each section of the beam are given below:

$0 < x < x_1$:

$$w_1(x,t) = (A_1 e^{-ik_f x} + B_1 e^{ik_f(x-x_1)} + C_1 e^{-k_f x} + D_1 e^{k_f(x-x_1)}) e^{i\omega t} \tag{3.12}$$

$$P_{f_1} = EIk_f^3 \omega \left(|A_1|^2 - |B_1|^2 - 2\, e^{-k_f x_1}\, \mathrm{Im}(C_1 D_1^*)\right) \tag{3.13}$$

$x_1 < x < x_2$:

$$w_2(x,t) = (A_2 e^{-ik_f^P(x-x_1)} + B_2 e^{ik_f^P(x-x_2)} + C_2 e^{-k_f^P(x-x_1)} + D_2 e^{k_f^P(x-x_2)}) e^{i\omega t} \tag{3.14}$$

$$P_{f_2} = \hat{E}_p I k_f^{P\,3} \omega \left(|A_2|^2 - |B_2|^2 - 2\, e^{k_f(x_1-x_2)}\, \mathrm{Im}(C_2 D_2^*)\right) \tag{3.15}$$

$x > x_2$:

$$w_3(x,t) = (A_3 e^{-ik_f(x-x_2)} + C_3 e^{-k_f(x-x_2)}) e^{i\omega t} \tag{3.16}$$

$$P_{f_3} = EIk_f^3 \omega \, |A_3|^2 \tag{3.17}$$

where A_1 and C_1 are the two complex coefficients of the incident flexural wave due to the disturbance (see equation (2.28)), which are defined by:

$$A_1 = \frac{-iF_f}{4EIk_f^3} \tag{3.18}$$

$$C_1 = \frac{-F_f}{4EIk_f^3} \tag{3.19}$$

In order to obtain the values of the eight unknown wave coefficients, the following flexural boundary conditions are applied at the two interfaces in x_1 and x_2 [59]:

(a) continuity of out-of-plane velocity v_w (x,t),

(b) continuity of angular velocity Θ_w (x,t),

(c) continuity of flexural moment M (x,t),

(d) continuity of shear force F_w(x,t),

where F_w, v_w, M, and Θ_w are defined in equations (2.15) to (2.18) respectively. These conditions are the continuity of the displacement, the second and third derivatives of the displacement, and the slope. An eight by eight matrix is then obtained (see Appendix B.1) and solved numerically for the wave coefficients. The associated flexural power flow reduction is expressed as:

$$T_f(\text{dB}) = 10 \times \text{Log}_{10}\left(\frac{|P_f^d|}{|P_{f_3}|}\right) \tag{3.20}$$

where P_f^d is the untreated flexural power flow due to the normal disturbance (see equation (2.29)).

3.2 Active Control System

The simultaneous active control of extensional and flexural power flows in an infinite uniform beam is implemented using two co-located (on either side of the beam) independent piezoelectric elements of applied complex voltages v_1 and v_2. The two extensional and flexural motions are studied separately (since assumed uncoupled), although both are present simultaneously within the beam for a point force excitation F at an angle θ with the neutral axis (this is valid for thin beams [4]). The purpose is to analytically determine the total power flow downstream of the actuators, and the optimal applied voltages associated with the minimum total farfield power flow. As mentioned earlier, this corresponds to a unique solution for the applied voltages v_1 and v_2 and the control voltages v_e and v_f. In order to determine the effectiveness of the active control system, the control effort and the control voltages will be examined. The control effort, which represents the energy to add in the system, may be defined as follows:

$$V_{eff} = \sqrt{|v_1|^2 + |v_2|^2} \tag{3.21}$$

Hereafter, only the equations for the extensional and flexural displacements in the farfield of the beam will be given, as the others can be determined easily from the previous cases.

3.2.1 Optimal Control of Extensional and Flexural Power Flows in Infinite Beams

In this study, the active control will result in minimizing the total power flow (sum of the extensional and flexural power flows) transmitted downstream of the actuators. In any active control method, the purpose is to minimize a cost function representing the unwanted vibration or noise, and in this case the cost function is chosen to be the total power flow transmitted. The total power flow transmitted represents the energy travelling in the farfield of the infinite beam, and is directly related to the coefficients of the farfield

propagating waves. As mentioned earlier, for both extensional and flexural motions, the primary disturbance field to be controlled is generated by a point force F applied at an angle θ in x=0 (see Figure 2.5). The secondary control source is implemented by two co-located independent piezoelectric actuators perfectly bonded on opposite sides of the beam, and placed at a given distance from the origin. Once active control is applied, the resulting displacements (extensional or flexural) downstream of the actuators are linear combinations of the displacements due to the primary and secondary sources. The associated total power flow in the farfield, expressed below according to equations (2.20) and (2.21), is thus a quadratic function of both the primary and secondary fields [26]:

$$P_t = P_e + P_f = \frac{ESk_e\omega}{2} |E_1|^2 + EIk_f^3\omega |A_1|^2 \qquad (3.22)$$

This quadratic power function has a unique minimum solution (optimal solution) in terms of the piezoelectric actuator voltages v_1 and v_2 (optimal voltages). To determine the optimal solution of the quadratic cost function the following procedure is followed [60]:

1. Calculate the total power flow (cost function), downstream of the actuators, as a function of the primary and secondary sources.
2. Take the partial derivatives of the cost function with respect to the real part and imaginary part of the applied voltages v_1 and v_2.
3. Set the partial derivatives equal to zero and find the associated optimal applied voltages v_1 and v_2.
4. Substitute these voltages into the cost function and verify that the total power flow is then close or equal to zero.

This procedure is used to calculate the optimal applied voltages in the case of the purely active control. After verifying that the minimum of the cost function is zero, an

easier procedure resulting in more efficient computation is followed for the active/passive control. The beam being a two dimensional system with only one travelling wave solution for extensional and flexural waves, it is possible to generate a secondary source (actuator input) which produces zero farfield power flow when superposed to the primary source (disturbance field) [26]. Thus, two co-located independent actuators should provide complete control of the total farfield power flow. The easier procedure consists of assuming that the farfield power flow is reduced to zero after active control. Since both extensional and flexural farfield power flows are only functions of the positive travelling wave (see equations (2.20) and (2.21)), the procedure for the active/passive control involves: expressing the total displacement transmitted along the beam in terms of the applied voltages, setting to zero the coefficients corresponding to the farfield extensional and flexural positive travelling waves (i.e. equivalent to zero farfield power flow), and solving this system for the unique applied voltages v_1 and v_2.

3.2.2 Active Control System for Extensional Motion

The model of the active system submitted to in-plane excitation is represented in Figure 3.2(a). The beam is again divided into three sections, section 2 being the beam section to which the actuators are bonded. Throughout this work, E_1 is the complex coefficient of the incident extensional wave due to the disturbance (see equation (3.9)). Also, the in-plane force F_0 due to the piezoelectric excitation in extension has been defined in equation (2.50) as proportional to the sum of the applied voltages v_1 and v_2.

The expressions for the extensional displacement u_3 and the associated extensional power flow in the farfield (i.e. for $x > x_2$) are given as:

$$u_3(x,t) = E_3 e^{-ik_e(x-x_2)} e^{i\omega t} \tag{3.23}$$

$$P_{e_3} = \frac{ESk_e\omega}{2} |E_3|^2 \tag{3.24}$$

(a) Extensional Excitation

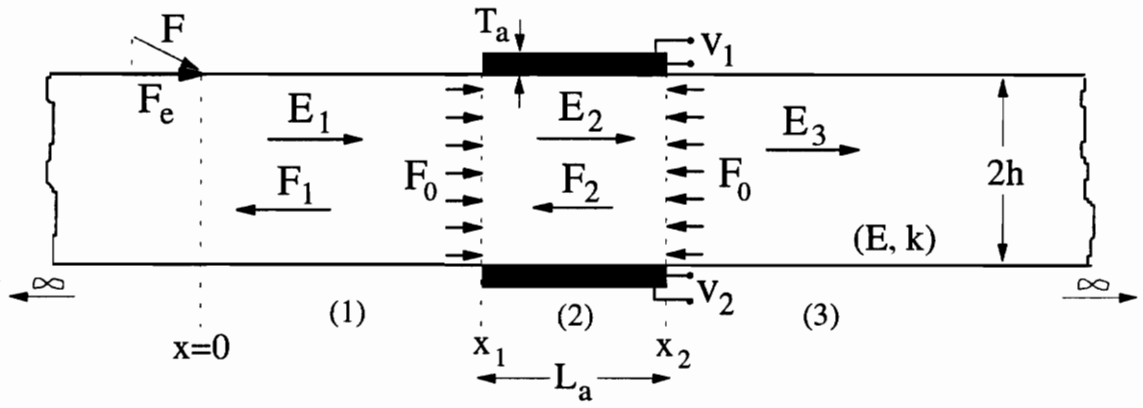

(b) Flexural Excitation

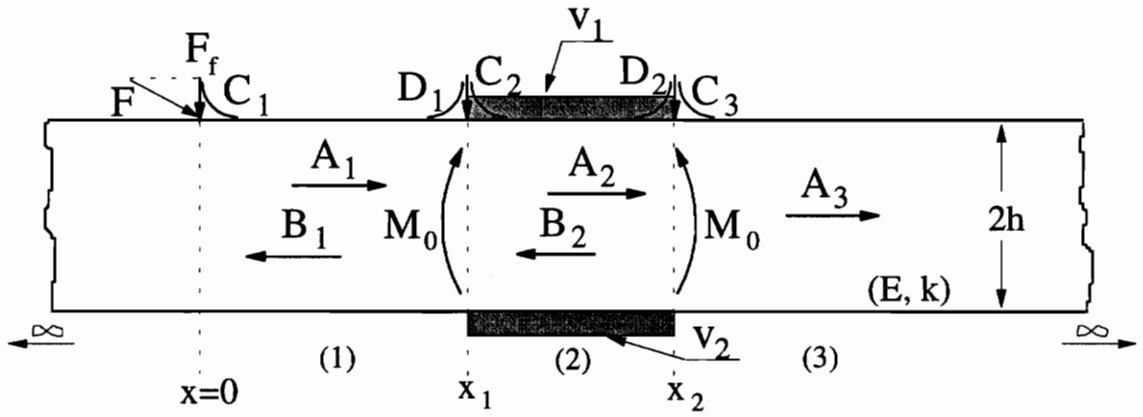

Figure 3.2 Schematic of the active control system for extensional and flexural excitations.

After applying the extensional boundary conditions in x_1 and x_2, a four by four matrix is obtained (see Appendix B.2) and solved analytically for the wave coefficients as functions of the primary and secondary fields.

3.2.3 Active Control System for Bending Motion

The active control of flexural vibrations in infinite beams is studied here and the system considered is detailed in Figure 3.2(b). In this thesis, the normal point force always results in a positive propagating wave of coefficient A_1 and a positive nearfield of coefficient C_1, defined in equations (3.18) and (3.19) respectively. The two co-located independent actuators induce bending motion through the moment M_0 proportional to the difference of the applied voltages v_1 and v_2 (see equation (2.51)).

The equations for the flexural displacement w_3 and the associated flexural power flow in the farfield of the beam (i.e. for $x > x_2$) are expressed below:

$$w_3(x,t) = (A_3 e^{-ik_f(x-x_2)} + C_3 e^{-k_f(x-x_2)}) e^{i\omega t} \tag{3.25}$$

$$P_{f_3} = EIk_f^3 \omega \, |A_3|^2 \tag{3.26}$$

The flexural boundary conditions are then applied in x_1 and x_2, resulting in an eight by eight matrix (see Appendix B.2) solved analytically for the unknown wave coefficients.

3.2.4 Optimal Applied Voltages for the Minimum of the Cost Function

As mentioned earlier, the cost function to be minimized is the total (i.e. flexural and extensional) farfield power flow. The farfield extensional power flow is directly proportional to the coefficient E_3 of the farfield positive propagating extensional wave (see equation (3.24)). Also, the farfield flexural power flow is directly proportional to the coefficient A_3 of the farfield positive propagating flexural wave (see equation (3.26)).

After analytically solving the matrices for the active system in extension and flexure (see Appendix B.2), the extensional and flexural propagating wave coefficients in the farfield are:

$$E_3 = \frac{iF_e(1-\nu^2)}{2ESk_e} e^{-ik_e x_2} + \frac{iK^e d_{31}}{2k_e T_a} (e^{-ik_e(x_2-x_1)} - 1)(v_1+v_2) \qquad (3.27)$$

$$A_3 = \frac{-iF_f}{4EIk_f^3} e^{-ik_f x_2} + \frac{K^f d_{31}}{4k_f^2 T_a} (1-e^{-ik_f(x_2-x_1)})(v_1-v_2) \qquad (3.28)$$

For both equations (3.27) and (3.28), the first term represents the beam response to the disturbance, and the second term describes the beam response to the actuator excitation. The farfield beam response is a superposition of the beam responses to the disturbance and the control sources. The total farfield power flow P_t to be minimized is equal to the sum of P_e^3 and P_f^3 defined as follows:

$$P_{e_3} = \frac{ESk_e\omega}{2} \left| \frac{iF_e(1-\nu^2)}{2ESk_e} e^{-ik_e x_2} + \frac{iK^e d_{31}}{2k_e T_a} (e^{-ik_e(x_2-x_1)} - 1)(v_1+v_2) \right|^2 \qquad (3.29)$$

$$P_{f_3} = EIk_f^3\omega \left| \frac{-iF_f}{4EIk_f^3} e^{-ik_f x_2} + \frac{K^f d_{31}}{4k_f^2 T_a} (1-e^{-ik_f(x_2-x_1)})(v_1-v_2) \right|^2 \qquad (3.30)$$

The total farfield power flow P_t is then expressed in a quadratic form and the optimal applied voltages associated with the minimum cost function are (see derivation in Appendix C):

$$v_1 = \frac{(1-\nu^2)T_a F_e}{2ESK^e d_{31}} \frac{e^{-ik_e x_2}}{1-e^{-ik_e(x_2-x_1)}} + \frac{iT_a F_f}{2k_f EIK^f d_{31}} \frac{e^{-ik_f x_2}}{1-e^{-ik_f(x_2-x_1)}} \qquad (3.31)$$

$$v_2 = \frac{(1-\nu^2)T_a F_e}{2ESK^e d_{31}} \frac{e^{-ik_e x_2}}{1-e^{-ik_e(x_2-x_1)}} - \frac{iT_a F_f}{2k_f EIK^f d_{31}} \frac{e^{-ik_f x_2}}{1-e^{-ik_f(x_2-x_1)}} \qquad (3.32)$$

Note in equations (3.31) and (3.32), that v_1 and v_2 are combinations of a first term dependent on characteristics of the extensional motion and a second term dependent on parameters of the flexural motion. This shows that v_1 and v_2 are able to simultaneously control extensional and flexural farfield power flows. Consequently, according to equation (2.50) the control voltage v_e responsible for minimum extensional power flow is found to be a function of parameters related to the extensional motion only:

$$v_e = \frac{(1-\nu^2)T_a F_e}{ESK^e d_{31}} \frac{e^{-ik_e x_2}}{1-e^{-ik_e(x_2-x_1)}} \qquad (3.33)$$

Also, according to equation (2.51) the control voltage v_f resulting in minimum flexural power flow is only a function of parameters associated with flexure:

$$v_f = \frac{iT_a F_f}{k_f EIK^f d_{31}} \frac{e^{-ik_f x_2}}{1-e^{-ik_f(x_2-x_1)}} \qquad (3.34)$$

Finally, the optimal applied voltages v_1 and v_2 are substituted back into the expression for the total farfield power flow P_t, in order to determine the minimum value of the power cost function. This minimum is found to be zero, which demonstrates that complete reduction of the total farfield power flow can be achieved using two co-located independent actuators. In the next models, as mentioned earlier, the optimal applied voltages will be calculated assuming that the farfield extensional and flexural power flows can be reduced to zero.

3.3 Active/Passive Control Systems (Hybrid Active Control Systems)

Passive control obtained with a viscoelastic insert, and active control achieved with two co-located independent piezoelectric actuators are combined here, in order to minimize farfield extensional and flexural power flows in an infinite thin beam. As mentioned in the introduction, passive approaches to minimize structural vibrations are limited concerning the amount of attenuation achieved, especially at low frequencies. Active control methods are effective for considerably reducing low frequency structural vibrations, but may require significant control effort. Thus, combining active and passive control methods appears attractive for cancellation of structural vibrations over a wider frequency range as the frequency domains of application for each method are complementary. Another expectation of this hybrid combination is to reduce the energy required by the active system, as the control effort is expected to be lower when passive control is added. In this section, three configurations for the active/passive system will be studied, depending on the location of the actuators with respect to the passive insert. The control effort V_{eff}, and control voltages v_e and v_f will be calculated for each active/passive system and compared with those for the purely active system. This is necessary in order to estimate the interest of adding passive methods to active ones.

3.3.1 Configuration 1

The first configuration corresponds to the most compact one with the piezoelectric actuators bonded on each side of the passive material insert as shown in Figure 3.3. The piezoelectric actuators are located in the middle of the passive insert resulting in a symmetrical configuration. The upper actuator is driven by a voltage v_1 and the lower one by a voltage v_2. The actuators act directly on the viscoelastic material, which one is assumed stiff enough in order to neglect the shear deformations inside the structure. In Section 4.1, the passive insert considered here will be shown to verify the thin beam

assumption, for which the shear deformations can be neglected. The in-plane and normal disturbances and control inputs are represented in Figure 3.3, as well as the extensional displacements u_i and flexural displacements w_i in each section of the beam.

The expressions for the extensional displacement and the extensional power flow in the farfield of the structure (i.e. for $x > x_4$) are defined below:

$$u_5(x,t) = E_5 \, e^{-ik_e(x-x_4)} \, e^{i\omega t} \tag{3.35}$$

$$P_{e_5} = \frac{ESk_e\omega}{2} \, |E_5|^2 \tag{3.36}$$

where E_5, the coefficient of the travelling extensional wave in the farfield, is set to zero resulting in zero farfield extensional power flow for the active/passive system.

The flexural displacement and the associated flexural power flow in the farfield (i.e. for $x > x_4$) are equal to:

$$w_5(x,t) = (A_5 e^{-ik_f(x-x_4)} + C_5 e^{-k_f(x-x_4)}) e^{i\omega t} \tag{3.37}$$

$$P_{f_5} = EIk_f^3\omega \, |A_5|^2 \tag{3.38}$$

where A_5, the coefficient of the farfield propagating flexural wave, is set to zero resulting in total control of the farfield flexural power flow. After applying the extensional and flexural boundary conditions at each interface and setting E_5 and A_5 to zero, the matrices (see Appendix B.3) will be solved numerically for the applied voltages v_1 and v_2.

3.3.2 Configuration 2

The analytical developments of configuration 2 will not be given in detail, since the same procedure used in the preceding configuration was followed. Configuration 2 locates the passive insert upstream of the active system location. For increasing x, the

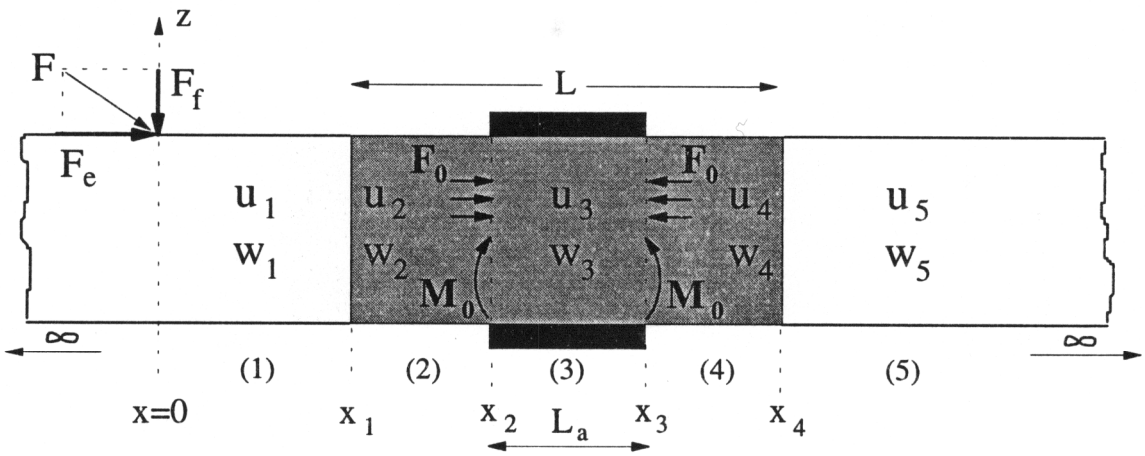

Figure 3.3 Schematic of the active/passive control system configuration 1.

extensional and flexural waves will first travel inside the viscoelastic material before propagating in the beam section located under the actuators (see Figure 3.4(a)). The active control procedure still results in setting to zero the coefficients of the propagating extensional and flexural waves in the farfield (downstream of the PZTs). The control effort and control voltages required by the actuators will be studied.

3.3.3 Configuration 3

The same procedure was again used for configuration 3 and will not be detailed here. The third configuration locates the piezoelectric actuators upstream of the passive insert (see Figure 3.4(b)). Active control results in cancellation of the extensional and flexural power flows downstream of the passive insert. The control effort and individual applied voltages will again be studied.

(a) Active/Passive System Configuration 2

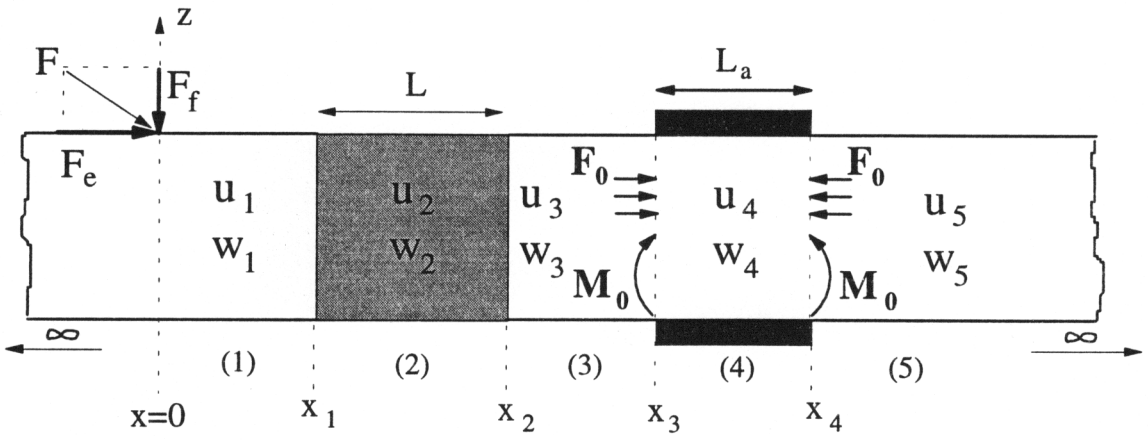

(b) Active/Passive System Configuration 3

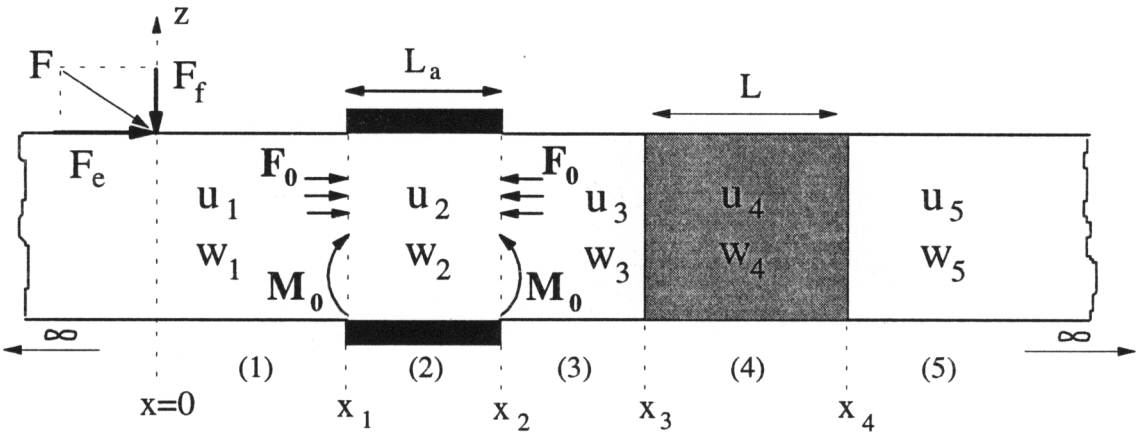

Figure 3.4 Schematic of the active/passive control system configurations 2 and 3.

Chapter 4
Results of the Control System Behavior Analysis

4.1 Characteristic Properties of the Control Systems

This section provides the physical characteristics of the control systems. Control is examined over a frequency range from 1 Hz to 1 kHz.

The disturbance point force is assumed to have a constant magnitude F applied at the angle θ with the beam neutral axis. The extensional and flexural power flows created in the infinite uniform beam by the disturbance (i.e. before any control treatment, passive and/or active, is applied) are referred to as the untreated extensional and flexural power flows. The value of θ is chosen to obtain approximately the same amount for the untreated extensional and flexural power flows (see equations (2.26) and (2.29)). Thus, a small angle θ is chosen so that the in-plane force is greater than the normal force, since the beam is significantly stiffer in extension than flexure. The characteristics of the point force used in the simulations are the following (see Figure 2.5):

- inclined force: $F = 1$ N
- angle: $\theta = 10^{o}$
- in-plane force: $F_e = 0.985$ N
- normal force: $F_f = 0.174$ N

The untreated extensional and flexural power flows, P_e^d and P_f^d respectively, associated

with this angle θ are approximately of the same order of magnitude, as seen in Figure 4.1. The average over the frequency range is about 1.2×10^{-5} W for the untreated extensional power flow and 1.3×10^{-5} W for the untreated flexural power flow. Thus, before treatment approximately the same amount of vibrational energy is carried by the extensional and flexural motions. The cost function to be minimized is the total farfield power flow. In order to control both motions properly when minimizing the cost function, both extensional and flexural power flows before treatment should be present in the beam, and none of them should be of dominant magnitude. Thus, to have control accuracy, the untreated extensional and flexural power flows are required to be approximately of similar magnitude.

The structure used in this work is an infinite steel beam with mechanical properties [61] and dimensions listed in Table 4.1. As mentioned in the introduction, the thin beam assumption is valid when the bending wavelength is over six times greater than the thickness of the beam. Similarly, shear deformations can be ignored for a wavelength to thickness ratio greater than 6 [4]. The wavelength for flexural waves is defined by:

$$\lambda_f = \frac{c_f}{f} = \frac{2\pi}{k_f} \tag{4.1}$$

where c_f is the flexural phase speed. The flexural wavelength is then proportional to the inverse of the square root of the frequency and the maximum frequency corresponds to the smallest wavelength. For the steel beam studied here, the wavelength to thickness ratio is always greater than 56 over the frequency range studied. Thus, the steel beam satisfies the requirements of the thin beam assumption at all frequencies of concern. The passive insert, of same cross sectional area as the beam, is made of hard rubber material characterized by a high loss factor. The values for loss factors vary significantly with changes in temperature and frequency. The loss factor for hard rubber is listed as varying between 0.1 and 1 [62], and the value of 0.4 chosen for the system studied here represents

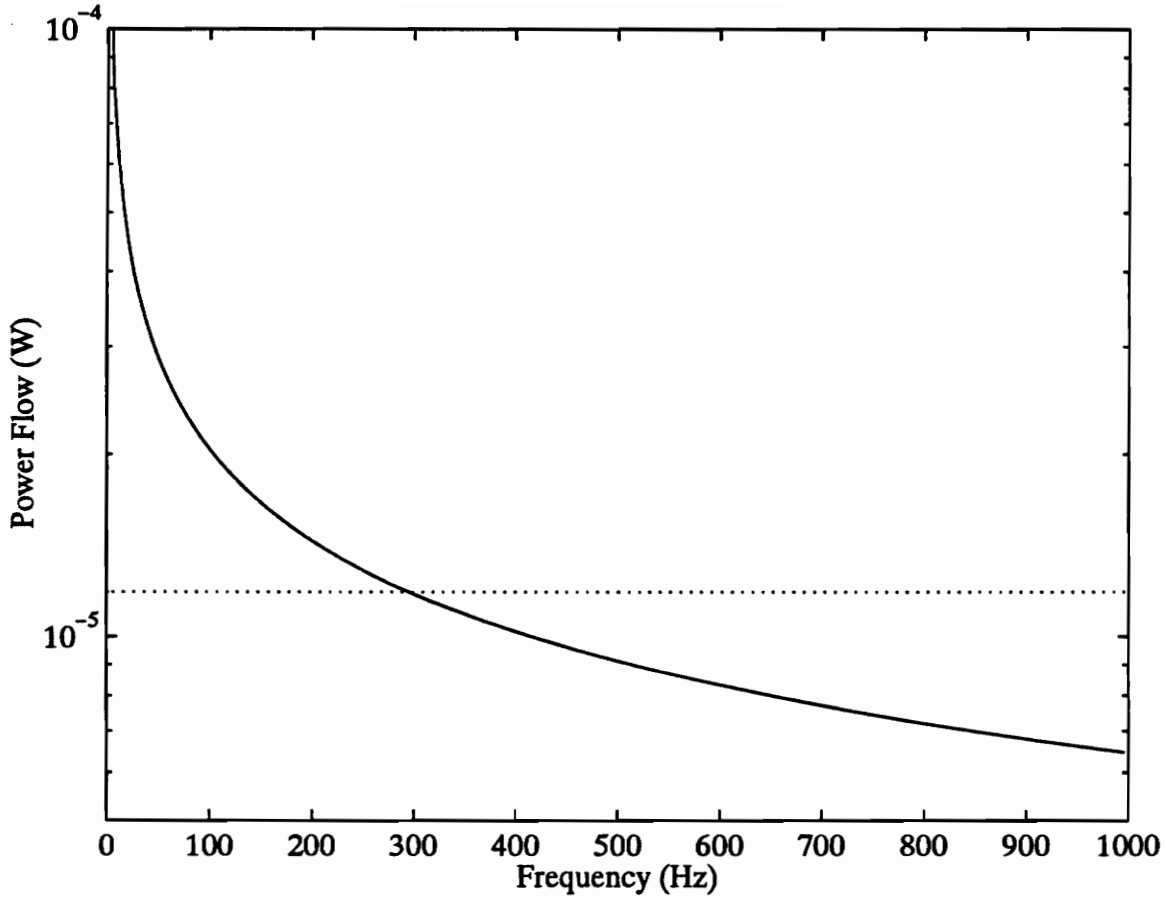

Figure 4.1 Extensional and flexural power flows P_e^d (·····) and P_f^d (——) before treatment.

Table 4.1 Mechanical properties and dimensions of the infinite steel beam.

Properties and Dimensions	Symbol	Value	Unit
Density	ρ	7700	kg/m^3
Young Modulus	E	21×10^{10}	N/m^2
Poisson Ratio	ν	0.28	non dimensional
Thickness	2h	3	mm
Width	w	7.5	cm

an average. The mechanical properties [61,62] and dimensions of the hard rubber insert are given in Table 4.2. The length of the insert primarily dictates the amount of attenuation obtained, but a practical length of 5 cm (in terms of ability to experimentally implement) is considered. The hard rubber section has a bending wavelength to thickness ratio always greater than 28 over the frequency range considered here. Thus, even for the hard rubber material, the thin beam assumption is valid. Note that if the viscoelastic material was soft rubber ($E=0.5\times10^7$ N/m^2 and $\rho=950$ kg/m^3), the wavelength to thickness ratio would equal 6.5 at the maximum frequency of 1 kHz. The validity of the thin beam assumption for soft rubber should then be considered more closely at high frequencies.

The two co-located actuators used for the active control are assumed to be G-1195 piezoelectric ceramic patches, of properties [53] and dimensions listed in Table 4.3. The maximum allowed field ε_{max} across each PZT is equal to 600 V/mm. Then, for a 0.18 mm thick PZT, the maximum voltage allowed is 108 V rms or 300 V peak to peak.

4.2 Passive Approach Results

The passive approach is analytically implemented using a hard rubber insert placed between two semi-infinite steel beams at x_1 and x_2 (see Figure 3.1):

- $x_1 = 1$ m,
- $x_2 = 1.05$ m.

Note that the axial location reference (i.e. the origin) is the position of the disturbance point force. For all of the systems, the first interface is placed far enough from the point force so that the nearfields created by the excitation do not reach this interface.

Figure 4.2 shows the power flow reductions obtained for the general case using a passive insert of length varying between 0.01 and 0.5 m. In this case, the extensional

Table 4.2 Mechanical properties and dimensions of the passive rubber insert.

Properties and Dimensions	Symbol	Value	Unit
Density	ρ_p	1100	kg/m^3
Young Modulus	E_p	0.2×10^{10}	N/m^2
Loss Factor	η_p	0.4	non dimensional
Poisson Ratio	ν_p	0.4	non dimensional
Thickness	2h	3	mm
Width	w	7.5	cm
Length	L	5	cm

Table 4.3 Mechanical properties and dimensions of the piezoelectric actuator (PZT G-1195).

Properties and Dimensions	Symbol	Value	Unit
Strain Coefficient	d_{31}	-166×10^{-12}	m/V
Density	ρ_a	7650	kg/m^3
Young Modulus	E_a	6.3×10^{10}	N/m^2
Loss Factor	η_a	0.001	non dimensional
Maximum Field	ε_{max}	600	V/mm
Thickness	T_a	0.18	mm
Length	L_a	3.8	cm
Width	w_a	6.5	cm

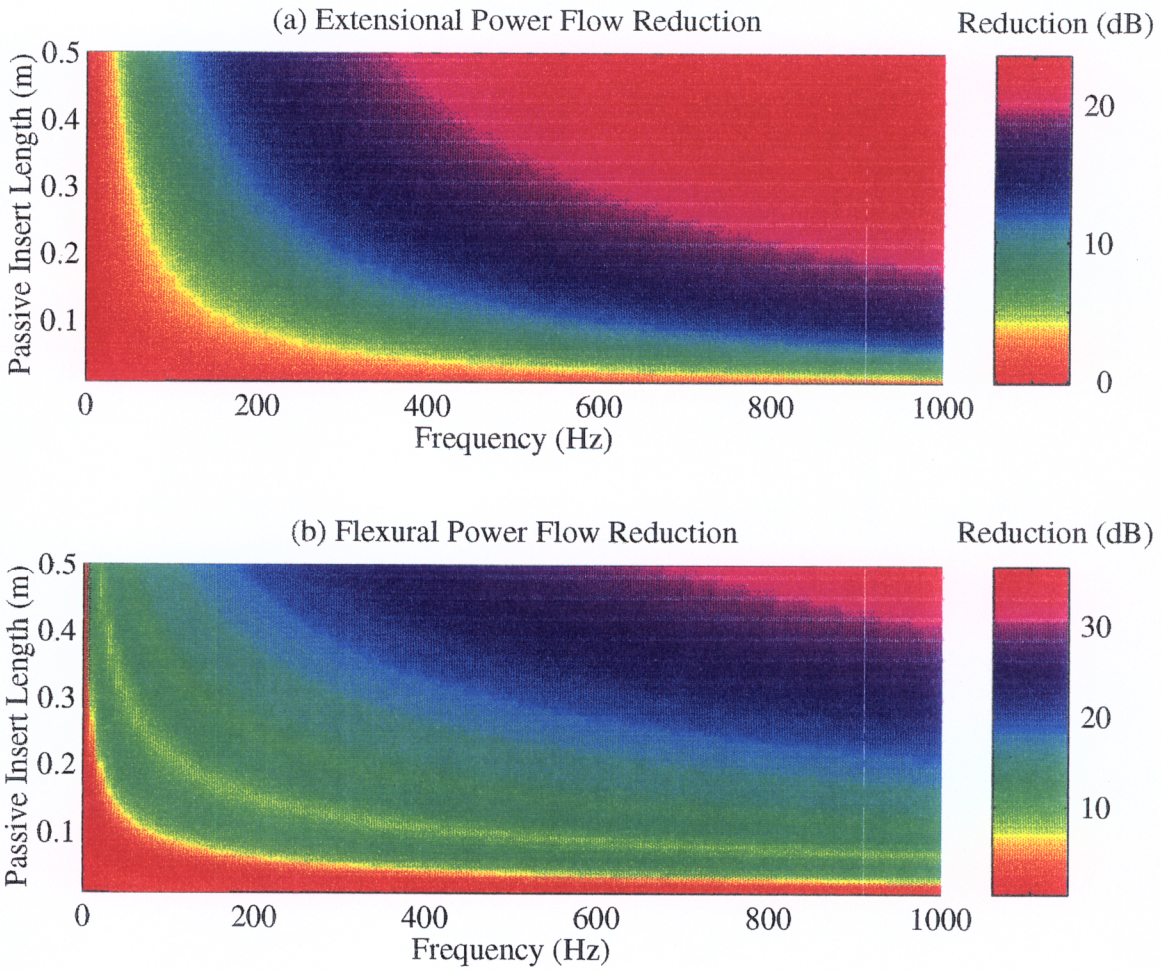

Figure 4.2 Extensional and flexural power flow reductions as functions of the frequency and the length of the passive hard rubber insert.

and flexural power flow reductions are now functions of the frequency and the passive insert length. Note that both extensional and flexural power flow reductions (see Figures 4.2(a) and 4.2(b) respectively) increase with increasing frequency and increasing insert length. This confirms that passive methods are more effective at high frequencies. Also, the flexural power flow reduction is always greater than the extensional power flow reduction, for the frequency range of concern. It appears to be easier to reduce flexural power flow than extensional power flow using a passive hard rubber insert. The passive approach results in more significant extensional and flexural power flow reductions for a long insert, but this does not apply to a practical situation.

Figure 4.3 contains the extensional and flexural power flow reductions as functions of only the frequency and with attenuation via a 5 cm long hard rubber insert. Again, the power flow reduction obtained for flexural waves is always greater than that obtained for extensional waves, over the entire frequency range. The maximum power flow reduction achieved here is about 12 dB for flexural waves and 10 dB for extensional waves. This particular case, which corresponds more to a realistic practical situation, is limited in the amount of power flow reduction achieved.

Figure 4.4 presents the magnitudes of the extensional and flexural displacements along the beam at the excitation frequency of 600 Hz, before and after insertion of the passive insert. The associated extensional and flexural power flows at this frequency are listed in Table 4.4 for each section of the beam. As expected, it can be seen in Table 4.4 that the extensional and flexural power flows are reduced after implementation of the passive approach. Note that in Figure 4.4, the two vertical dotted lines correspond to the location of the hard rubber insert. The extensional and flexural displacements before the passive approach are the in-plane and out-of-plane disturbances that would propagate within a uniform infinite beam. Attenuation of the extensional and flexural displacements can be observed downstream of the passive rubber insert. However, upstream of the

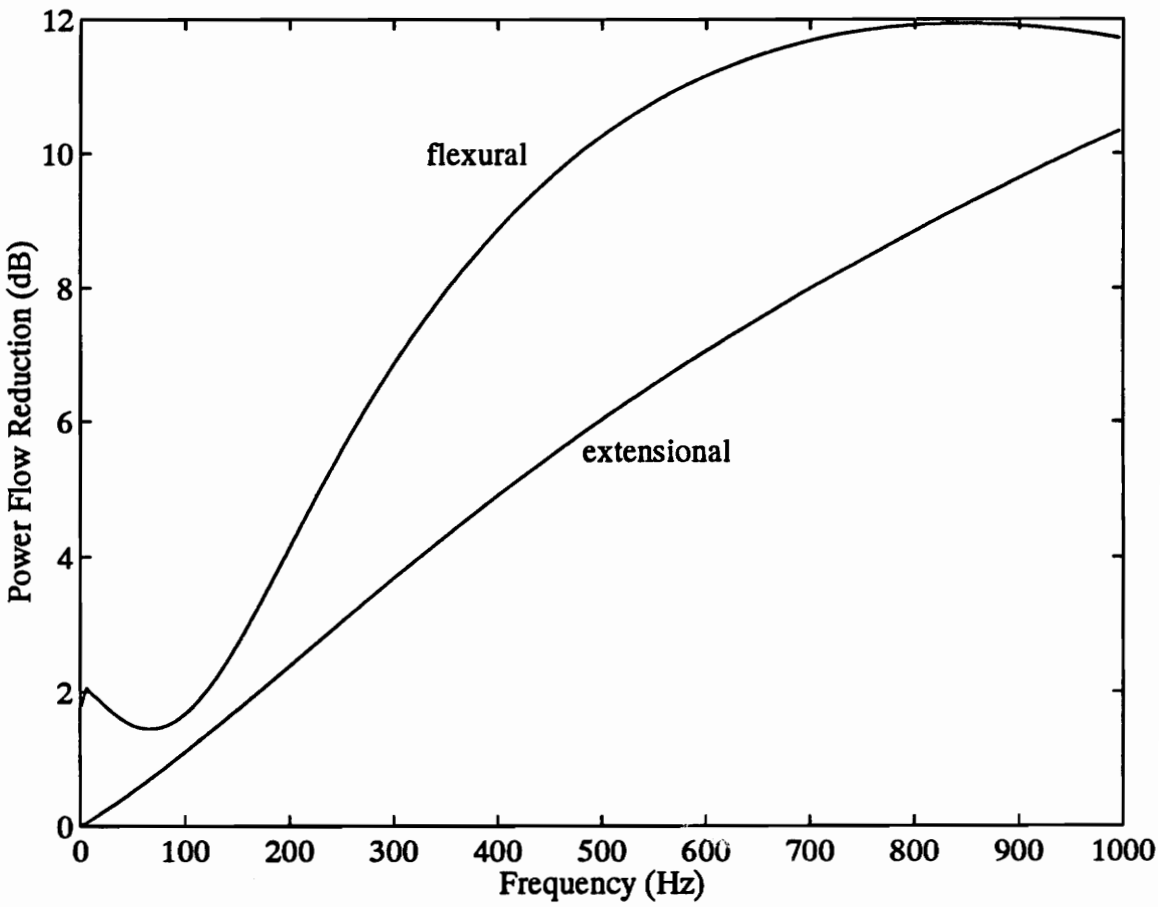

Figure 4.3 Extensional and flexural power flow reductions using a passive hard rubber insert.

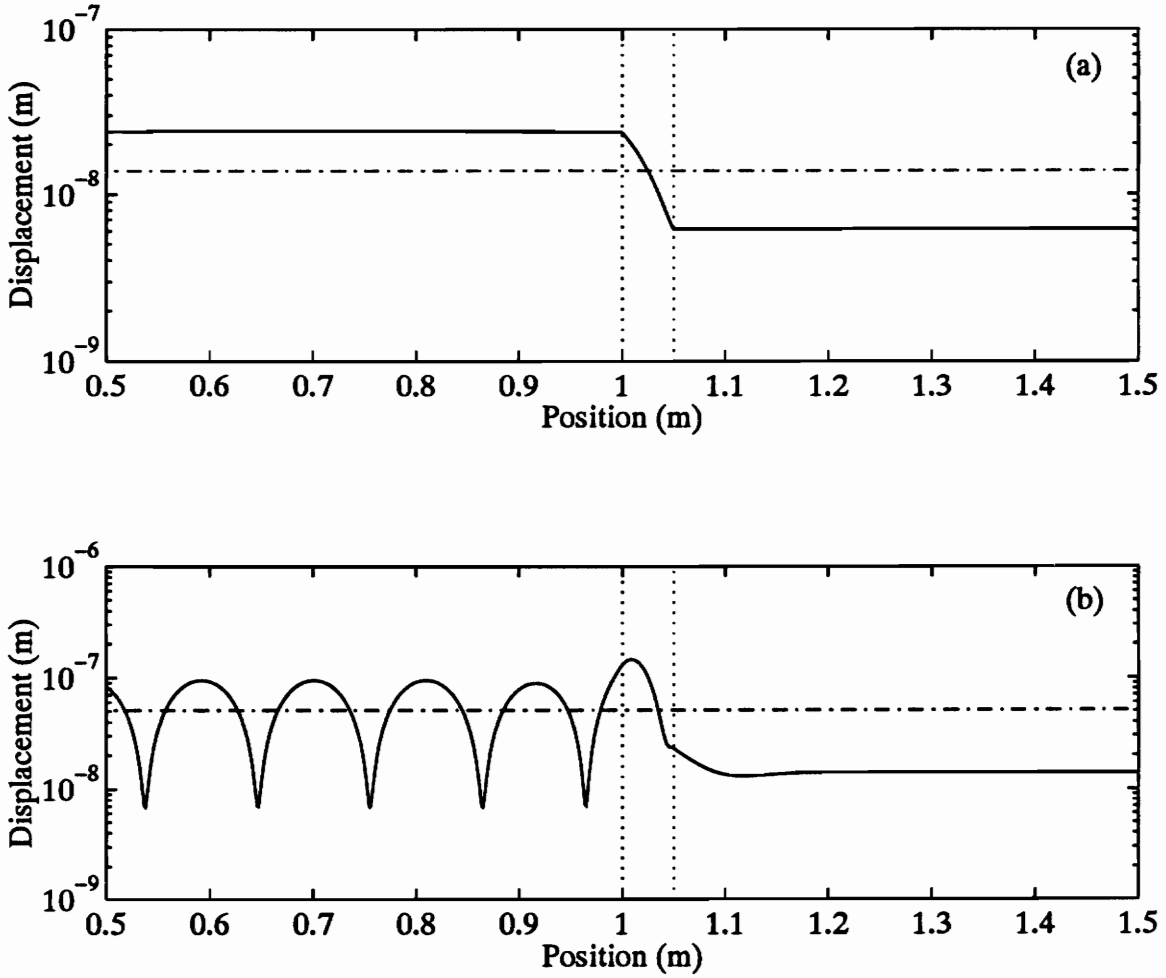

Figure 4.4 Magnitudes of (a) the extensional and (b) the flexural displacements for f=600 Hz (– · – before passive approach, —— after passive approach).

Table 4.4 Extensional and flexural power flows in each section before and after passive approach for f=600 Hz.

Power Flow (W)	Section 1 (upstream)	Section 2 (passive insert)	Section 3 (downstream)
P_e^d before passive approach	1.2×10^{-5}		
P_e after passive approach	5.2×10^{-6}	3.2×10^{-6}	2.3×10^{-6}
P_f^d before passive approach	8.3×10^{-6}		
P_f after passive approach	2.1×10^{-6}	1.85×10^{-6}	6.4×10^{-7}

passive insert the extensional and flexural displacements are increased (see Figure 4.4). A flexural standing wave is created upstream of the passive insert due to reflections at the interfaces, resulting in reactive attenuation (see Figure 4.4(b)). Also, Figure 4.4(a) shows that at 600 Hz little reactive attenuation occurs for the extensional motion, since no standing wave exists between the origin and the insert. At this frequency, most of the extensional reduction is due to damping within the passive material. Note that at the frequency of 1500 Hz, a first extensional standing wave appears between the origin and the insert. Thus, after insertion of the passive insert, reflections of waves are induced at the beam-rubber interfaces due to the impedance mismatches at the changes of material. These negative travelling waves, in the first beam section after control, result in higher displacement levels since displacements are the summation of the positive and negative wave terms. On the contrary, the extensional and flexural power flows upstream of the passive insert are decreased, when compared with the untreated power flows (see Table 4.4). Note that the extensional and flexural power flows consist of the positive wave term minus the negative wave term and minus the nearfield influence term for bending waves. The coefficients E_1, A_1 and C_1 are the same before and after insertion of the passive insert, or after addition of any control technique. Thus, the untreated extensional power flow should always be greater than the extensional power flow upstream of the control system location, which is expressed as:

$$|E_1|^2 > |E_1|^2 - |F_1|^2 \tag{4.2}$$

Here, the untreated flexural power flow is also greater than the flexural power flow upstream of the passive insert, which is expressed by the following inequality:

$$|A_1|^2 > |A_1|^2 - |B_1|^2 - 2\, e^{-k_f x_1}\, \mathrm{Im}(C_1 D_1^*) \tag{4.3}$$

This means that the nearfield interaction term has to be positive or negative and less than the negative propagating wave term ($|B_1|^2$).

4.3 Active Control Results

The results obtained for the purely active control system are presented in this section. The beam is a uniform infinite steel beam with two independent PZTs bonded on each side of the beam. The location of the actuators on the beam is given by (see Figures 3.2):

- $x_1 = 1$ m,
- $x_2 = 1.038$ m.

Figure 4.5 gives the magnitudes of the extensional and flexural displacements along the beam before and after active control, at the frequency of 600 Hz. Note that the two vertical dotted lines indicate the location of the actuators. For the three beam sections, the corresponding extensional and flexural power flows before and after active control are listed in Table 4.5. Table 4.5 shows that downstream of the actuators, complete cancellation of the extensional and flexural power flows is achieved, since infinitely small values on the order of 10^{-34}-10^{-36} correspond to the computational machine zero. This confirms that the farfield extensional and flexural power flows can be simultaneously reduced to zero using two co-located independently driven actuators. Under active control, the extensional and flexural power flows are found to be decreased in every section of the beam. Also, similarly to the passive approach, the magnitudes of the extensional and flexural displacements after active control are increased upstream of the PZTs due to the reflected waves at the interfaces (see Figure 4.5). This phenomenon will be observed in all the following systems. In Figure 4.5(a), the extensional displacement magnitude is found to be infinitely small downstream of the actuators. Thus, reducing to zero the farfield extensional power flow results in cancelling the extensional displacement downstream of the actuators. Thus, the farfield for extensional waves starts precisely after the last interface. This was expected since both the farfield extensional power flow and the extensional displacement in section 3 depend only on the

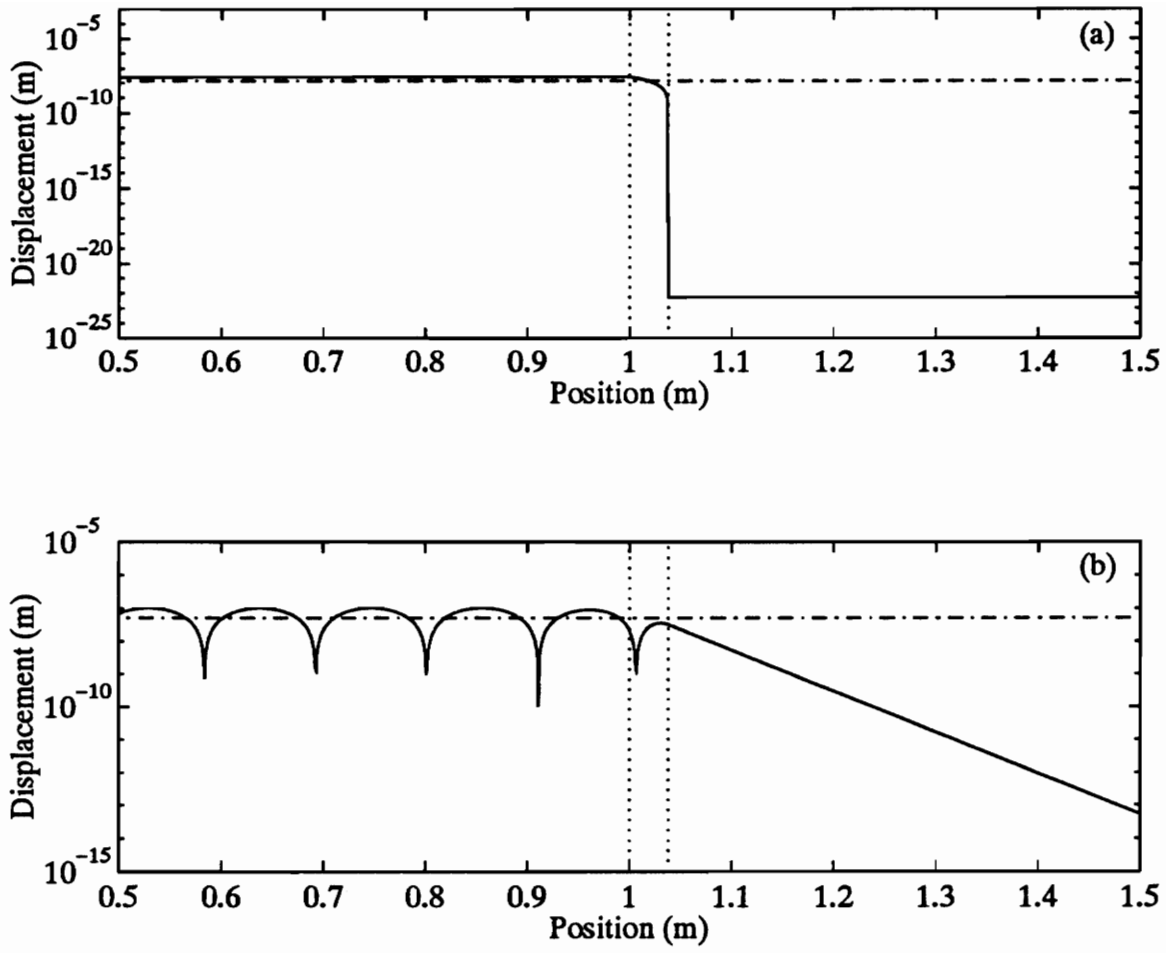

Figure 4.5 Magnitudes of (a) the extensional and (b) the flexural displacements for f=600 Hz (– · – before control, —— after active control).

Table 4.5 Extensional and flexural power flows in each section before control and after active control for f=600 Hz.

Power Flow (W)	Section 1 (upstream)	Section 2 (PZTs location)	Section 3 (downstream)
P_e^d before control	1.2×10^{-5}		
P_e after active control	1.7×10^{-9}	9×10^{-8}	1.7×10^{-34} ~ 0
P_f^d before control	8.3×10^{-6}		
P_f after active control	2.5×10^{-8}	8.4×10^{-10}	2.7×10^{-36} ~ 0

coefficient E_3 (see equations (3.23) and (3.24)). On the Contrary, setting to zero the farfield flexural power flow does not cancel the flexural displacement downstream of the actuators, since the positive decaying flexural wave is not part of the cost function (see Figure 4.5(b)). Indeed, the positive decaying wave is present in the expression of the flexural displacement in section 3 (see equation (3.25)) and not in the equation of the farfield flexural power flow (see equation (3.26)). Although it is not shown in Figure 4.5(b), the evanescent wave downstream of the actuators decays rapidly with x to completely disappear at x=2.2 m, resulting in zero flexural displacement. The farfield for flexural waves starts at the distance from the last interface where the flexural displacement equals zero, which is defined by a distance greater than five wavelengths. This behavior will be observed for the three active/passive control systems.

Finally, the study of the control effort V_{eff} defined in equation (3.21), and the control voltages v_e and v_f expressed in equations (3.32) and (3.33) is presented. The values for the control effort showed in Figure 4.6(a) are relatively high at low frequencies but reach practical values in terms of experimental implementation limits (i.e. actuator maximum allowed voltage) approximately above 100 Hz, for a disturbance force input of 1N. Thus, for the active system and the following active/passive systems, the values for the voltages below 100 Hz will be ignored. The magnitudes of the control voltages cancelling extensional and flexural power flows are shown in Figure 4.6(b), in order to understand the active control of both types of power flow separately. Note that the magnitude of the control voltages v_e and v_f similarly decrease as a function of frequency. However, the magnitude of the voltage v_e controlling the extensional power flow is about ten times higher than that of the voltage v_f cancelling the flexural power flow. Recall that before control approximately the same amount of extensional and flexural power flow is induced in the beam by the disturbance. This implies that for an infinite steel beam and the disturbance considered here, more energy is required to actively control the extensional power flow than the flexural power flow. This is again associated with the

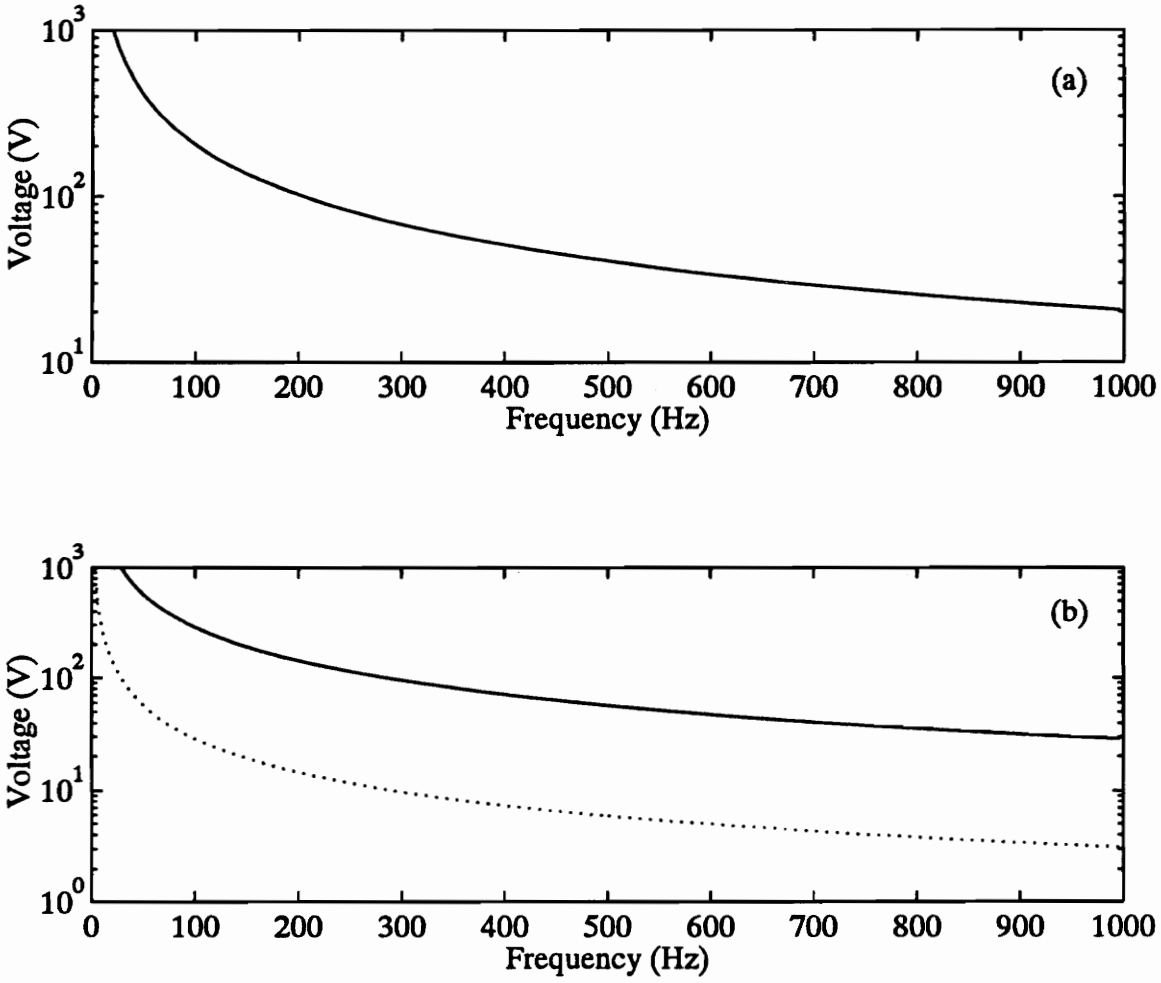

Figure 4.6 (a) Control effort V_{eff} and (b) magnitudes of the control voltages v_e (——) and v_f (·····) obtained for active control.

beam being much stiffer in extension than flexure. It appears that reducing the voltage v_e controlling the extensional power flow should result in the most significant reduction of the control effort, since control of the extensional motion is the most challenging.

4.4 Active/Passive Control Results

The results obtained for the active/passive control systems are outlined in this section. As mentioned earlier, three configurations are examined in order to determine if combining these two control techniques is always advantageous. The purpose is to find which configuration is the most effective in terms of lower control effort required.

4.4.1 Configuration 1

The first configuration is the most compact one with the actuators bonded to the hard rubber insert. For this configuration, the coordinates of Figure 3.3 are the following:

- $x_1 = 1$ m,
- $x_2 = 1.006$ m,
- $x_3 = 1.044$ m,
- $x_4 = 1.05$ m,

with the insert located between x_1 and x_4, and the actuators between x_2 and x_3. These coordinates will be represented by vertical dotted lines in the graphs of the displacements.

Figure 4.7 shows the magnitudes of the extensional and flexural displacements before and after active/passive control, for the frequency of 600 Hz. The corresponding extensional and flexural power flows in each section of the beam, before and after control are given in Table 4.6. It appears that total control of the extensional power flow is achieved downstream of the actuators (see Table 4.6). Thus, the small last section of rubber past the actuators (i.e. section 4) does not contribute to the cancellation of the

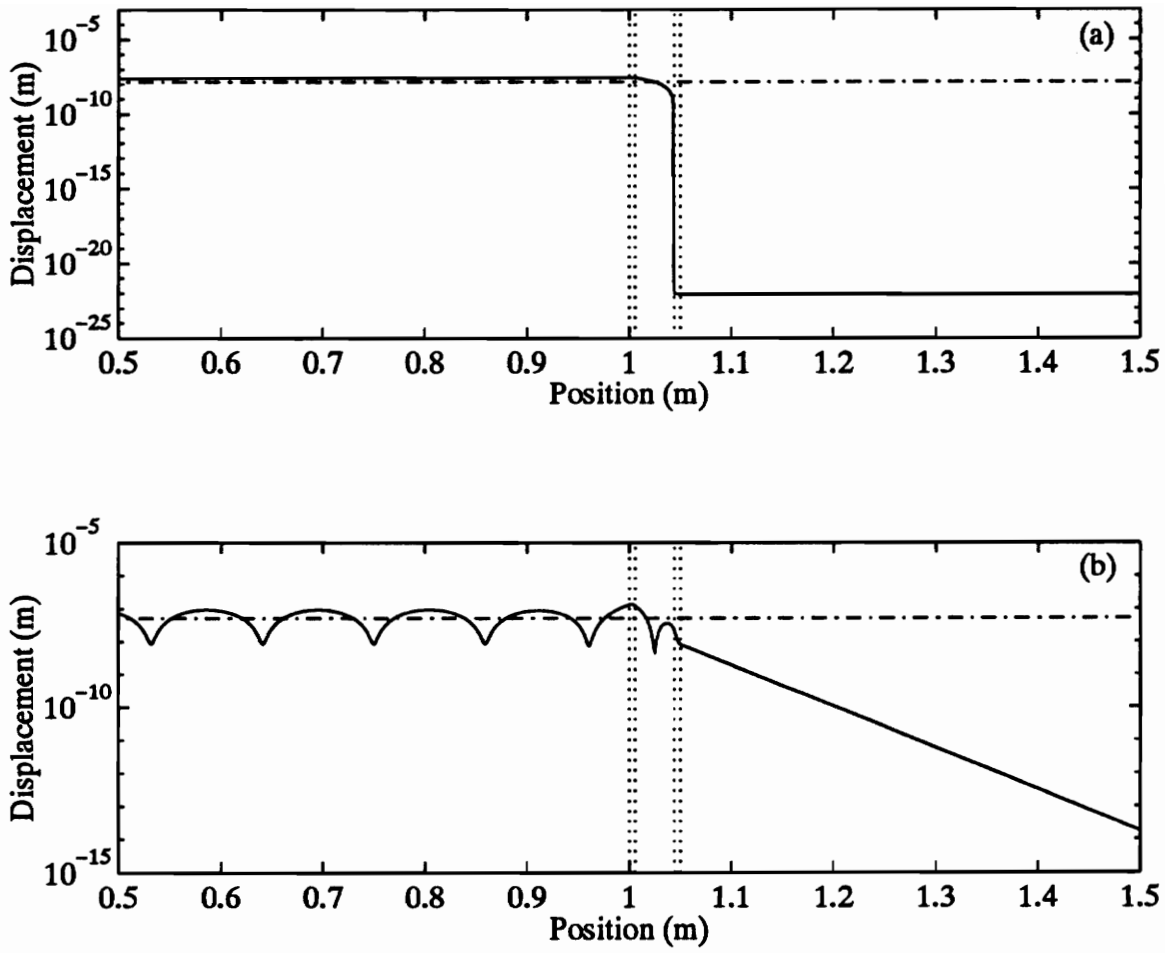

Figure 4.7 Magnitudes of (a) the extensional and (b) the flexural displacements for f=600 Hz (– · – before control, —— after active/passive control configuration 1).

Table 4.6 Extensional and flexural power flows in each section before control and after active/passive control configuration 1 for f=600 Hz.

Power Flow (W)	Section 1 (upstream)	Section 2 (passive insert)	Section 3 (PZTs on passive insert)	Section 4 (passive insert)	Section 5 (down-stream)
P_e^d before control	1.2×10^{-5}				
P_e after active/passive control	1.7×10^{-9}	1.8×10^{-8}	1.8×10^{-6}	0	0
P_f^d before control	8.3×10^{-6}				
P_f after active/passive control	2.5×10^{-6}	8.5×10^{-7}	3.9×10^{-7}	4.9×10^{-8}	0

extensional power flow. On the contrary, zero flexural power flow is only obtained in section 5 of the system (i.e. the farfield). This can be associated with the nearfield interactions present in sections 1 through 4 of the system. As seen in Figure 4.7, the displacement magnitudes are slightly increased for both extensional and flexural waves upstream of the passive insert. Again, for each section of the beam, the extensional and flexural power flows after active/passive control are lower than the ones before control (see Table 4.6).

The study of the control effort V_{eff} and the control voltages v_e and v_f for the configuration 1 of the active/passive system is now examined. In order to show the possible advantage of combining active and passive control techniques, the purpose is to compare the control effort and control voltages required for the active/passive system with those required for the purely active system.

Figure 4.8 presents the comparison of the control effort for active control and active/passive control configuration 1. A significant reduction in the required control effort V_{eff} is obtained, over the entire frequency range, when passive control is combined with active control. On average, the control effort is reduced by a factor of ten when passive control is combined with active control using this configuration. This demonstrates the effectiveness, in terms of lower control effort, of combining passive control techniques with active control techniques using this first configuration.

The comparison of the control voltages magnitudes for the active/passive control configuration 1 and the active control is investigated in Figure 4.9. This in order to show which control voltage is at the origin of a lower control effort. Note in Figure 4.9(b) that the magnitude of the voltage v_f, cancelling the flexural power flow, changes very little between the active/passive control configuration 1 and the active control. About the same amount of energy is then necessary to reduce to zero the farfield flexural power flow

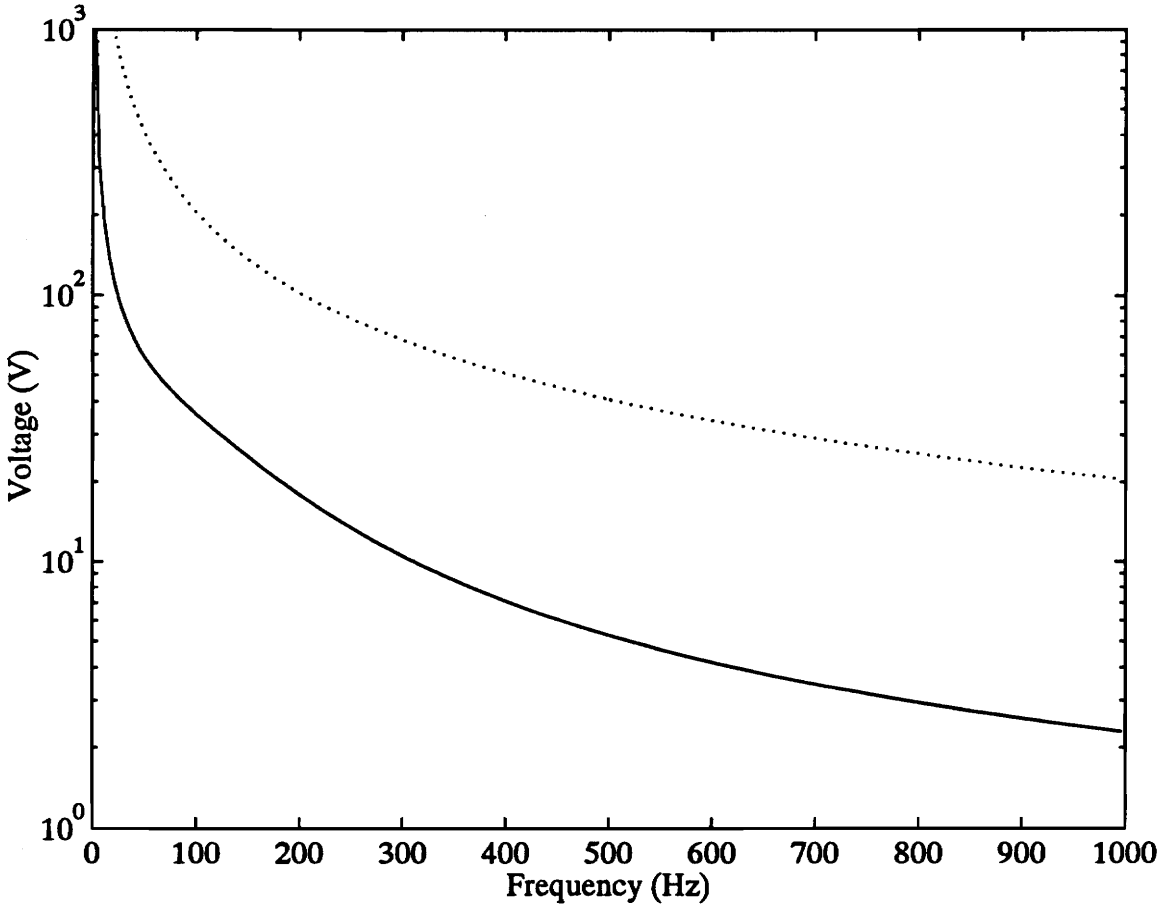

Figure 4.8 Comparison of the control effort V_{eff} for active control (·····) and active/passive control configuration 1 (——).

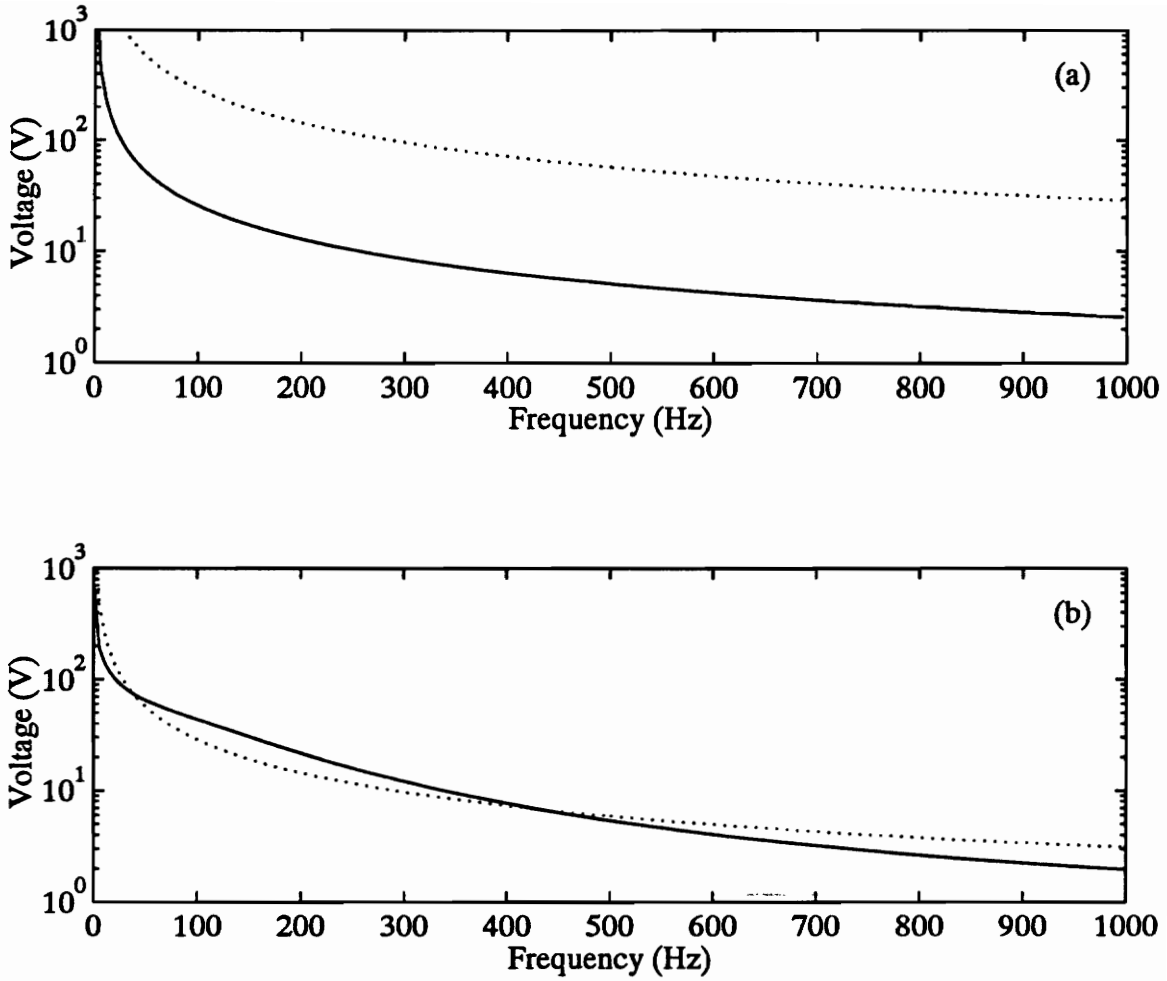

Figure 4.9 Comparison of the control voltages (a) v_e and (b) v_f for active control (·····) and active/passive control configuration 1 (——).

using the active control or the active/passive control configuration 1. Thus, having the actuators bonded to the passive insert does not result in a major change in the control voltage v_f. On the contrary, the magnitude of the control voltage v_e (see Figure 4.9(a)), cancelling the extensional power flow, is significantly reduced when the passive control is added to the active control using the configuration 1. Also, similarly to the control effort, the control voltage v_e is approximately reduced by a factor of ten with the active/passive configuration 1. Thus, less control voltage required by the PZTs to cancel the extensional power flow for the active/passive configuration 1, is at the origin of a lower control effort. This result will be given further consideration in Section 4.5.

4.4.2 Configuration 2

The active/passive system configuration 2 locates the passive insert upstream of the actuators (see Figure 3.4(a)) and the coordinates along the beam are the following:

- $x_1 = 1$ m,
- $x_2 = 1.05$ m,
- $x_3 = 1.06$ m,
- $x_4 = 1.098$ m,

with the insert located between x_1 and x_2, and the PZTs between x_3 and x_4. The insert is only 10 cm from the PZTs resulting in a relatively compact active/passive arrangement.

As previously, the extensional and flexural displacements magnitudes for the active control and the active/passive control configuration 2 at a frequency of 600 Hz are first compared in Figure 4.10. The associated extensional and flexural power flows before and after control are also given in Table 4.7 for each section of the system. Note in Table 4.7 that, as expected, simultaneous cancellation of the extensional and flexural power flows is achieved in the farfield of the beam (i.e. downstream of the PZTs). Table 4.7 shows attenuated values of the power flows downstream of the passive insert that are different from the values for the passive approach alone (see Table 4.4). This means that

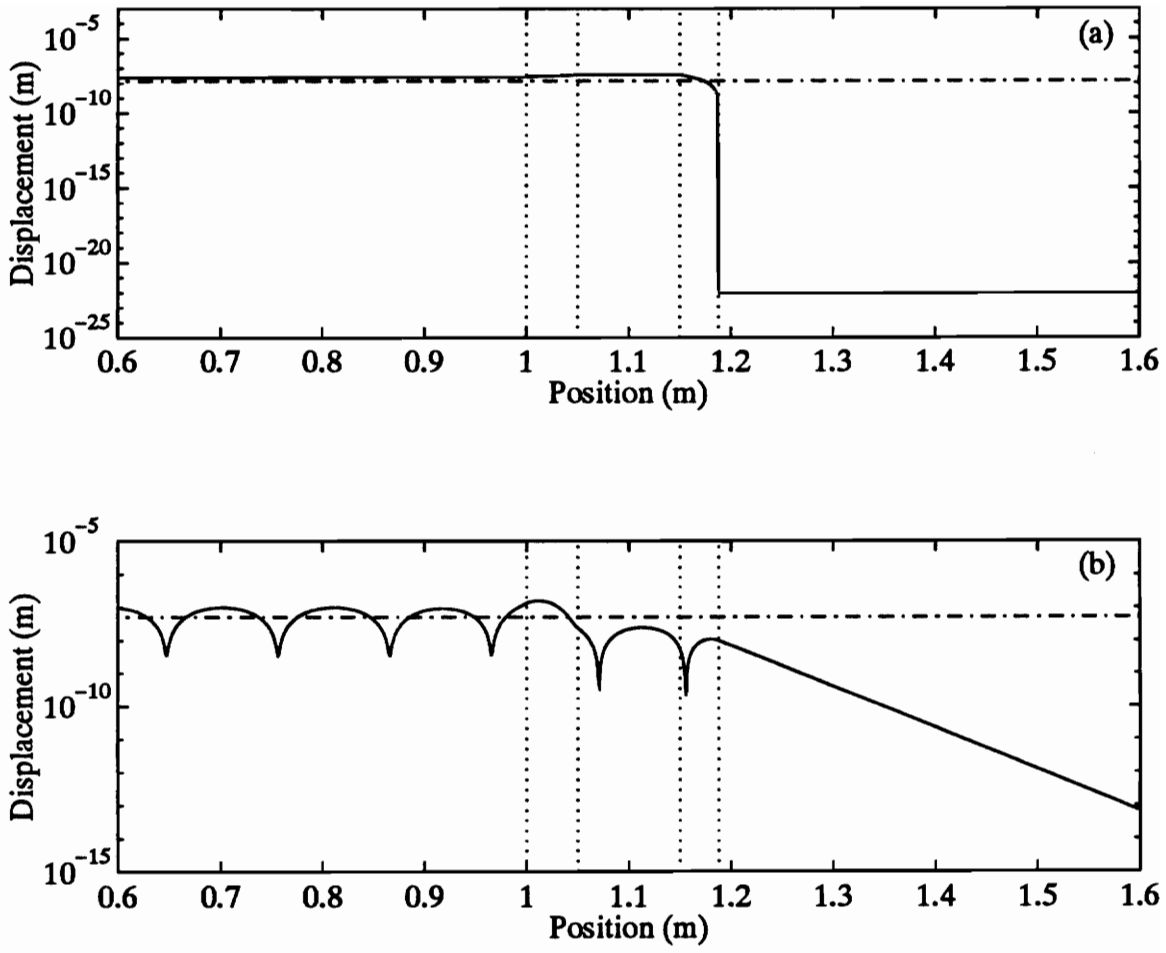

Figure 4.10 Magnitudes of (a) the extensional and (b) the flexural displacements for f=600 Hz (– · – before control, ——— after active/passive control configuration 2).

Table 4.7 Extensional and flexural power flows in each section before control and after active/passive control configuration 2 for f=600 Hz.

Power Flow (W)	Section 1 (upstream)	Section 2 (passive insert)	Section 3	Section 4 (PZTs location)	Section 5 (down-stream)
P_e^d before control	1.2×10^{-5}				
P_e after active/passive control	7.4×10^{-7}	1.5×10^{-6}	3.9×10^{-10}	1.6×10^{-7}	0
P_f^d before control	8.3×10^{-6}				
P_f after active/passive control	1.1×10^{-6}	6.7×10^{-7}	8.5×10^{-11}	2.7×10^{-10}	0

the active/passive control system with the passive insert upstream of the actuators cannot be considered as a superposition of the passive attenuation first and then the active control, since both controls are simultaneous. Zero farfield extensional power flow is associated with zero farfield extensional displacement past the last interface, as seen in Figure 4.10(a). Again, although it does not appear in Figure 4.10(b), zero farfield flexural power flow results in zero farfield flexural displacement, which starts 5λ away from the last interface. Also, as previously, the displacement magnitude for both flexural and extensional waves is slightly increased in section 1 (i.e. before the insert).

The comparison of the control efforts V_{eff} required for the active/passive control configuration 2 and the active control is now plotted in Figure 4.11. Note that the control effort necessary for the active/passive control configuration 2 is somewhat greater than the control effort obtained for the active control alone, especially at high frequencies. It appears that with this active/passive combination, more effort is required to simultaneously control extensional and flexural power flows than without the passive insert. Thus, in this case it is not useful to add the passive insert, since simultaneous control is perfectly achieved using only the PZTs and with less control effort required.

In attempt to explain the preceding result, the comparison of the control voltages v_e and v_f for the active control and the active/passive control configuration 2 is given in Figure 4.12. Note that the control voltage v_e required for the active/passive configuration 2 is greater than that for the purely active system, especially in the high frequency region (see Figure 4.12(a)). However, in Figure 4.12(b), the control voltage v_f required for the active/passive configuration 2 is lower than that for the purely active system at most of the frequencies. Thus, the increased control effort for the active/passive configuration 2 is associated with a higher control voltage v_e. An explanation for this can be the importance of the standing wave upstream of the PZTs, resulting in high input impedance of the section which is thus hard to drive with external sources (i.e. the actuators).

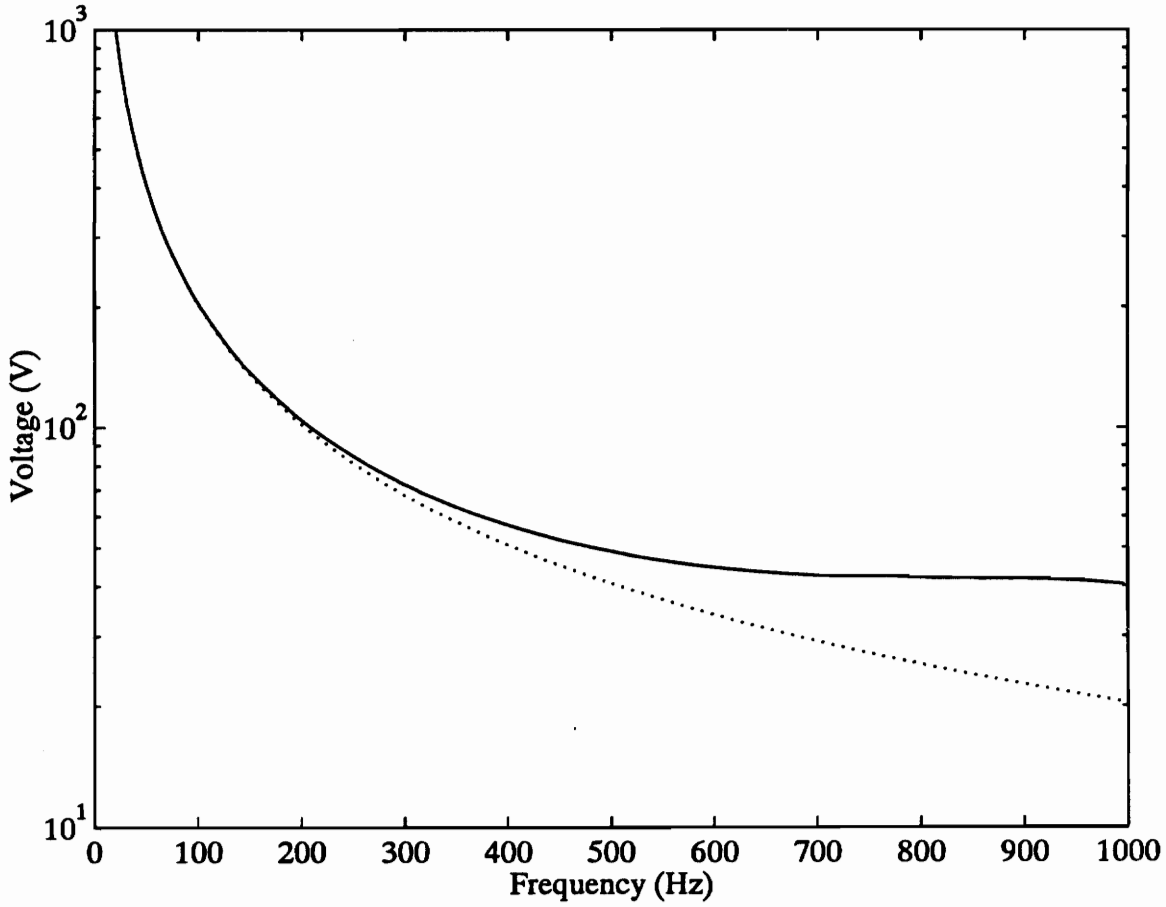

Figure 4.11 Comparison of the control effort V_{eff} for active control (·····) and active/passive control configuration 2 (——).

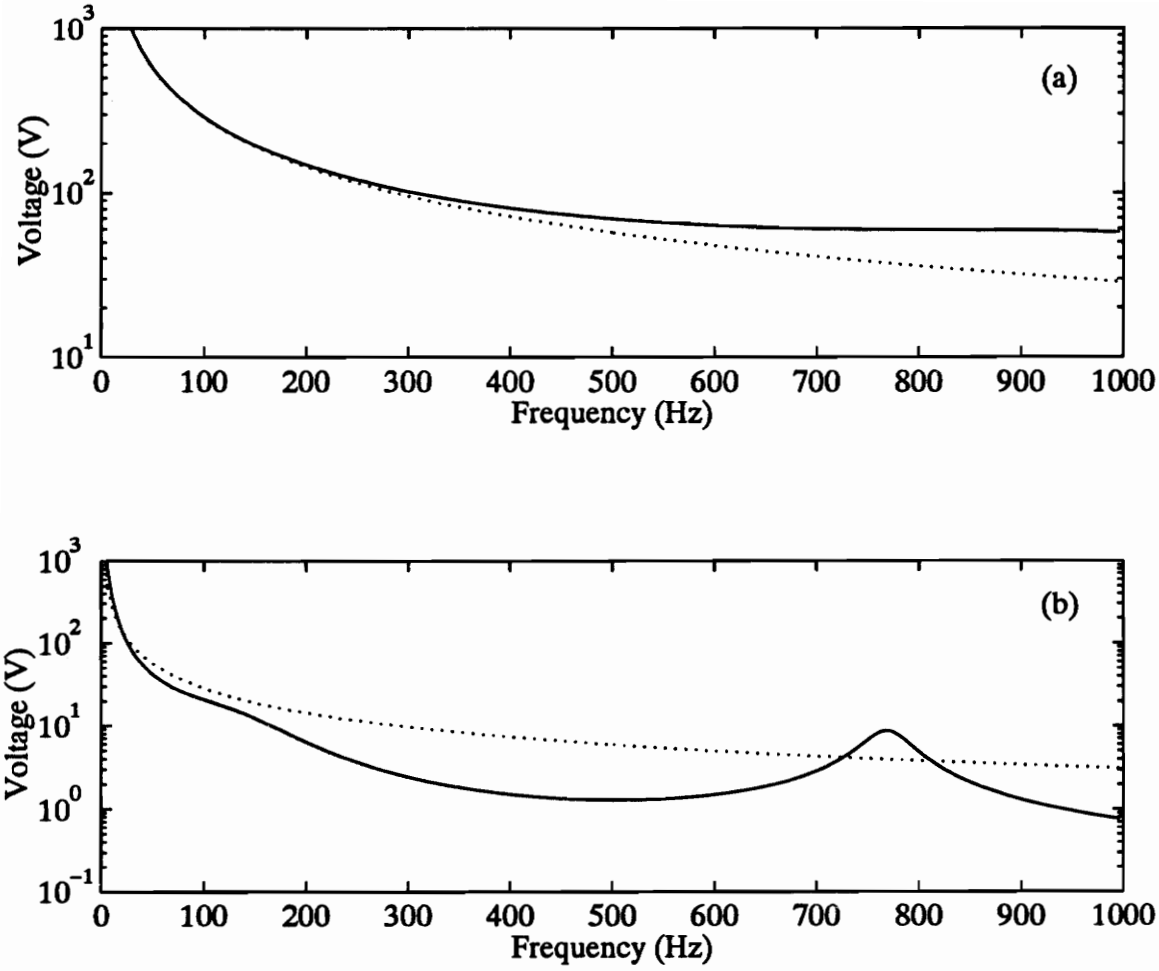

Figure 4.12 Comparison of the control voltages (a) v_e and (b) v_f for active control (·····) and active/passive control configuration 2 (——).

4.4.3 Configuration 3

The results obtained for the active/passive control system using the third configuration are examined here. The configuration 3 has the actuators upstream of the passive insert (see Figure 3.4(b)), and the coordinates along the beam are the following:

- x_1 = 1 m,
- x_2 = 1.038 m,
- x_3 = 1.048 m,
- x_4 = 1.098 m,

with again 10 cm between the piezoelectric actuators and the passive insert.

First, the magnitudes of the extensional and flexural displacements along the beam before and after control are plotted in Figure 4.13 for f=600 Hz. As in the preceding systems, the flexural and extensional displacement magnitudes are increased in section 1. The associated extensional and flexural power flows in each section of the beam before and after control are listed in Table 4.8. Note in Table 4.8 that while minimizing the total power flow in section 5 (i.e. after passive insert), the extensional power flow is already cancelled in sections 3 and 4. Comparing these results with those for the purely active system (see Table 4.5), the same values are obtained for the extensional power flows after control in sections 1 (before PZTs) and 2 (PZTs location). Thus, when extensional waves first travel through the active system and then through the passive insert, the extensional power flow reduction is seen as only due to the active system. An explanation is that once the extensional power flow has been considerably reduced downstream of the PZTs, the attenuation due to the insert is insignificant. This behavior is not observed for the flexural power flow due to the decaying waves in both directions, resulting in a more complex system. The flexural power flow is equal to zero only in the farfield of the beam, i.e. where the cost function is minimized. This configuration is not expected to result in lower control effort than the purely active system, since the extensional power flow reduction is not affected by the insert.

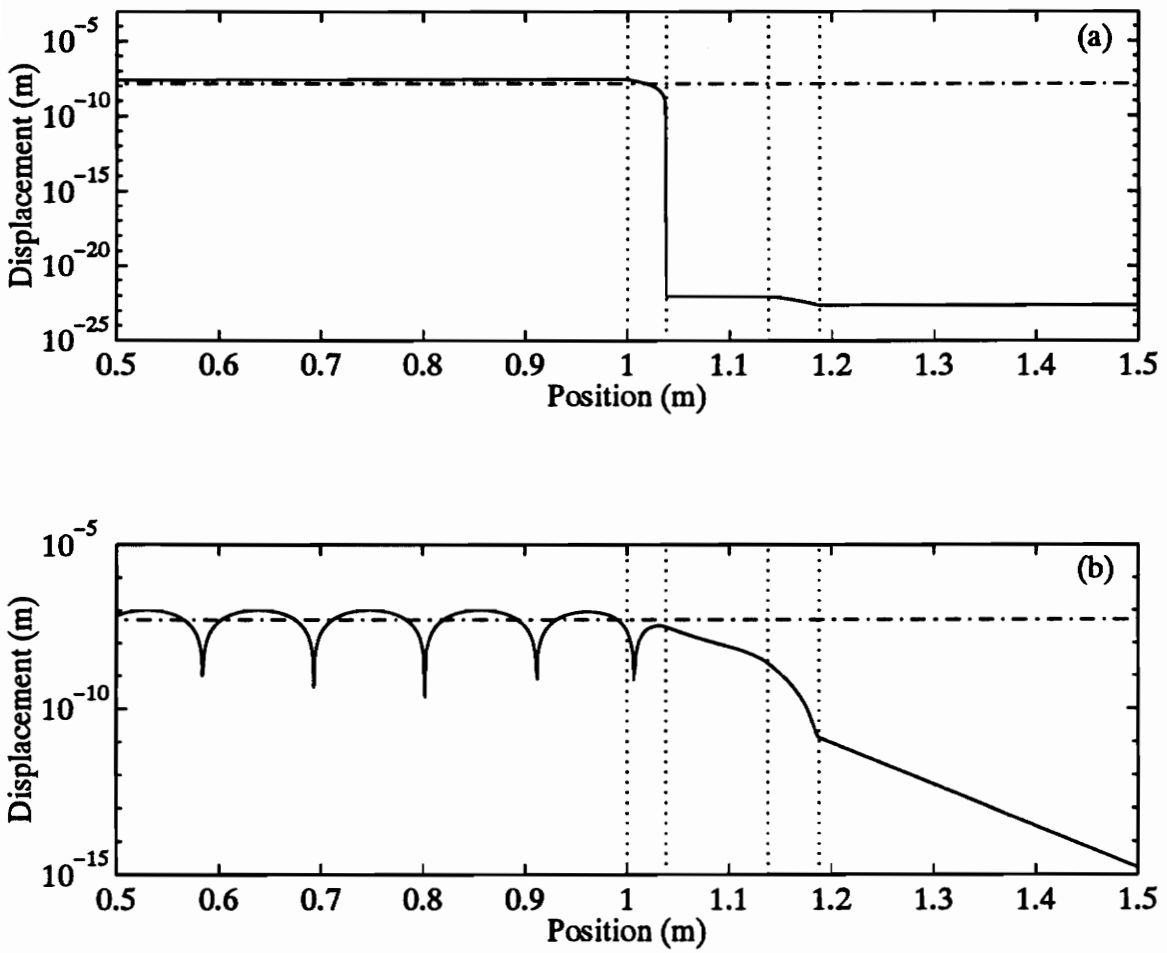

Figure 4.13 Magnitudes of (a) the extensional and (b) the flexural displacements for f=600 Hz (– · – before control, —— after active/passive control configuration 3).

Table 4.8 Extensional and flexural power flows in each section before control and after active/passive control configuration 3 for f=600 Hz.

Power Flow (W)	Section 1 (upstream)	Section 2 (PZTs location)	Section 3	Section 4 (passive insert)	Section 5 (down-stream)
P_e^d before control	1.2×10^{-5}				
P_e after active/passive control	1.7×10^{-9}	9×10^{-8}	0	0	0
P_f^d before control	8.3×10^{-6}				
P_f after active/passive control	2.1×10^{-8}	1.7×10^{-8}	1.1×10^{-10}	3.4×10^{-12}	0

To demonstrate this, the control efforts and control voltages obtained for the active/passive control configuration 3 and the active control are plotted in Figure 4.14 and 4.15 respectively. It is interesting to notice in Figure 4.14 that the control efforts are found to be exactly the same for the active/passive control configuration 3 and the active control alone. This results from the fact that the control voltage v_e is not changed when the passive insert is added downstream of the actuators (see Figure 4.15(a)). Also, note that the control voltage v_f, required to cancel the flexural power flow, is only slightly modified when the passive insert is placed downstream of the PZTs (see Figure 4.15(b)).

4.5 Actuator Power Transfer and Impedance Matching

In Section 4.4, it was shown that the lowest control voltage required to cancel the extensional power flow and consequently the lowest control effort, are obtained for the actuators located on the hard rubber insert. The purpose here is to first verify that for a given actuator input, more extensional power flow is induced by the PZTs in a rubber beam than in a steel beam. This is similar to requiring less control effort to cancel a given extensional power flow with the PZTs on rubber material instead of steel material. Then, in order to explain the physics of this phenomenon from an impedance point of view, the PZTs mechanical impedance is compared to that of the steel and rubber beams.

Consider the case of the pair of actuators excited by a given control effort equal to +141 V, while no primary disturbance is apply to the beam. One infinite beam is made of steel and the other is made of hard rubber (i.e. the passive material). In order to induce extensional power flow in the beam, the upper and lower PZTs are submitted to the same complex voltage (i.e. $v_1=v_2=100\ e^{i\phi}$). Flexural power flow is induced in the beam by driving the upper and lower PZTs with voltages of same magnitude but 180° out-of-phase (i.e. $v_1=100\ e^{i\phi}$ and $v_2=100\ e^{i(\phi+\pi)}$). Here, the only vibration sources are

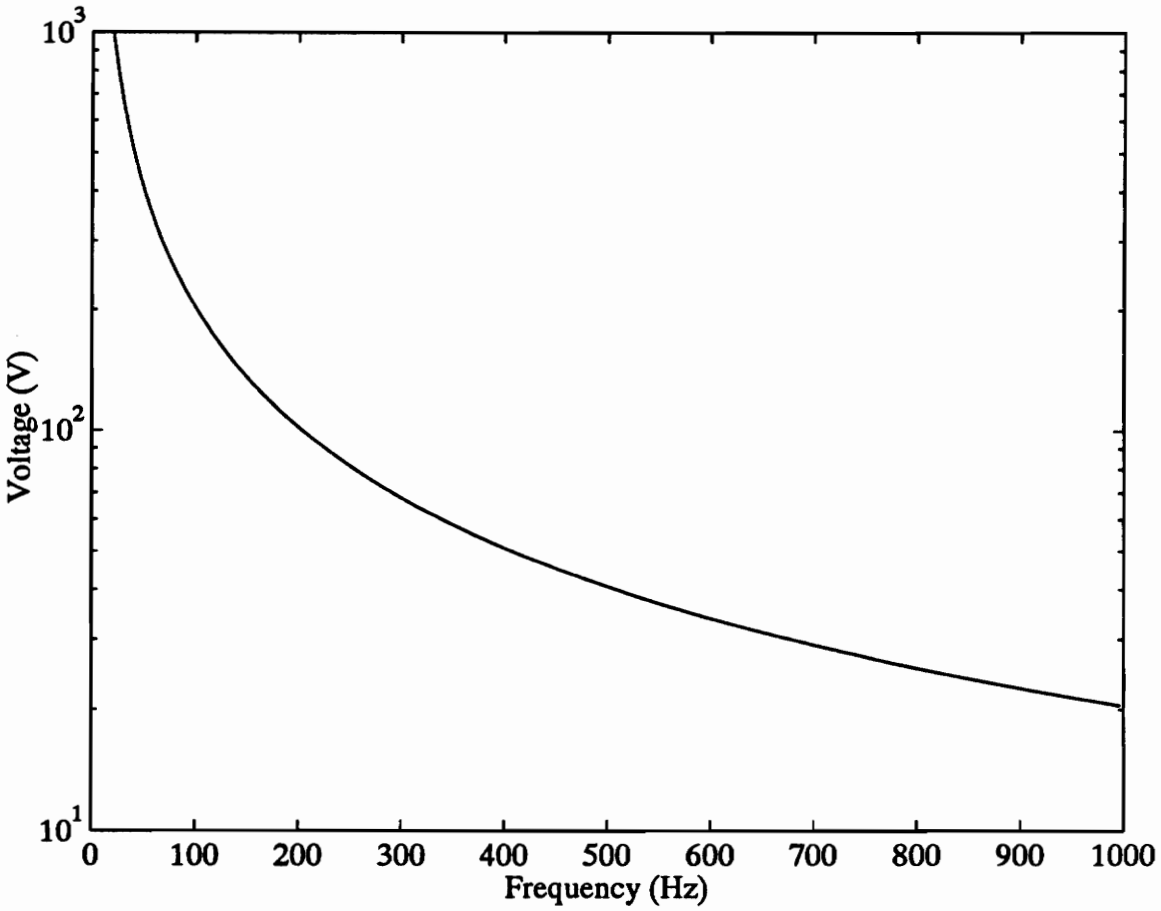

Figure 4.14 Comparison of the control effort V_{eff} for active control (·····) and active/passive control configuration 3 (——).

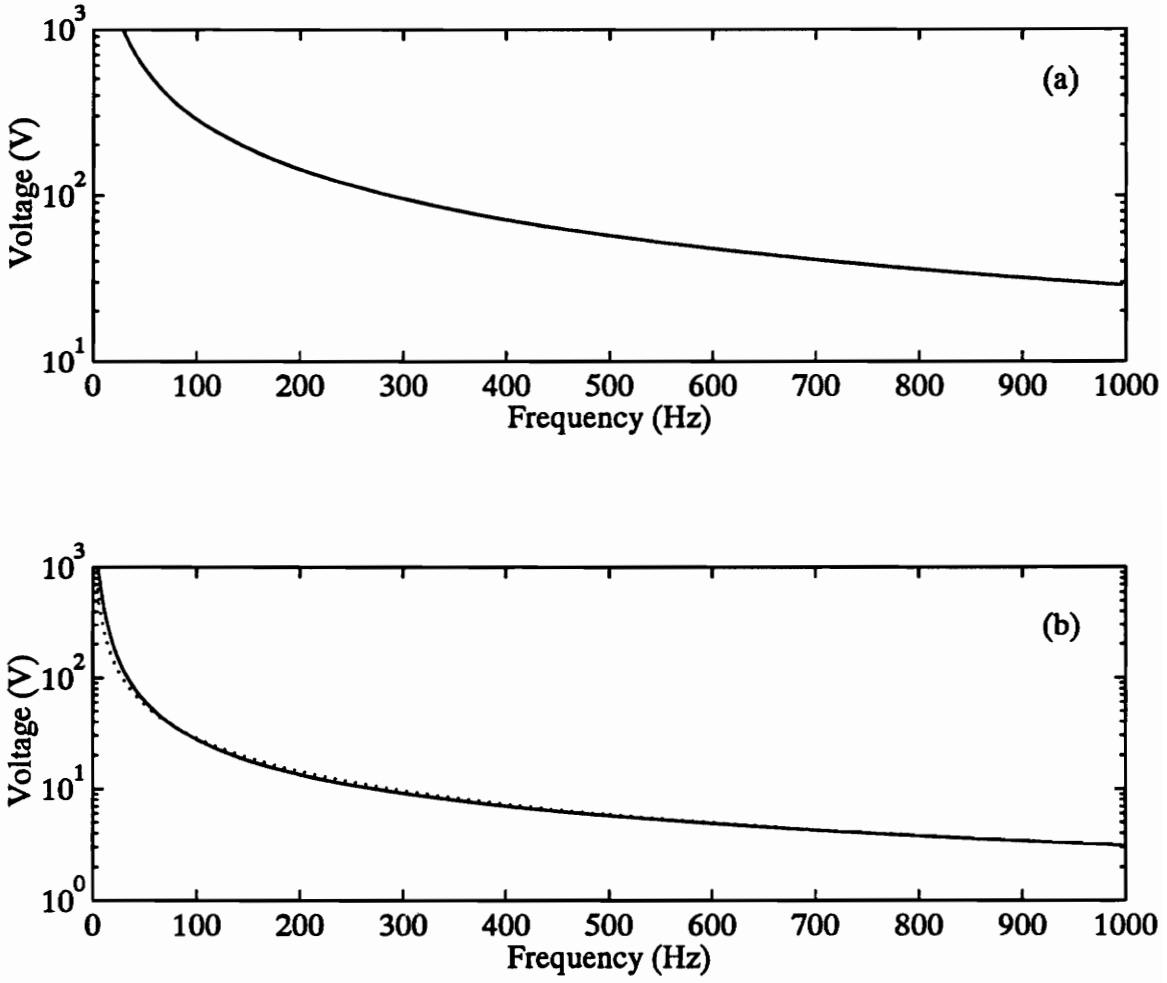

Figure 4.15 Comparison of the control voltages (a) v_e and (b) v_f for active control (·····) and active/passive control configuration 3 (——).

the actuators with the same power flow induced left and right of the actuators. The power flows induced by the PZTs, which excite separately the beam in extension and flexure, are plotted in Figure 4.16 for both the steel and rubber beam. Figure 4.16(a) shows that, over the entire frequency range, the extensional power flow induced by the PZTs in the rubber beam is greater than that induced in the steel beam. On the contrary, figure 4.16(b) indicates that the flexural power flow induced by the PZTs is almost the same for the rubber beam and the steel beam. Thus, two co-located actuators, driven by a given control effort, are found to induce about ten times more extensional power flow in a rubber beam than in a steel beam, and approximately equal amount of flexural power flow in both beams. As expected, higher actuator power transfer is achieved for extensional waves with the actuators on rubber material instead of steel material.

The ability of an actuator to transfer power to its host structure at any frequency depends on the mechanical impedances of the actuator and the structure. When the power transferred from a PZT to a structure is maximized, the amount of control effort required by the PZT is minimized. Note that an actuator provides the maximum input power when the structural mechanical impedance matches the actuator mechanical impedance. Impedance matching between a PZT and its host structure only occurs when the actuator and structural impedances are complex conjugate [63]. In this section, the magnitudes of the mechanical impedances of the actuators and of the two different beam materials are compared. The following expressions for the different mechanical impedances are all based on the impedance method developed by Liang et al. [63].

First, the mechanical impedance Z_a of a PZT actuator defined as the ratio of the actuation force to the velocity, is expressed as:

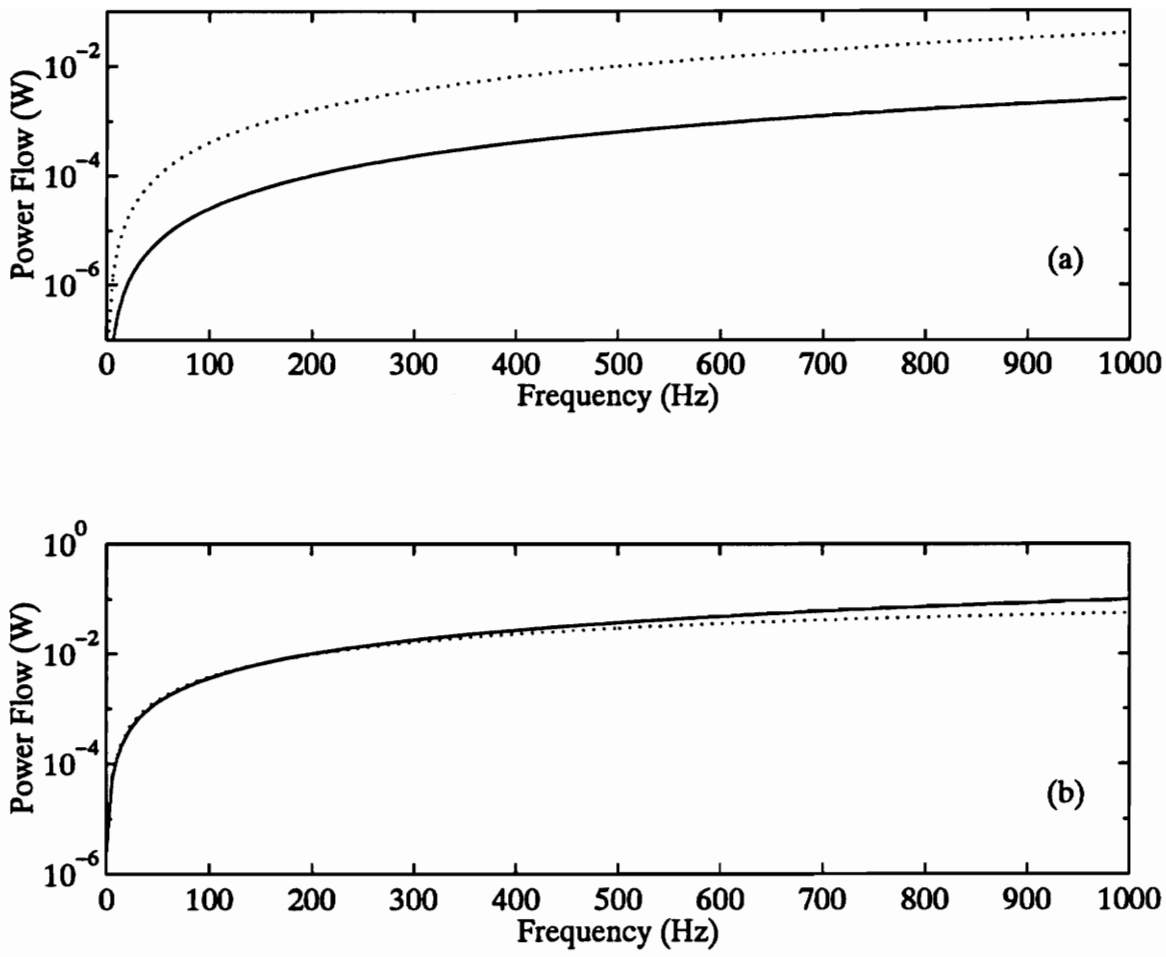

Figure 4.16 Comparison of (a) the extensional and (b) the flexural power flows induced by two PZTs on a steel beam (——) and a rubber beam (·····).

$$Z_a = \frac{-K_a(1+\eta_a i)}{\omega} \frac{k_a L_a}{\tan(k_a L_a)} i \tag{4.4}$$

where K_a is the static stiffness of the PZT given by $E_a w_a T_a/L_a$ and k_a is the extensional wavenumber of the PZT defined as follows:

$$k_a = \omega \sqrt{\frac{\rho_a}{E_a(1+\eta_a i)}} \tag{4.5}$$

Note that the mechanical impedance of the actuator used in this study has to be doubled since the thickness of the equivalent actuator is doubled using two actuators on top and bottom of the beam. Also, whether the two actuators are exciting the beam in extension or flexure, the PZT impedance is the same since the actuators are always either in compression or extension (i.e. submitted to axial motion).

The beam mechanical impedances (in N.s/m) Z_e and Z_f corresponding to actuator loading for extensional motion and flexural motion respectively are now examined. The actuators are located between x_1 and x_2 on the beam, resulting in two equal and opposite forces F_0 for in-plane excitation and two equal and opposite moments M_0 for normal excitation. These forces and moments are located at the actuator ends in x_1 and x_2. The beam mechanical impedance Z_e for in-plane excitation is expressed below as the ratio of the PZTs induced force to the difference of the in-plane velocities at the PZTs ends:

$$Z_e = \frac{F_0}{v_u(x_2) - v_u(x_1)} \tag{4.6}$$

The beam equivalent mechanical impedance Z_f for flexural excitation is proportional to the ratio of the PZTs induced moment to the difference of the angular velocities at the PZTs ends:

$$Z_f = \frac{2}{(2h+T_a)^2} \frac{M_0}{\Theta_w(x_2) - \Theta_w(x_1)} \tag{4.7}$$

Note that the ratio of the PZTs induced moment to the difference of the angular velocities at the PZTs ends corresponds to the rotational structural impedance. By multiplying the rotational impedance by $2/(2h+T_a)^2$ the rotational impedance is modified into an equivalent linear impedance. Then, this equivalent mechanical impedance can be compared to the PZTs mechanical impedance [63].

The actuators mechanical impedance and the structural impedances for the steel and rubber beams are now calculated, considering again the actuators driven by the control effort of +141 V and no disturbance applied to the beam. The three mechanical impedances (i.e. PZTs, steel beam, rubber beam) are compared in Figure 4.17, over the entire frequency range, for the beam in extension and the beam in flexure. Note that for the beam in extension, the actuators impedance is much closer to the rubber beam impedance than the steel beam impedance (see Figure 4.17(a)). On the contrary, for the beam in bending, the actuators impedance is found to be slightly closer to the steel beam impedance than the rubber beam impedance (see Figure 4.17(b)). This demonstrates that for extensional motion, better impedance matching exists between the actuators and the rubber material than between the actuators and the steel material. For bending motion, slightly better impedance matching exists between the PZTs and the steel material than between the PZTs and the rubber material. It has been proved that the active/passive configuration with the PZTs on the hard rubber insert resulted in the lowest control effort required by the actuators, due to the best impedance matching in extension. Note that these results are only for the specific physical system studied here, and they may vary for different beam or actuator thicknesses for instance.

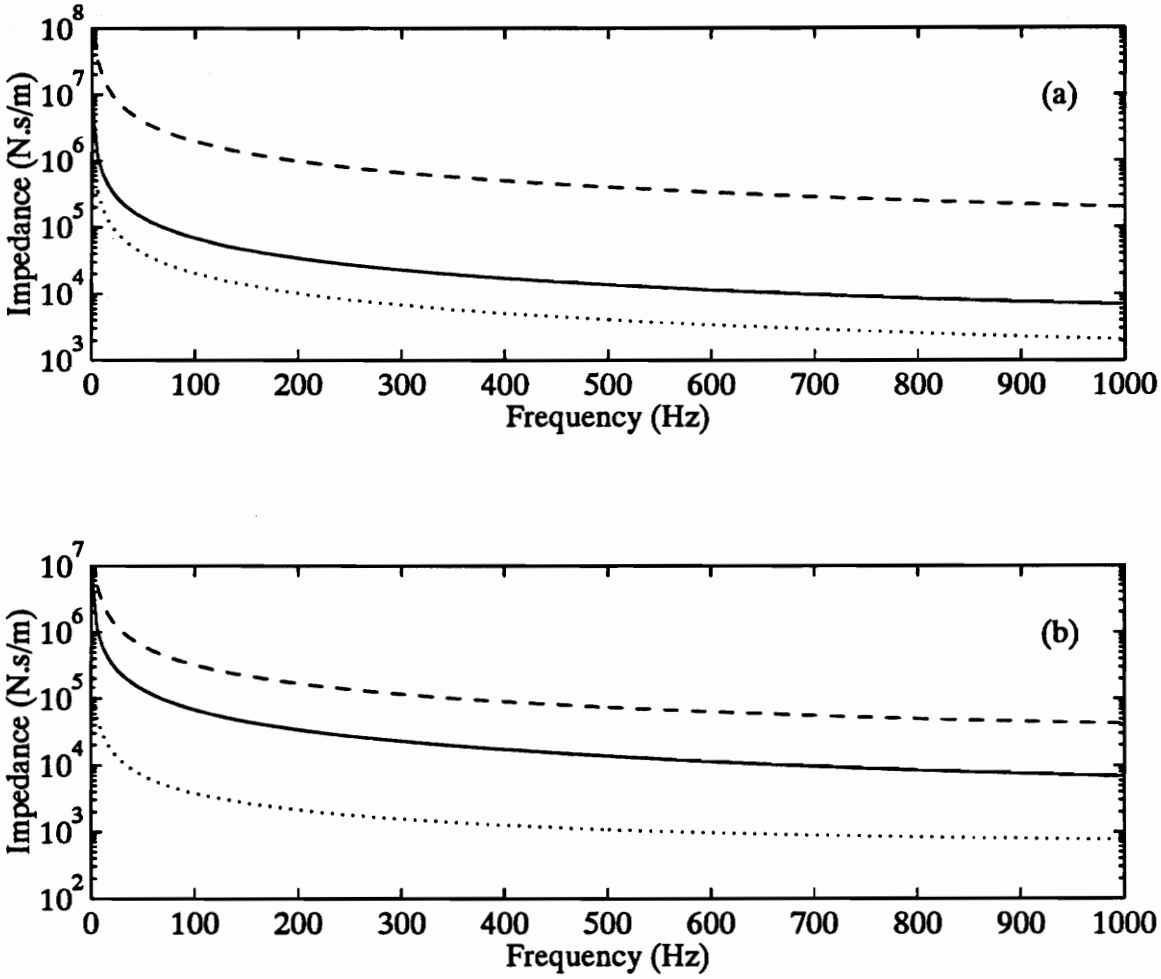

Figure 4.17 Comparison of the PZTs impedance (——), the steel beam impedance (- - -) and the rubber beam impedance (·····) for the beam in (a) extension and (b) flexure.

4.6 Summary

Control techniques involving purely passive control, purely active control and hybrid active/passive control of total farfield power flow in infinite thin beams were analytically studied. For the disturbance used in this study (i.e. point force excitation at an angle), approximately equal amount of extensional and flexural power flows were induced in the infinite beam before control treatment. This allowed to know which power flow (extensional or flexural) was reduced most using the different control methods.

For the passive approach, consisting of a 5 cm long hard rubber insert in an infinite uniform beam, a maximum of 10 dB reduction for the farfield extensional power flow and 12 dB reduction for the farfield flexural power flow were achieved. It was verified that the effectiveness of the passive approach increases with frequency and insert length. Throughout the studied frequency range (1-1000 Hz), the flexural power flow reduction was found to be higher than the extensional power flow reduction. This is due to the fact that the beam is considerably stiffer in extension than in flexure, and thus control of extensional motion is more difficult. Thus, the passive approach was shown to be effective to some extent and limited in the amount of attenuation achieved at low frequencies. A longer passive insert could be used to increase the amount of attenuation obtained, but this may not be practical in real applications.

Active control using piezoelectric actuators resulted in complete cancellation of the total power flow in the farfield of the beam. Thus, the analytical results for the active control indicated that two co-located independent piezoelectric patches are effective control actuators for simultaneously reducing the farfield extensional and flexural power flows to zero. Also, about ten times more control voltage was required to cancel the extensional power flow than the flexural power flow, although the untreated extensional and flexural power flows were approximately of same magnitude. This is an important

result which shows that the active control is less effective on extensional vibrations than flexural vibrations, due to the large stiffness of the beam in extension.

Finally, the combination of the active and passive control systems was investigated and three locations of the actuators with respect to the passive insert were studied. The results demonstrated that the most effective active/passive control system, in terms of lower control effort, is when the actuators are directly located on the passive hard rubber insert as opposed to the actuators being mounted on the beam (i.e. upstream or downstream of the insert). Also, the two other active/passive systems (i.e. with actuators upstream or downstream of insert) were shown to add no benefit to the purely active system. The lower control effort obtained with the actuators on the passive insert was found to be associated with a lower control voltage required to cancel the farfield extensional power flow. Thus, when the actuators are bonded directly to the rubber material instead of being bonded to the steel material, less control voltage is required to control a given extensional power flow, and reciprocally more extensionl power flow is induced by the actuators driven by a given voltage. This result was demonstrated to be associated with a better impedance match for extensional motion between the actuators and the rubber material than between the actuators and the steel material.

Chapter 5
Simulation of Vibration Flanking Paths

5.1 Introduction

The purpose of this section is to study the influence of flanking paths on the attenuation performance and the control effort required by the active/passive control system configuration 1 (i.e. with the actuators on the passive insert). Flanking or acoustic leaks can be defined as noise or vibration transmission through paths different from the direct expected path [1]. These flanking paths parallel to the direct path corresponding to vibration propagation within the beam could, for instance, approximate secondary acoustic paths through a heavy fluid surrounding the beam. When subsonic vibrational waves propagating within a fluid-loaded beam reach an interface, an exchange of vibrational energy occurs via a coupling between the fluid and the vibrating structure due to structural nearfield waves. A fluid-loaded beam is also characterized by a coupling of the different types of waves, but in the following systems coupling of extensional and flexural waves is still neglected. Thus, in the following models, only the energy exchange between the structure and the flanking paths, and not that between the different vibrational waves, is taken into account. In this study, the flanking paths connect the two points of the beam corresponding to the beginning and the end of the control section. Thus, the vibrational energy that propagates through the flanking paths does not propagate through the control section (such as the insert or/and the beam section below the PZTs). In terms of the purely active control system, this is expected to result in higher control effort required by the actuators to cancel the total farfield power flow.

In order to understand the behavior of the active/passive system configuration 1 associated with flanking paths, the purely active system with flanking paths and the purely passive system with flanking paths are first investigated. To study these systems, the flanking paths are approximated and simulated using an axial and a torsional spring, both connected between the first and last interface of the system. The axial spring represents a flanking path for extensional waves, while the torsional spring simulates a flanking path for bending waves, as shown in Figure 5.1. The axial and torsional springs have complex spring constants $\hat{K}_l$ in N/m and $\hat{K}_t$ in N·m respectively, defined by:

$$\hat{K}_l = K_l (1 + \eta_K i) \tag{5.1}$$

$$\hat{K}_t = K_t (1 + \eta_K i) \tag{5.2}$$

where the terms K_l and K_t (i.e. the real values) of the axial and torsional spring constants represent the spring stiffness and η_K is the damping ratio. This is similar to having an axial and a torsional spring-damper system and would approximate loss of energy due to radiation damping. Note that the method or theory involved in solving the different systems will not be repeated here and the reader can refer to Chapter 3 if necessary.

Since both the axial and torsional springs will be in parallel with a finite section of the beam, it is interesting to calculate the equivalent spring constant of this section. This would give an idea of the values necessary for the axial and torsional spring constants to affect the results presented previously. For a length l of beam section in extension, the equivalent spring constant $K_{eq}^{\ e}$ (in N/m) of the section is defined by [64]:

$$K_{eq}^{\ e} = \frac{ES}{l} \tag{5.3}$$

For the same beam section in bending, the equivalent spring constant $K_{eq}^{\ f}$ (in N·m) is expressed as follows [64]:

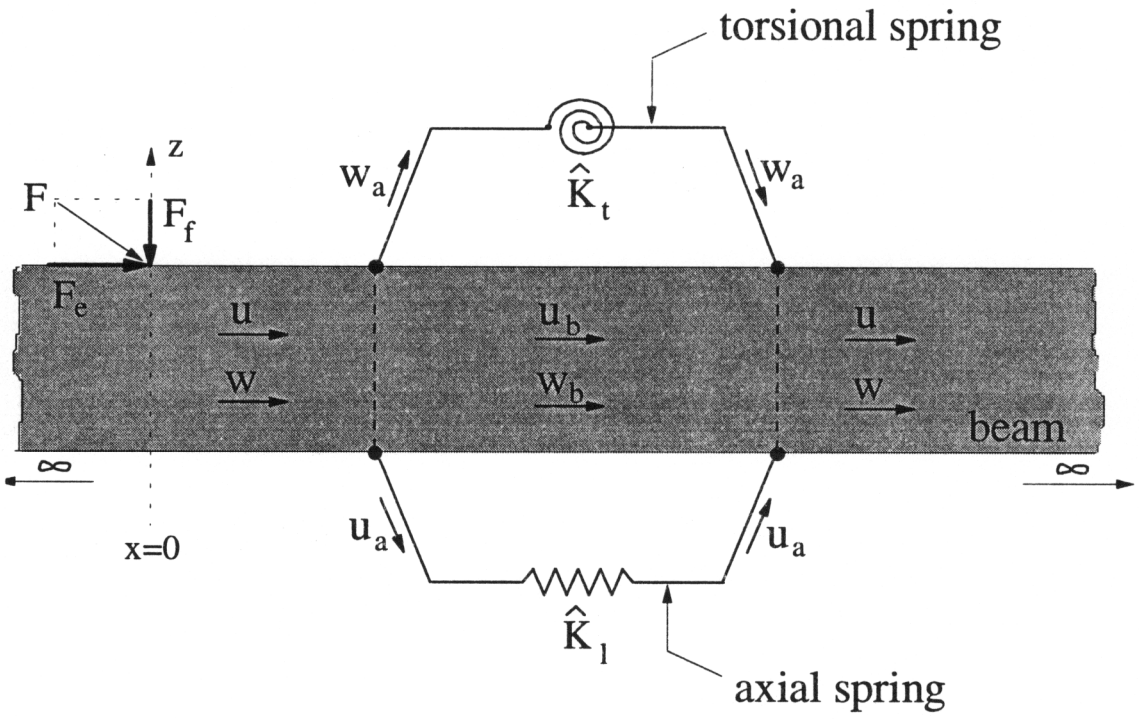

Figure 5.1 Simulation of vibration flanking paths using axial and torsional springs.

$$K_{eq}^{f} = \frac{EI}{l} \tag{5.4}$$

For the active system with flanking (see Figure 5.2(a)), the springs are in parallel with the beam section to which the PZTs are bonded (i.e. length L_a=0.038 m). For the passive system with flanking (see Figure 5.2(b)) and the active/passive system configuration 1 with flanking (see Figure 5.3), the springs are in parallel with the passive insert (i.e. length L=0.05 m). The equivalent spring constants are presented in Table 5.1 for the different flanking systems mentioned. The results confirm that, for any system, the equivalent stiffness in extension is significantly high. Thus, the linear spring constant associated with flanking would have to be very large to affect the extensional direct energy path. The equivalent stiffness in bending is much smaller than that in extension. Therefore, it is expected that a lower value of flanking stiffness associated with flexure will change the way energy travels along the beam. This can be seen from an impedance point of view, with the impedance of the beam section being in parallel with the impedance of the spring. This is similar to the influence of a fluid loading on a beam, which acts like a radiation impedance load.

Table 5.1 Equivalent spring constants of the different sections of beam in parallel with the axial and torsional springs.

Beam section below actuators (active system)		Passive insert section (passive and active/passive systems)	
Extension (N/m)	Flexure (N·m)	Extension (N/m)	Flexure (N·m)
1.2×10^{10}	932	$(9 + 3.6\,i) \times 10^{6}$	$6.8 + 2.7\,i$

(a) Active Control System with Flanking

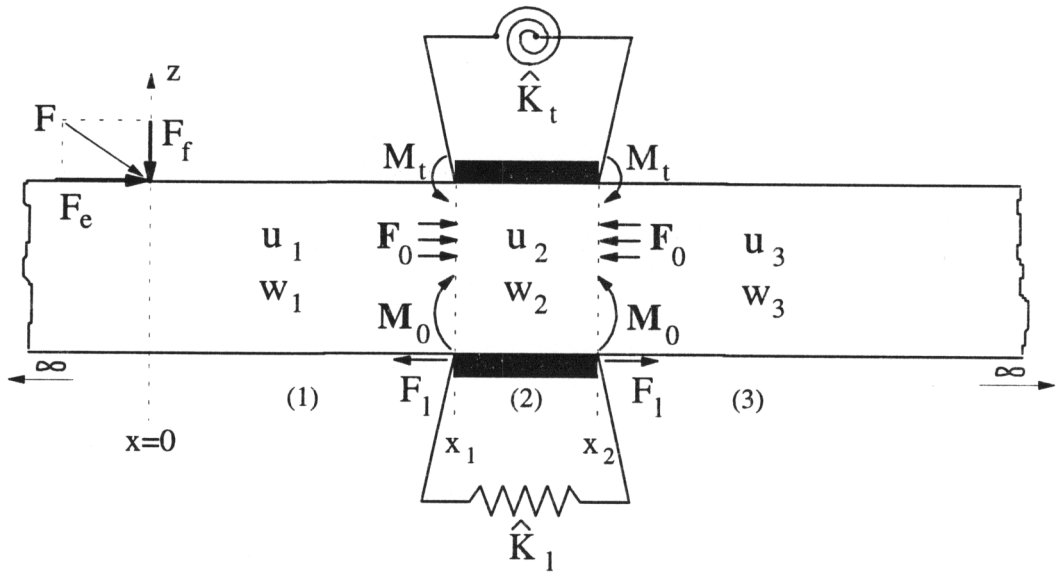

(b) Passive Control System with Flanking

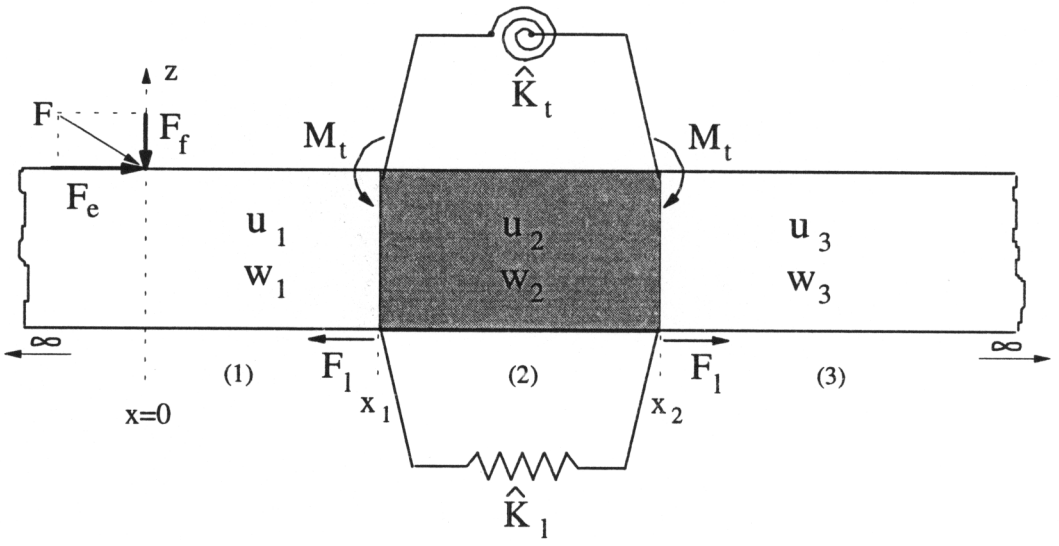

Figure 5.2 Schematic of the active and passive systems associated with flanking paths.

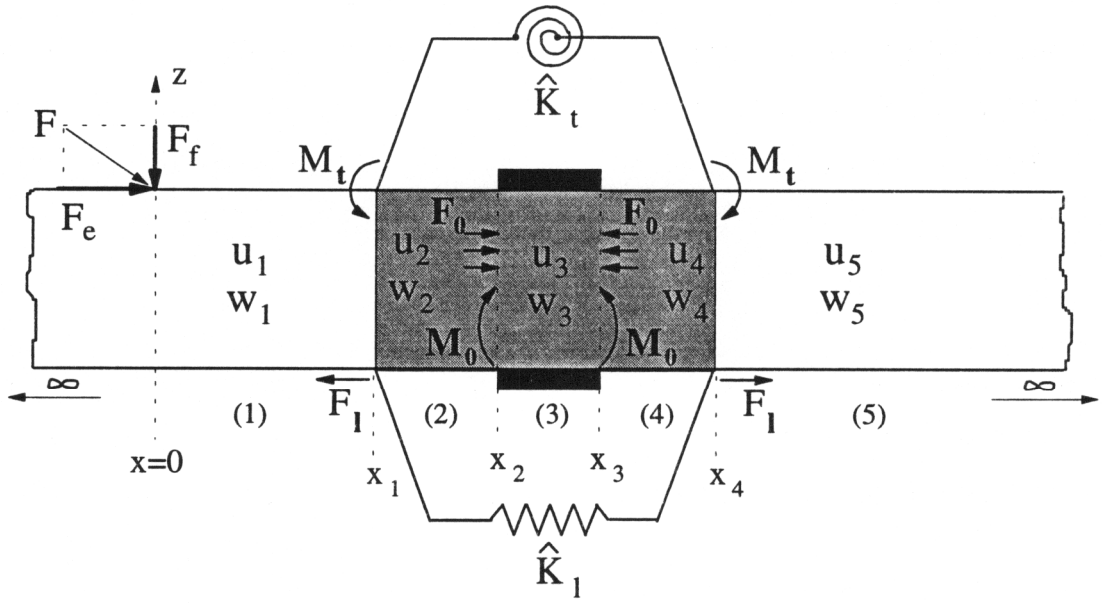

Figure 5.3 Schematic of the active/passive control system configuration 1 associated with flanking paths.

5.2 Association of Flanking Paths with the Active and Passive Systems

The study of the purely active and purely passive systems associated with flanking paths for both extensional and flexural vibrations is developed in this section.

5.2.1 Description of the Active and Passive Systems with Flanking

The active and passive systems with flanking are depicted in Figures 5.2(a) and 5.2(b) respectively. The only difference between these systems and those detailed in Sections 3.1 and 3.2 is the presence of new forces and moments induced by the springs. The axial spring induces two equal and opposite linear forces of amplitude F_l, located at the spring attachment points (i.e. in x_1 and x_2). This force F_l, for both active and passive systems, is expressed below in terms of the extensional displacements in x_1 and x_2 [48]:

$$F_l = \hat{K}_l \, [u_2(x_2) - u_1(x_1)] \tag{5.5}$$

The torsional spring induces two equal and opposite moments M_t, also located at the spring attachment points. For both control systems, the expression for the moment M_t is given below as a function of the slopes (i.e. first derivative of displacement with respect to x) in x_1 and x_2 [48,50]:

$$M_t = \hat{K}_t \, [\frac{\partial w_2(x_2)}{\partial x} - \frac{\partial w_1(x_1)}{\partial x}] \tag{5.6}$$

After applying the extensional and flexural boundary conditions at each interface for both systems, the matrices describing the extensional and flexural motions are determined. Then, the control effort and control voltages required by the active system with flanking and the extensional and flexural power flow reductions obtained for the passive approach with flanking are calculated.

5.2.2 Influence of Flanking Paths on the Active Control Results

After solving the active control system with flanking in extension and flexure simultaneously, the influence of flanking on the control effort and control voltages required by the actuators is examined. To determine the influence of flanking, the results for the active system with flanking are compared to that for the active system without flanking given in Chapter 4. In all of the systems, only the values for the real spring constants K_l and K_t will be given, and the damping ratio η_K will always equal 0.1 (i.e. 10 % damping). In addition, the influence of flanking on the different systems was examined for several values of K_l and K_t, but only the results for two values of K_l and K_t indicative of the influence will be presented. The results for the active system with flanking are given here for K_l equals 10^8 and 10^{10} N/m and K_t equals 10^3 and 10^4 N.m.

Figure 5.4 shows the comparison of the control effort V_{eff} required by the PZTs for the active system without and with flanking. For K_l equals 10^8 N/m and K_t equals 10^3 N.m, the control effort are found to be the same without and with flanking (see Figure 5.4(a)). This is also the case for smaller values of K_l and K_t. Thus, for K_l smaller than $K_{eq}^{\ e}$ of the steel section below the actuators and K_t greater than $K_{eq}^{\ f}$ of this same section, the effect of flanking on the control effort is negligible. On the contrary, for K_l equals 10^{10} N/m and K_t equals 10^4 N.m, the control effort for the active system with flanking is found to be greater than that for the active system without flanking, over the entire frequency range (see Figure 5.4(b)). Thus, as expected, in the presence of springs simulating flanking paths and appropriate spring constants, more control effort is required to reduce the farfield extensional and flexural power flows to zero.

To verify that both motions (extensional and flexural) are responsible for a higher control effort, the control voltages v_e and v_f cancelling the extensional and flexural power flows respectively are now examined for the system without and with flanking. Figures 5.5(a) and 5.5(b) present the control voltage v_e without and with the axial spring, for

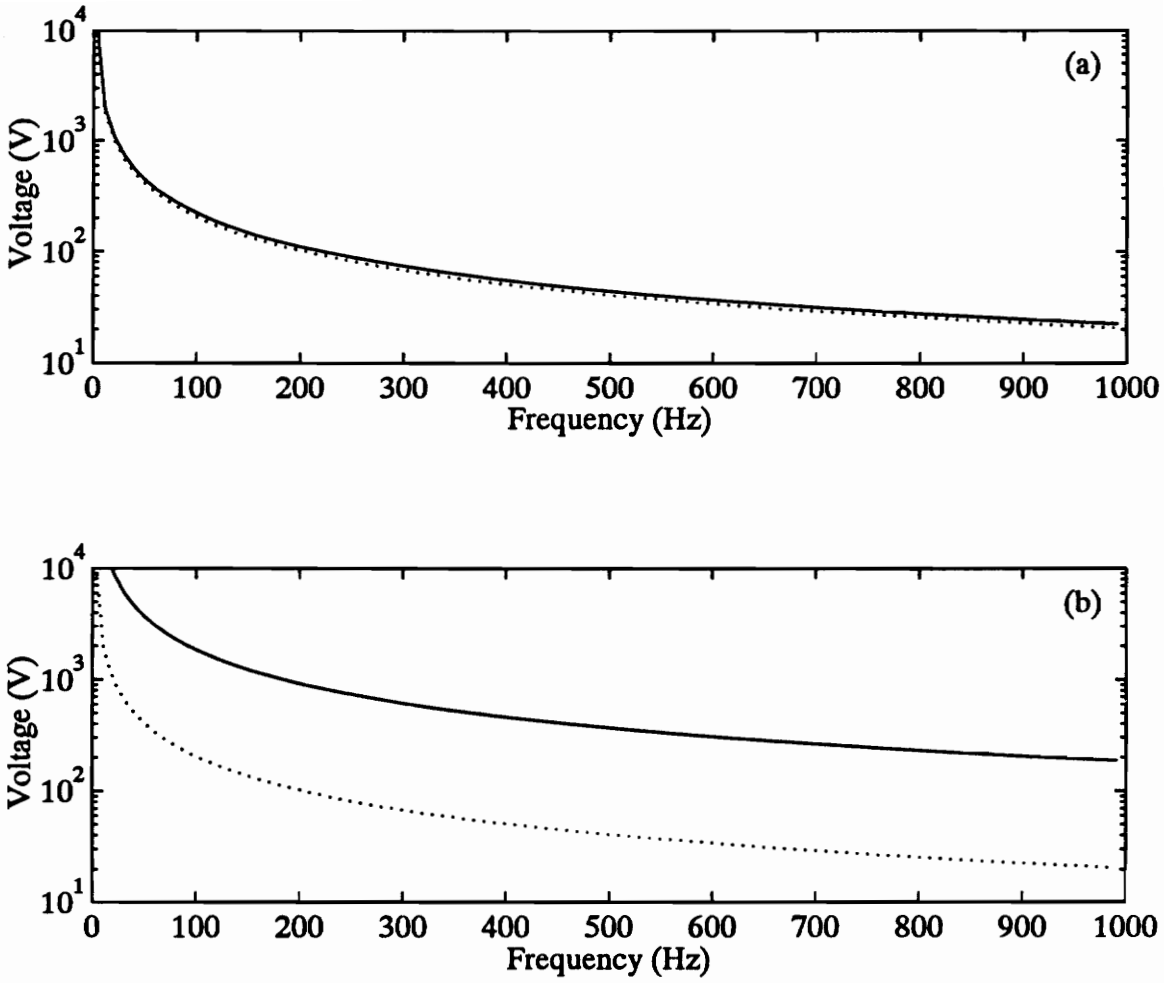

Figure 5.4 Control effort V_{eff} for active control without flanking (·····) and with flanking (——).

(a) $K_l=10^8$ N/m, $K_t=10^3$ N.m (b) $K_l=10^{10}$ N/m, $K_t=10^4$ N.m

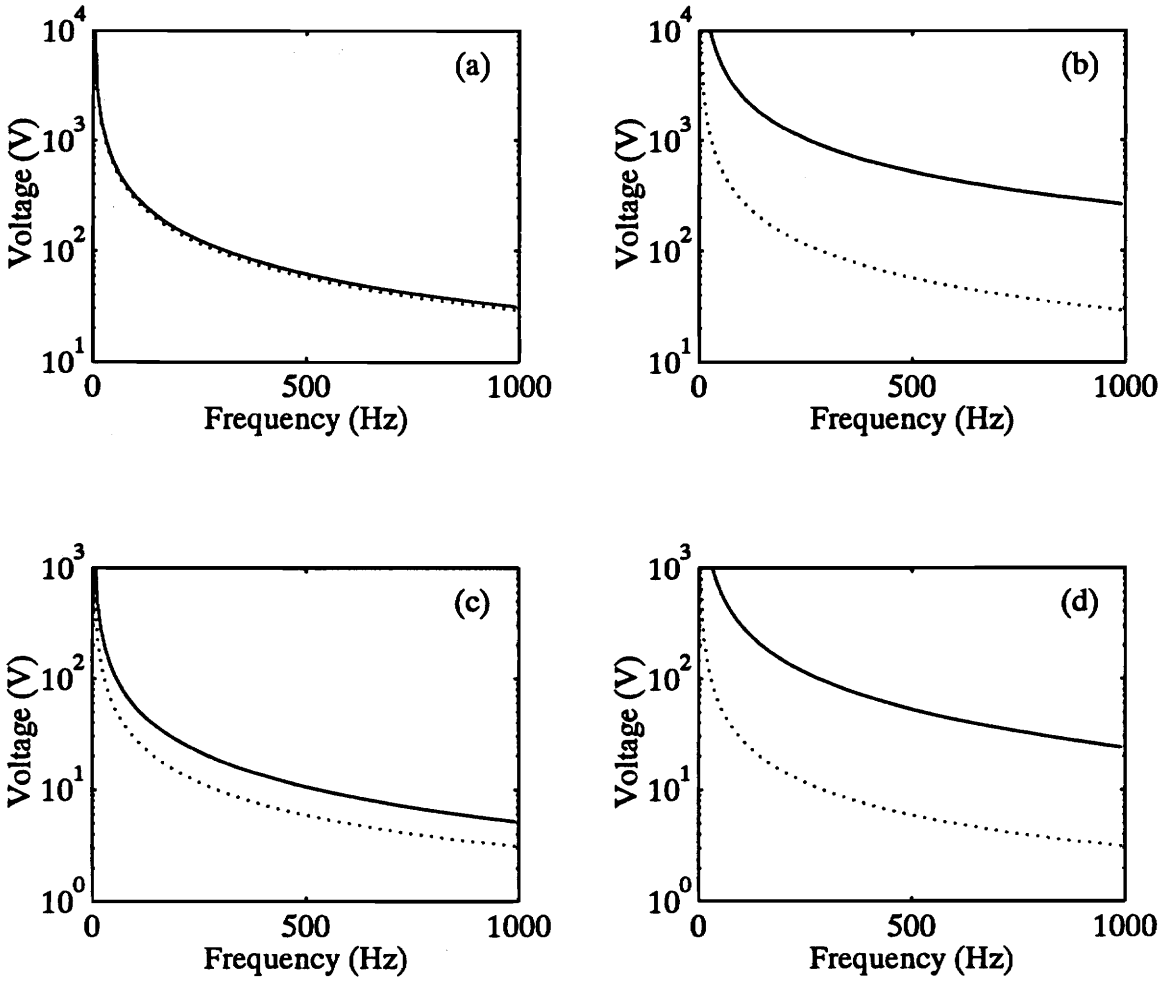

Figure 5.5 Control voltages (a), (b) v_e and (c), (d) v_f for active control without flanking (·····) and with flanking (——).

(a) $K_l=10^8$ N/m (b) $K_l=10^{10}$ N/m (c) $K_t=10^3$ N.m (d) $K_t=10^4$ N.m

values of K_l equal to 10^8 and 10^{10} N/m. Note that the control voltage v_e is unchanged for K_l equals 10^8 N/m, which is below the equivalent stiffness K_{eq}^e of the beam in extension (see Table 5.1). It was verified that the control voltage v_e and consequently the control effort are increased for values of K_l greater than 10^9 N/m. Thus, only high values of flanking stiffness K_l slightly smaller or greater than the equivalent beam stiffness in extension can affect the extensional direct energy path, resulting in an increase of the control effort. Figures 5.5(c) and 5.5(d) display the comparison of the control voltage v_f for active control without and with the torsional spring for the two values of K_t mentioned previously. Note that for both values of K_t the control voltage v_f is found to be higher with the torsional spring than without. Also, both of these stiffness values are greater than the equivalent spring constant of the beam in flexure (see Table 5.1). For the first value of K_t, the control voltage v_f is not increased enough to result in higher control effort (see Figure 5.5(c)). However, for the second value of K_t (see Figure 5.5(d)), the control voltage v_f is increased by a factor of ten, which means that the flexural energy path is significantly changed, resulting in an increased control effort. Thus, both the axial and torsional springs contribute into a higher control effort when their respective stiffness is close to or greater than the equivalent stiffness of the beam in extension and flexure respectively. Also, it appears that the energy mainly travels through the path which has the largest stiffness.

5.2.3 Influence of Flanking Paths on the Passive Approach Results

The passive system with flanking was solved for both extensional and flexural motions. The effect of flanking on both extensional and flexural power flow reductions induced by the passive insert is now studied. The results obtained for the purely passive system with flanking are compared to the ones for the purely passive system without flanking examined in Chapter 4. The passive system is studied for two values of K_l equal to 10^7 and 10^8 N/m and two values of K_t equal to 100 and 2000 N.m. Also, the frequency range studied here is extended to 4 kHz, in order to have a better understanding

of the phenomenon occurring after the addition of flanking.

Figure 5.6 compares the extensional and flexural power flow reductions induced by the passive insert for the system without and with flanking. Figures 5.6(a) and 5.6(b) show the extensional power flow reduction without and with the axial spring for the two values of K_l. For K_l equals 10^7 N/m, which is almost equal to K_{eq}^e of the insert, the extensional power flow reduction is already modified and found to be reduced. Then, for K_l equals 10^8 N/m, the extensional power flow reduction is significantly reduced with only 3 dB reduction at 4000 Hz. For large values of extensional flanking stiffness greater than K_{eq}^e of the insert, the passive insert is less effective in the frequency range studied as the energy path is redirected through the axial spring. Figures 5.6(c) and 5.6(d) display the flexural power flow reduction without and with the torsional spring for the two values of K_t. The flexural power flow reduction without flanking (i.e. the dotted line) is found to have maxima and minima in the 1-4000 Hz frequency range. These correspond to maxima and minima of absorption, which occur at specific frequencies depending on the properties and dimensions of the passive insert. Note that this behavior is observed in any absorption phenomenon and for any type of wave, with the maxima of absorption corresponding to the anti-resonances of the system. Note that maxima and minima also exist for the extensional power flow reduction, but they occur at much higher frequencies. This is associated with the fact that extensional waves have a much longer wavelength than flexural waves. It was verified that the first two maxima for the extensional power flow reduction happen at 7 kHz and 22 kHz, which means that the maxima of absorption occur for the length L of insert equal to $\lambda/4$, $3\lambda/4$, and so forth. Also, when flanking is added to the passive insert in extension with K_l equals 10^7 N/m, the first maximum is reduced and the second one is increased. Then, for K_l above 10^8 N/m, both maxima of the extensional power flow reduction are significantly reduced. Concerning the flexural power flow reduction for the passive system without flanking, the first two maxima occur in the 1-4000 Hz frequency range at approximately 800 Hz and 3200 Hz. The maxima

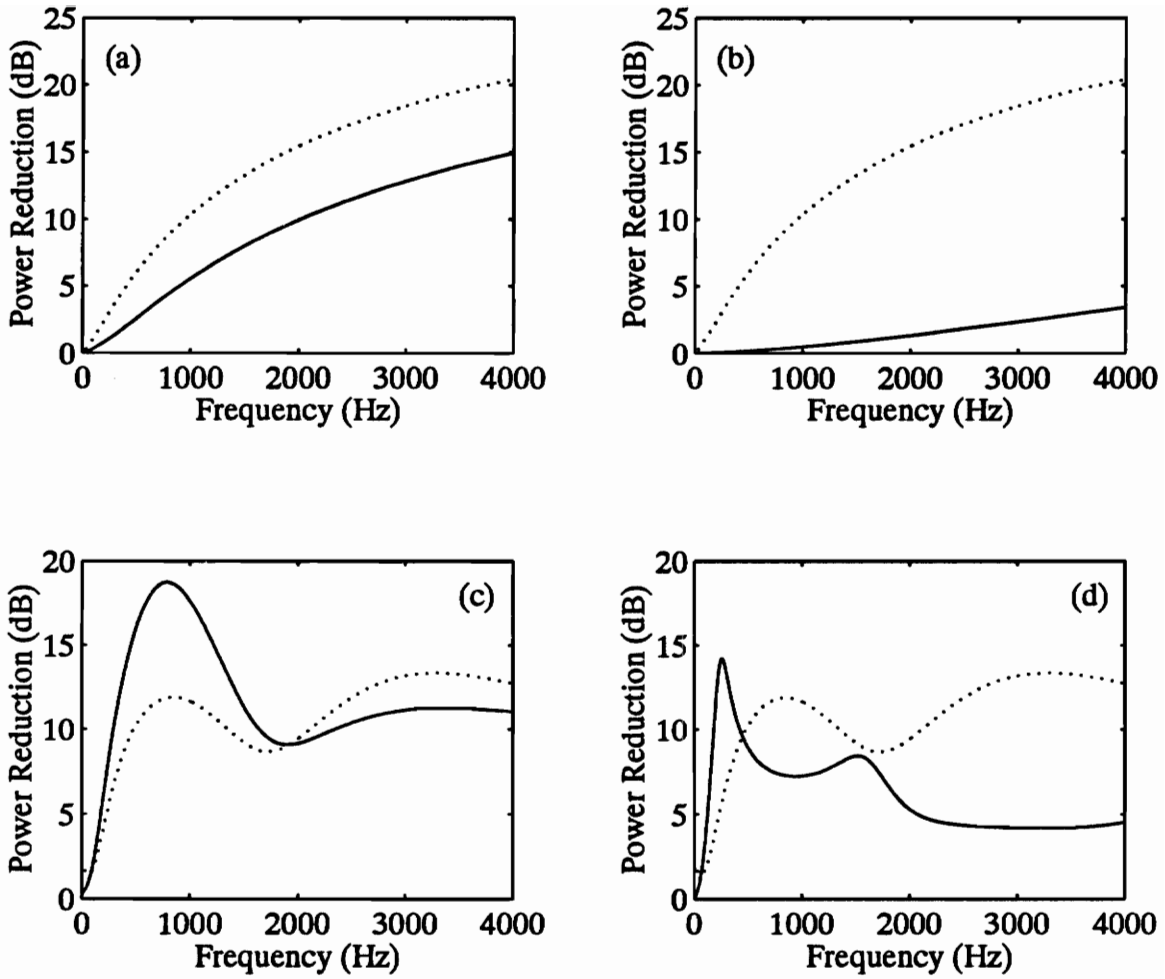

Figure 5.6 (a), (b) extensional and (c), (d) flexural power flow reductions for passive system without flanking (·····) and with flanking (——).

(a) $K_l=10^7$ N/m (b) $K_l=10^8$ N/m (c) $K_t=100$ N.m (d) $K_t=2000$ N.m

of absorption for the passive system in flexure do not happen for the length L multiple of $\lambda/4$, due to the dispersive nature of flexural waves. For the passive system in flexure with K_t equals 100 N.m, the first maximum is increased while the second one is decreased (see Figure 5.6(c)). Then, for a higher value of K_t equal to 2000 N.m, the first maximum is split into two maxima at the frequencies of about 200 and 1600 Hz, while the second maximum is considerably reduced (see Figure 5.6(d)). It was verified that as K_t is increased above 2000 N.m, the new maximum at 200 Hz is strongly reduced, resulting in the flexural power flow reduction with flanking always inferior to that without flanking. Thus, when flanking is added to the passive system, the maxima of absorption for extensional and flexural motions happen at modified frequencies, due to the fact that the system is no longer continuous. Also, in the presence of flanking paths parallel to the insert, more extensional and flexural power flow reductions can be obtained at some frequencies, especially for K_l and K_t less than 10^8 N/m and 2000 N.m respectively. This can be associated with the fact that the springs parallel to the insert add more discontinuities to the system, inducing more reflections at the interfaces for some frequencies and consequently less power flow downstream of the insert.

5.3 Association of Flanking Paths with the Active/Passive System Configuration 1

5.3.1 Description of the Active/Passive System Configuration 1 with Flanking

The active/passive control system configuration 1 with flanking is represented in Figure 5.3 of Section 5.1. The axial and torsional springs still connect the upstream and downstream of the control section, in x_1 and x_4. As earlier, the axial spring of complex spring constant $\hat{K}_l$ results in two equal and opposite forces of amplitude F_l expressed in

terms of the extensional displacements in x_1 and x_4:

$$F_l = \hat{K}_l \, [u_4(x_4) - u_1(x_1)] \tag{5.7}$$

Also, the torsional spring of complex spring constant $\hat{K}_t$ creates two equal and opposite moments of magnitude M_t function of the slopes in x_1 and x_4:

$$M_t = \hat{K}_t \, [\frac{\partial w_4(x_4)}{\partial x} - \frac{\partial w_1(x_1)}{\partial x}] \tag{5.8}$$

The extensional and flexural boundary conditions were applied at each interface of the beam. Then, the control effort and control voltages at the actuators were calculated in order to cancel the total farfield power flow, as previously in Sections 5.2.2 and 5.2.3.

5.3.2 Influence of Flanking Paths on the Active/Passive Control Results

The influence of the flanking paths on the active/passive control results is expected to be a combination of the influence on the active control results and the influence on the passive control results. The values here for the spring constants K_l and K_t are chosen equal to the ones for the passive system with flanking. The active/passive system with flanking requires smaller values of K_l and K_t than the active system with flanking to observe modification of the results. This is due to the fact that the springs are in parallel with the passive insert, which has smaller values of $K_{eq}^{\ e}$ and $K_{eq}^{\ f}$ in both extension and flexure. Figure 5.7 presents the control effort V_{eff} obtained for the active/passive control system without and with flanking. Note that for K_l equals 10^7 N/m and K_t equals 100 N.m (i.e. values slightly above $K_{eq}^{\ e}$ and $K_{eq}^{\ f}$ respectively), the control effort required by the actuators is slightly increased when compared to the system without flanking (see Figure 5.7(a)). Then, for higher values of K_l and K_t the control effort is clearly increased, which agrees with the energy travelling through the springs and not being controlled. To verify that this behavior is a combination of that of the active system with flanking and that of the passive system with flanking, the control voltages v_e and v_f

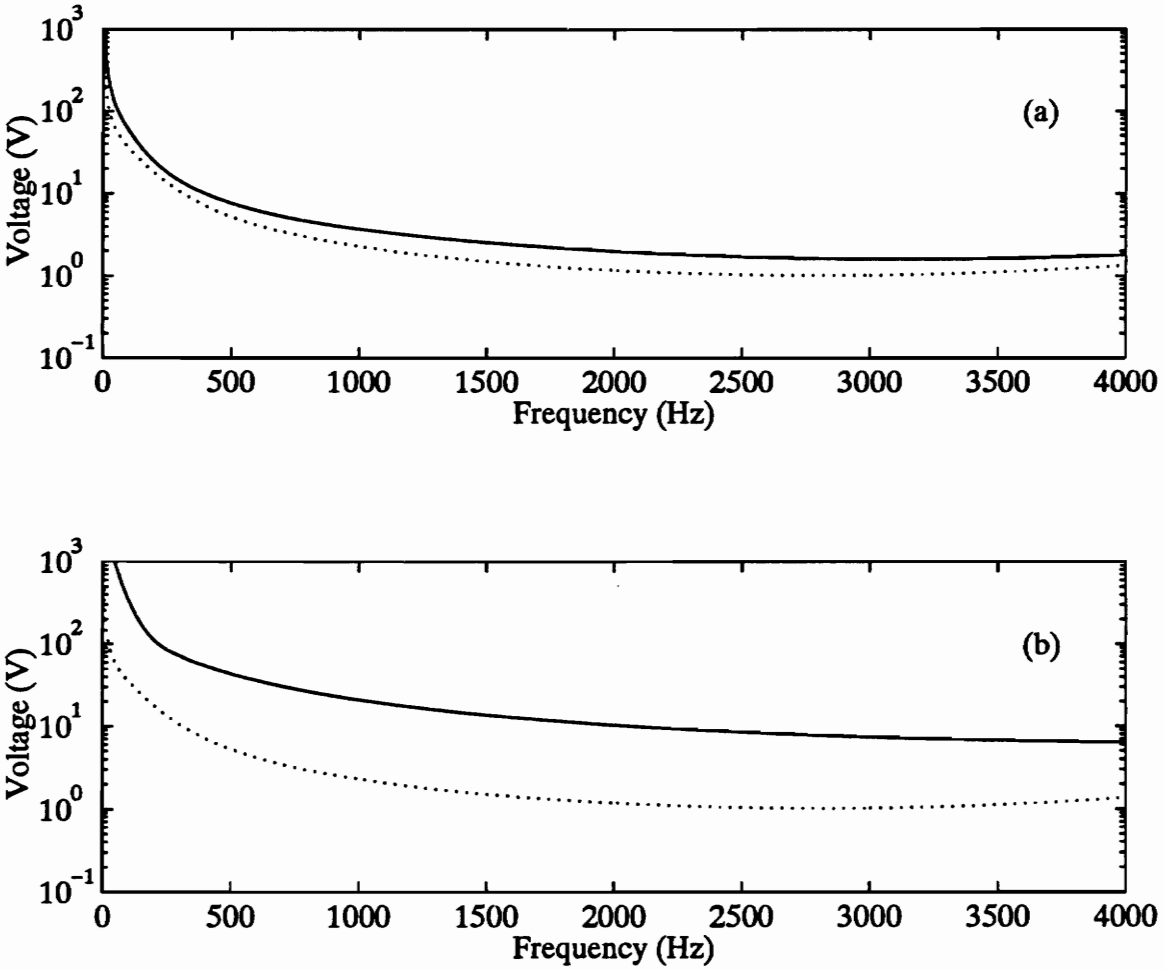

Figure 5.7 Control effort V_{eff} for active/passive control configuration 1 without flanking (·····) and with flanking (——).

(a) $K_l=10^7$ N/m, $K_t=100$ N.m (b) $K_l=10^8$ N/m, $K_t=2000$ N.m

without and with flanking are plotted in Figure 5.8. According to Figures 5.8(a) and 5.8(b), the control voltage v_e for the active/passive system configuration 1 is increased for both values of K_l (greater than K_{eq}^e of the insert). This result combines the decrease of the extensional power flow reduction for the passive system with flanking and the increase of the control effort for the active system with flanking. The control voltages v_f for the active/passive system without and with flanking are compared in Figures 5.8(c) and 5.8(d) for the two values of K_t. Note that at the frequencies where the flexural power flow reduction was found to have a local maximum, the control voltage v_f should have a local minimum once the passive system is added to the active one. Indeed, for K_t equals 100 N.m (see Figure 5.8(c)), v_f has a local minimum around 800 Hz due to the first maximum of absorption of the passive system in flexure with flanking (see Figure 5.6(c)). Also, for K_t equals 2000 N.m (see Figure 5.8(d)), v_f is always increased but two local minima exist at 200 Hz and 1600 Hz, which correspond to the frequencies of the two maxima of absorption of the passive system (see Figure 5.6(d)). Although, due to the active/passive combination, the local minima for the control voltage v_f are not as noticeable as the corresponding local maxima of absorption of the passive system with flanking. Thus, the influence of flanking on the control voltage v_f for the active/passive system is also a combination of the influence of flanking on v_f for the active system and that on the flexural power flow reduction for the passive system.

5.4 Summary

The passive system, active system and active/passive system configuration 1 associated with flanking paths were analytically studied. The extensional flanking path was simulated by a linear spring and the flexural one by a torsional spring. In all of the systems, the direct energy path through the beam was only modified for values of spring constants close to or greater than the equivalent stiffness of the section in parallel.

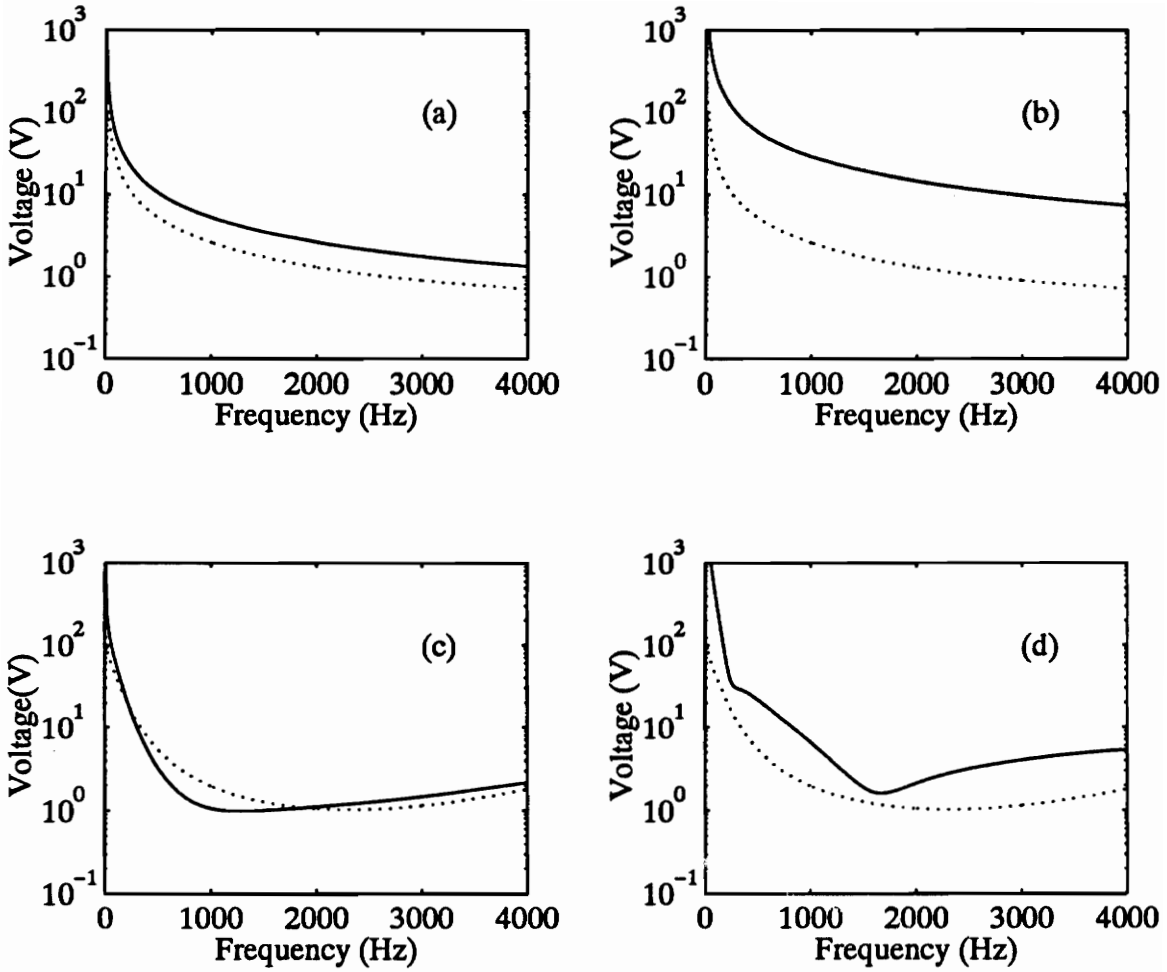

Figure 5.8 Control voltages (a), (b) v_e and (c), (d) v_f for active/passive control configuration 1 without flanking (·····) and with flanking (——).

(a) $K_l=10^7$ N/m (b) $K_l=10^8$ N/m (c) $K_t=100$ N.m (d) $K_t=2000$ N.m

For the active system with flanking, more control effort was found to be required by the actuators than for the active system without flanking. This was expected and was associated with higher control voltages v_e and v_f for the active system with flanking. Thus, for springs of stiffness higher than the equivalent stiffness of the section in parallel, the energy appeared to mainly travel through the springs parallel to the actuators.

The association of flanking with the passive system was found to result in a complex behavior. The passive system without flanking was characterized by local maxima of absorption, for both motions, dependent on the properties and dimensions of the insert. Some of the maxima of absorption were increased after addition of flanking, which disagreed with loss of energy through the flanking paths. This was explained by the fact that the springs parallel to the insert create new discontinuities, which induce more reflections at the interfaces for some frequencies, and result in higher power flow reduction. However, for K_l greater than 10^8 N/m and K_t greater than 2000 N.m, most of the energy was found to travel through the flanking paths, resulting in less power flow attenuation.

The influence of flanking on the active/passive system configuration 1 was shown to be a combination of the influence of flanking on the active system and that on the passive system. The local maxima of absorption present in the passive system with flanking, were found in the active/passive system with flanking as local minima in the plots of the control voltages. Also, the control effort required by the actuators was found to be increased for K_l and K_t greater than 10^7 N/m and 100 N.m respectively. In conclusion, the active/passive system with flanking was proved to require more control effort, to cancel the total farfield power flow, when secondary flanking paths are added in parallel with the control section.

Chapter 6
Conclusions and Recommendations

The goal of this work was to analytically demonstrate the advantages of combining passive and active control methods to attenuate the total farfield vibrational power flow in infinite beams subjected to a point force excitation. The objective was also to find the optimal active/passive configuration, with respect to minimum control effort required, by comparing the control results for the purely active system with the ones for the different active/passive systems. Then, a last study consisted of combining the optimal active/passive system with vibration flanking paths simulating heavy fluid loading and examining the effect of flanking on the control results. Control was examined, for most cases, over a frequency range from 1 Hz to 1 kHz. The point force was applied at an angle θ with the neutral axis of the beam in order to simultaneously induce extensional and flexural motion. The total farfield power flow was equal to the summation of the extensional and flexural power flows in the farfield of the beam. For the different control systems studied, the extensional response was expressed in terms of propagating waves and the flexural response in terms of both propagating and decaying waves.

First, the purely passive approach consisted of a 5 cm long passive hard rubber insert located between two identical semi-infinite steel beams. The passive insert resulted in two attenuation mechanisms: induced reflections due to impedance mismatch at the interfaces and absorption within the insert due to high damping. The extensional and flexural power flow reductions induced by the passive insert were studied as functions of the frequency. Then, purely active control was implemented using two co-located

independent PZTs on each side of the beam for the control inputs. For the active control, the cost function to be minimized was defined as the total farfield power flow expressed in terms of the disturbance force and the control inputs. The passive approach and active control technique were then combined and studied for three different configurations, depending on the location of the actuators with respect to the passive insert. Configuration 1 consisted of the actuators directly bonded to the insert, configuration 2 located the actuators downstream of the insert, and configuration 3 had the actuators upstream of the insert. The purpose was to evaluate which of the piezoelectric actuator locations was the most effective, i.e. resulted in the lowest control effort required. The control effort is a combination of the complex voltages v_1 and v_2 respectively applied to the upper and lower actuators. For the three different active/passive systems, the cost function to be minimized was again the total power flow in the farfield of the beam.

Finally, the influence of flanking paths on some of the control systems was examined. The flanking paths parallel to the direct energy path (i.e. propagation within the beam) were simulated using an axial spring as the extensional flanking path and a torsional spring as the flexural flanking path. The interest of this study was to give an approximation of the effects of a surrounding heavy fluid on the control performances.

A summary of the main conclusions of this work is as follows:

1. The purely passive approach was verified to have an increasing effectiveness with increasing frequency and increasing length of the passive insert. In the frequency range studied, the maximum extensional power flow reduction of the system studied was 10 dB and the maximum flexural power flow reduction 12 dB.

2. The passive insert resulted in more flexural power flow reduction than extensional power flow reduction, throughout the entire frequency range. This was associated with the beam being much stiffer in extension than in flexure. Thus, the passive approach was found to be effective to some extent but limited in the amount of

attenuation achieved at low frequencies for multi-wave propagation.

3. Two co-located independent piezoelectric actuators (i.e. purely active system) were shown to be effective to simultaneously reduce the farfield extensional and flexural power flows. The minimum of the cost function was found to be zero since there was equal number of control inputs and variables to be minimized. Thus, active control resulted in complete cancellation of the total power flow in the farfield of the beam.

4. Approximately ten times more control voltage was required to actively cancel the extensional power flow than the flexural power flow, even though the extensional and flexural power flows before treatment were approximately of same magnitude. This result was due, once again, to the larger stiffness of the beam in extension than flexure.

5. The most effective active/passive combination was obtained when the actuators were bonded directly to the passive insert (instead of being mounted upstream or downstream of the insert). The optimal active/passive configuration resulted in less control voltage required to cancel the extensional power flow than with the purely active system. Consequently, the control effort was significantly reduced. This was associated with the fact that the actuators were found to induce ten times more extensional power flow when located on a rubber beam than on a steel beam. A physical explanation was that for extensional motion, better impedance matching exists between the actuators and the rubber material than between the actuators and the steel material. Thus, the extensional power flow is more effectively induced and controlled in the rubber material than in the steel material.

6. The flanking paths (simulated by springs) were found to have an effect on the control results only for spring stiffness approximately equal to or greater than the equivalent stiffness of the beam section in parallel with them. As expected, for the extensional motion, large values of flanking stiffness were required to affect the direct energy path. On the contrary, relatively small values of torsional spring stiffness modified the way the flexural energy travelled in the systems.

7. In most cases, the control performance was decreased when flanking paths of

appropriate flanking stiffness were added to the systems. However, at some frequencies, the passive approach with flanking resulted in more flexural power flow reduction than that without flanking. This was thought to be associated with the fact that the springs parallel to the insert created new discontinuities, inducing more reflections at the interfaces, and resulting in higher power flow reduction.

A few recommendations for future work are listed below:

1. For the passive insert used in this work, only one kind of material (a general type) was considered but it would be interesting to investigate several viscoelastic materials and compare their effectiveness.

2. In the analytical systems developed, the disturbance was assumed to be harmonic single frequency excitation, although, in practice a disturbance may often contain random or broadband frequency content. Thus, it would be useful to apply this work to a broadband excitation. However, using the complex loss factor model of damping would no longer be valid for this form of disturbance and another model, valid with broadband excitation, would have to be considered.

3. In this study, the size of the piezoelectric actuators was chosen to be constant. Since the control performance is function of the actuator size, an optimization of the actuator geometry and material could be of interest.

4. This work being only analytical, experiments should be performed for the active/passive system in order to validate the results obtained.

5. In practice, more complex structures such as plates, cylinders and shells with fluid loading are frequently used. Thus, a generalization of the active/passive model to 2-D and 3-D structures could be interesting. This would facilitate the work to a future realistic application of the active/passive control of extensional and flexural waves in piping systems for example.

Bibliography

[1] C. E. Wilson (1989) *Noise Control: Measurement, Analysis, and Control of Sound and Vibration*, Harper and Row Inc., New York.

[2] L. L. Beranek and I. L. Vér (1992) *Noise and Vibration Control Engineering: Principles and Applications*, John Wiley & Sons, Inc., New York.

[3] Y. J. Kang, W. Tsoi and J. S. Bolton (1993) "The Effect of Mounting on the Acoustical Properties of Finite-Depth Polyimide Foam Layers", Noise-Con 93,Williamsburg, Virginia.

[4] L. Cremer, M. Heckl, and E. E. Ungar (1973) *Structure-Borne Sound: Structural Vibrations and Sound Radiation*, Springer Verlag, Berlin.

[5] B. B. Baker, and E. T. Copson (1950) *The Mathematical Theory of Huygens' Principle*, Oxford, Clarendon Press, Second Edition.

[6] P. Lueg (1936) *Process of Silencing Sound Oscillations*, US Patent, No. 2043416.

[7] H. L. Olson and E. G. May (1953) "Electronic Sound Absorber", Journal of the Acoustical Society of America, Vol. 25, No. 6, pp. 1130-1136.

[8] W. B. Conover (1955) "Recent Contributions to Transformers Audible Noise Control", AIEE Transactions, Applications and Industry, Vol.74, Part D, pp. 77-86.

[9] W. B. Conover (1956) "Fighting Noise with Noise", Noise Control, Vol. 2, No. 1, pp. 78-82.

[10] G. E. Warnaka (1982) "Active Attenuation of Noise: The State of the Art", Noise Control Engineering, Vol. 18, No. 3, pp. 100-110.

[11] J. E. Ffowcs-Williams (1984) "Anti-Sound", Proceedings of the Royal Society of London, A 395, pp. 63-88.

[12] M. Jessel and G. A. Mangiante (1972) "Active Absorbers in an Air Duct", Journal of Sound and Vibration, Vol. 23, No. 3, pp. 383-390.

[13] M. A. Swinbanks (1973) "The Active Control of Sound Propagation in Long Ducts", Journal of Sound and Vibration, Vol. 27, No. 3, pp. 411-436.

[14] B. Chaplin (1983) "Anti-Noise-The Essex Breakthrough", Chartered Mechanical Engineering, pp. 41-47.

[15] C. R. Fuller (1987) *Apparatus and Method for Global Noise Reduction*, US Patent, No. 4715599.

[16] J. D. Jones and C. R. Fuller (1987) "Active Control of Sound Fields in Elastic Cylinders by Vibrational Inputs", Proceedings of Noise-Con 87, pp. 413-418.

[17] C. R. Fuller and J. D. Jones (1987) "Experiments on Reduction of Propeller Induced Interior Noise by Active Control of Cylinder Vibration", Journal of Sound and Vibration, Vol. 112, No. 2, pp. 389-395.

[18] C. H. Hansen, S. D. Snyder, and C. R. Fuller (1989) "Reduction of Noise Radiated by a Vibrating Rectangular Panel by use of Active Sound Sources and Active Vibration Sources", Proceedings of the 1989 International Conference on Noise and Vibration, Singapore, pp. E50-E57.

[19] L. Meirovitch and M. A. Norris (1984) "Vibration Control", Proceedings of Inter-Noise 84, Noise Control Foundation, New York, pp.477-482.

[20] D. K. Lindner, W. T. Baumann, E. Bielecki (1991) "Modal Domain Optical Fiber Sensors for Control of Acoustic Radiation", Proceedings of the Conference on Recent Advances in Active Control of Sound and Vibration, Blacksburg, VA, April 15-17, pp. 839-850.

[21] B. R. Mace (1984) "Wave Reflection and Transmission in Beams", Journal of Sound and Vibration, Vol. 97, No. 2, pp.237-246.

[22] A. H. von Flotow (July-Aug. 1986) "Travelling Wave Control for Large Spacecraft Structures", Journal of Guidance, Control, and Dynamics, Vol. 9, pp. 462-468.

[23] A. H. von Flotow, and B. Schafer (Nov-Dec. 1986) "Wave-Absorbing Controllers for a Flexible Beam", Journal of guidance, Control, and Dynamics, Vol. 9, pp. 673-680.

[24] W. Redman-White, P. A. Nelson, and A. R. D. Curtis (1987) "Experiments on the Active Control of Flexural Wave Power", Journal of Sound and Vibration, Vol. 112, No. 1, pp. 187-192.

[25] L. O. Gonidou, and C. R. Fuller (1989) "Further Research on Active Control of Flexural Power Flow in Elastic Thin Beams", Journal of the Acoustical Society of America, Vol. 85, No. S1, pp. 573.

[26] G. Gibbs (1993) "Simultaneous Active Control of Flexural and Extensional Power Flow in Thin Beams", Ph. D. Dissertation, Virginia Polytechnic Institute and State University.

[27] D. W. Miller, S. R. Hall, and A. H. von Flotow (1989) "Optimal Control of Power Flow at Structural Junctions", Proceedings of the American Control Conference.

[28] K. W. Ng (July 1995) "Applications of Active Control", The 1995 International Symposium on Active Control of Sound and Vibration, Active 95, Newport Beach, CA.

[29] A. H. von Flotow, A. Beard, and D. Bailey (May 1994) "Adaptive Tuned Vibration Absorbers: Tuning Laws, Tracking Agility, Sizing, and Physical Implementations", Proceedings of Noise-Con 94, Ft. Lauderdale, FL, pp. 437-454.

[30] D. R. Halwes, W. A. Simmons (1980) *Vibration Suppression System*, US Patent, No. 4236607.

[31] M. V. Gandhi, B. S. Thompson (1992) *Smart Materials and Structures*, Chapman and Hall, London, England.

[32] Y. Choi, A. F. Spencer, and H. Conrad (January 1990) "Vibration Characteristics of a Composite Beam Containing an Electro-Rheological Fluid", Journal of Intelligent Material Systems and Structures, Vol. 1, pp. 91-104.

[33] D. Guicking, and E. Lorenz (1984) "An Active Sound Absorber with Porous Plate", Journal of Vibration, Acoustics, Stress and Reliability in Design, Vol. 106, pp. 389-392.

[34] L. D. Lafleur, F. D. Shields, and J. E. Hendrix (1991) "Acoustically Active Surface Using Piezorubber", Journal of the Acoustical Society of America, Vol. 90, No. 3, pp. 1230-1237.

[35] A. Baz (February 1993) "Active Constrained Layer Damping", Proceedings of Damping 93 Conference, San Francisco, CA.

[36] S. Beyene, and R. A. Burdisso (1995) "A New Hybrid Passive/Active Noise Absorption System", submitted to the Journal of the Acoustical Society of America (to appear).

[37] C. R. Fuller, M. J. Bronzel, C. A. Gentry, and D. E. Whittington (May 1994) "Control of Sound Radiation/Reflection with Adaptive Foams", Proceedings of Noise-Con 94, Ft Lauderdale, Florida, pp.429-436.

[38] C. A. Rogers (Fall 1992) "Smart Material Systems", Lecture Notes, pp.15.

[39] R. L. Forward, and C. J. Swigert (January/February 1981) "Electronic Damping of Orthogonal Bending Modes in a Cylindrical Mast - Theory", Journal of Spacecraft and Rockets.

[40] E. E. Crawley and J. de Luis (October 1987) " The Use of Piezoelectric Actuators as Elements of Intelligent Structures", AIAA Journal, Vol. 25, No. 10, pp. 1373-1385.

[41] E. F. Crawley, and K. B. Lazarus (1989) "Induced Strain Actuation of Isotropic and Anisotropic Plates", AIAA Paper 89-1326, 30th AIAA Structures, Structural Dynamics and Materials Conference.

[42] E. K. Dimitriadis, C. R. Fuller, and C. A. Rogers (1991) "Piezoelectric Actuators for Distributed Vibration Excitation of Thin Plates", Journal of Vibration and Acoustics, Vol. 113, pp. 100-107.

[43] M. W. Lin, and C. A. Rogers (April 1992) "Formulation of a Beam Structure with Induced Strain Actuators Based on an Approximated Linear Shear Stress Field", Proceedings, 33rd SDM Conference, Dallas, Texas, pp. 896-904.

[44] C. Liang, and C. A. Rogers (August 1989) "Behavior of Shape Memory Alloy Actuators Embedded in Composites", Proceedings of the 1989 International Composites Conference, Beijing, China.

[45] J. L. Fanson, and J. C. Chen (1986) "Structural Control by the Use of Piezoelectric Active Members", Proceedings of NASA-DOD Control-Structures Interaction Conference, NASA CP-2447, Part II.

[46] E. F. Crawley and E. H. Anderson (1990) "Detailed Models of Piezoceramic Actuation of Beams", Journal of Intelligent Material Systems and Structures, Vol. 1, January, pp 4-25.

[47] C. R. Fuller, G. P. Gibbs, and R. J. Silcox (1990) "Simultaneous Active Control of Flexural and Extensional Power Flows in Beams", Journal of Intelligent Materials Systems and Structures, Vol. 1, No. 2, pp. 235-247.

[48] L. Meirovitch (1986) *Elements of Vibration Analysis*, New York: Mc Graw-Hill, Second Edition.

[49] M. C. Junger, and D. Feit (1986) *Sound, Structures, and Their Interaction*, Cambridge: The MIT Press, Second Edition.

[50] F. J. Fahy (1985) *Sound and Structural Vibration: Radiation, Transmission and Response*, Academic Press, Orlando Florida.

[51] J. Pan and C. H. Hansen (March 1990) "Active Control of Total Power Flow Along a Beam", Proceeding from the International Congress on Recent Developments in Air and Structure-Borne Sound and Vibration, Auburn University, AL.

[52] Z. Chaudhry and C. A. Rogers (November 1992) "A Mechanics Approach to Induced Strain Actuation of Structures", Proceedings of the Third International Conference on Adaptive Structures, San Diego, CA.

[53] Piezo systems (1987). *Piezoelectric Motor/Actuator Kit Manual*, Piezoelectric Products Inc., Cambridge, MD.

[54] R. M. Jones (1975). *Mechanics of Composite Materials*, Scripta Book Company, Washington, D.C.

[55] J. C. Snowdon (1968) *Vibration and Shock in Damped Mechanical Systems*, Wiley, New York.

[56] A. D. Nashif, D. I. G. Jones, and J. P. Henderson (1985) *Vibration Damping*, Wiley, New York.

[57] S. H. Crandall (1970) "The Role of Damping in Vibration Theory", Journal of Sound and Vibration, Vol. 11, No. 1, pp. 3-18.

[58] R. H. Scanlan (1970) "Linear Damping Models and Causality in Vibrations", Journal of Sound and Vibration, Vol. 13, No. 4, pp. 499-509.

[59] J. F. Doyle (1989) *Wave Propagation in Structures: An FFT-Based Spectral Analysis Methodology*, Springer-Verlag New-York, Inc.

[60] P. A. Nelson, and S. J. Elliott (1992) *Active Control of Sound*, Academic Press Inc., San Diego, CA.

[61] L. E. Kinsler, A. R. Frey, A. B. Coppens, and J. V. Sanders (1982) *Fundamentals of Acoustics*, John Wiley & Sons, New York.

[62] B. J. Lazan (1968) *Damping of Materials and Members in Structural Mechanics*, Pergamon Press, New York.

[63] C. Liang, F. P. Sun, and C. A. Rogers (April 1993) "An Impedance Method for Dynamic Analysis of Active Material Systems", 34th AIAA Structures, Structural Dynamics and Materials Conference, La Jolla, CA, pp. 3587-3599.

[64] R. D. Blevins (1993) *Formulas for Natural Frequency and Mode Shape*, Krieger Publishing Company, Malabar, FL.

[65] W. H. Beyer (1981) *CRC Standard Mathematical Tables*, CRC Press Inc., Boca Raton, FL.

[66] P. V. O'Neil (1991) *Advanced Engineering Mathematics*, Wadsworth Inc., Belmont, CA.

Appendix A
Infinite Beam Response to a Point Force Excitation

A.1 Extensional Response to a Point Force

The extensional equation of motion of an infinite beam subjected to an in-plane force $F_e\, e^{i\omega t}$ at x=0, where F_e is the magnitude in Newtons, is of the form:

$$\frac{\partial^2 u_d(x,t)}{\partial x^2} - \frac{\rho(1-\nu^2)}{E}\frac{\partial^2 u_d(x,t)}{\partial t^2} = \frac{F_e(1-\nu^2)}{ES}\delta(x)\, e^{i\omega t} \qquad \text{(A.1)}$$

where $u_d(x,t)$ is the total extensional displacement due to the disturbance and $\delta(x)$ is the Dirac function (in m^{-1}). Equation (A.1) can be rewritten as:

$$\frac{\partial^2 u_d(x,t)}{\partial x^2} + k_e^2\, u_d(x,t) = \frac{F_e(1-\nu^2)}{ES}\delta(x)\, e^{i\omega t} \qquad \text{(A.2)}$$

where k_e is the extensional wavenumber defined in equation (2.3).

Since the beam is infinite, an appropriate method of solving $u_d(x,t)$ is to use the spatial Fourier transform [68] of equation (A.2), which is expressed as:

$$\int_{-\infty}^{+\infty} \frac{\partial^2 u_d(x,t)}{\partial x^2} e^{-ik_x x} dx + k_e^2 \int_{-\infty}^{+\infty} u_d(x,t) e^{-ik_x x} dx = \int_{-\infty}^{+\infty} \frac{F_e(1-\nu^2)}{ES} \delta(x)\, e^{i\omega t} e^{-ik_x x} dx \qquad \text{(A.3)}$$

since the spatial Fourier transform of $u_d(x,t)$ is defined by:

$$\tilde{u}_d(k_x,t) = \int_{-\infty}^{+\infty} u_d(x,t)\, e^{-ik_x x} dx \qquad \text{(A.4)}$$

then, knowing that the spatial Fourier transform of the Delta function $\delta(x)$ is:

$$\int_{-\infty}^{+\infty} \delta(x)\, e^{-ik_x x} dx = 1 \qquad \text{(A.5)}$$

also, assuming that:

$$\frac{\partial^n u_d(x,t)}{\partial x^n} = 0 \qquad \text{at } x = \pm\infty \ , \quad \text{for } n = 1,2... \qquad \text{(A.6)}$$

and that:

$$\int_{-\infty}^{+\infty} \frac{\partial^n u_d(x,t)}{\partial x^n} e^{-ik_x x} dx = (ik_x)^n\, \tilde{u}_d(k_x,t) \qquad \text{for } n = 1,2... \qquad \text{(A.7)}$$

equation (A.3) can be simplified into:

$$(ik_x)^2\, \tilde{u}_d(k_x,t) + k_e^2\, \tilde{u}_d(k_x,t) = \frac{F_e(1-\nu^2)}{ES} e^{i\omega t} \qquad \text{(A.8)}$$

which gives:

$$\tilde{u}_d(k_x,t) = \frac{F_e(1-\nu^2)}{ES\,(k_e^2 - k_x^2)} e^{i\omega t} \qquad \text{(A.9)}$$

Then, $u_d(x,t)$ is found by applying the inverse spatial Fourier transform to equation (A.9):

$$u_d(x,t) = \frac{1}{2\pi}\int_{-\infty}^{+\infty}\tilde{u}_d(k_x,t)\, e^{ik_x x}\, dk_x = \frac{F_e(1-\nu^2)}{2\pi ES}\, e^{i\omega t}\int_{-\infty}^{+\infty}\frac{e^{ik_x x}}{k_e^2 - k_x^2}\, dk_x \qquad \textbf{(A.10)}$$

Using the method of residues [69] to solve the integral in equation (A.10), the in-plane displacement for x>0 due to a point force of amplitude F_e located at x=0 on the beam is expressed as a single positive travelling wave generated at x=0:

$$u_d(x,t) = \frac{iF_e(1-\nu^2)}{2ESk_e} e^{-ik_e x} e^{i\omega t} \qquad \textbf{(A.11)}$$

A.2 Flexural Response to a Point Force

The flexural equation of motion of an infinite beam submitted to an out-of-plane force $F_f\, e^{i\omega t}$ at x=0, where F_f is the magnitude in Newtons, is presented as follows:

$$EI\frac{\partial^4 w_d(x,t)}{\partial x^4} + \rho S\frac{\partial^2 w_d(x,t)}{\partial t^2} = F_f\delta(x)\, e^{i\omega t} \qquad \textbf{(A.12)}$$

where $w_d(x,t)$ is the total flexural displacement due to the disturbance. Equation (A.12) can also be written as:

$$\frac{\partial^4 w_d(x,t)}{\partial x^4} - k_f^4 w_d(x,t) = \frac{F_f}{EI}\delta(x)\, e^{i\omega t} \qquad \textbf{(A.13)}$$

where k_f is the flexural wavenumber. The spatial Fourier transform of equation (A.13) is presented as follows:

$$\int_{-\infty}^{+\infty}\frac{\partial^4 w_d(x,t)}{\partial x^4}\, e^{-ik_x x}\, dx - k_f^4\int_{-\infty}^{+\infty} w_d(x,t)\, e^{-ik_x x}\, dx = \int_{-\infty}^{+\infty}\frac{F_f}{EI}\delta(x)\, e^{i\omega t}\, e^{-ik_x x}\, dx \qquad \textbf{(A.14)}$$

Using the same assumptions as in the previous section, equation (A.4) is reduced to:

$$k_x^4 \, \tilde{w}_d(k_x,t) - k_f^4 \, \tilde{w}_d(k_x,t) = \frac{F_f}{EI} e^{i\omega t} \qquad \text{(A.15)}$$

which gives:

$$\tilde{w}_d(k_x,t) = \frac{F_f}{EI(k_x^4 - k_f^4)} e^{i\omega t} \qquad \text{(A.16)}$$

The inverse Fourier transform is now applied to equation (A.16), resulting in:

$$w_d(x,t) = \frac{F_f \, e^{i\omega t}}{2\pi EI} \int_{-\infty}^{+\infty} \frac{e^{ik_x x}}{k_x^4 - k_f^4} dk_x \qquad \text{(A.17)}$$

Finally, after application of the method of residues [69] to equation (A.17), the flexural displacement for $x>0$ due to the normal force F_f at $x=0$ is determined to be:

$$w_d(x,t) = \frac{iF_f}{4EIk_f^3}(-e^{-ik_f x} + ie^{-k_f x}) e^{i\omega t} \qquad \text{(A.18)}$$

Thus, an out-of-plane force of magnitude F_f applied to an infinite beam creates two flexural waves: a propagating wave (first term) of phase velocity k_f and a non-propagating evanescent wave (second term).

Appendix B

Matrices For Control System Analysis

In this section, the following variables are used in order to simplify the matrices.

Extensional variables:

$$W = \frac{S_p E_p k_e^p}{S E k_e} \tag{B.1}$$

$$\alpha_e = \frac{K^e d_{31}}{T_a} \tag{B.2}$$

Flexural variables:

$$X = \frac{k_f^p}{k_f} \tag{B.3}$$

$$Y = \frac{E_p I_p k_f^{p^2}}{E I k_f^2} \tag{B.4}$$

$$Z = \frac{E_p I_p k_f^{p^3}}{E I k_f^3} \tag{B.5}$$

$$\alpha_f = \frac{K^f d_{31}}{T_a} \tag{B.6}$$

Distances:

$$x_{21} = x_2 - x_1 \quad , \quad x_{32} = x_3 - x_2 \quad , \quad x_{43} = x_4 - x_3 \tag{B.7}$$

B.1 Passive Control System

Extensional Vibrations:

$$\begin{bmatrix} 1 & -1 & -e^{-ik_e^p x_{21}} & 0 \\ 1 & W & -We^{-ik_e^p x_{21}} & 0 \\ 0 & e^{-ik_e^p x_{21}} & 1 & -1 \\ 0 & -We^{-ik_e^p x_{21}} & W & 1 \end{bmatrix} \begin{bmatrix} F_1 \\ E_2 \\ F_2 \\ E_3 \end{bmatrix} = \begin{bmatrix} -E_1 e^{-ik_e x_1} \\ E_1 e^{-ik_e x_1} \\ 0 \\ 0 \end{bmatrix} \tag{B.8}$$

Flexural Vibrations:

$$\begin{bmatrix} M_1 & M_2 \end{bmatrix} \begin{bmatrix} B_1 \\ D_1 \\ A_2 \\ B_2 \\ C_2 \\ D_2 \\ A_3 \\ C_3 \end{bmatrix} = \begin{bmatrix} -A_1 e^{-ik_f x_1} - C_1 e^{-k_f x_1} \\ iA_1 e^{-ik_f x_1} + C_1 e^{-k_f x_1} \\ A_1 e^{-ik_f x_1} - C_1 e^{-k_f x_1} \\ -iA_1 e^{-ik_f x_1} + C_1 e^{-k_f x_1} \\ 0 \\ 0 \\ 0 \\ 0 \end{bmatrix} \tag{B.9}$$

where M_1 and M_2 are eight by four matrices defined on the following page.

$$M_1 = \begin{bmatrix} 1 & 1 & -1 & -e^{-ik_f^p x_{21}} \\ i & 1 & iX & -iXe^{-ik_f^p x_{21}} \\ -1 & 1 & Y & Ye^{-ik_f^p x_{21}} \\ -i & 1 & -iZ & iZe^{-ik_f^p x_{21}} \\ 0 & 0 & e^{-ik_f^p x_{21}} & 1 \\ 0 & 0 & -iXe^{-ik_f^p x_{21}} & iX \\ 0 & 0 & -Ye^{-ik_f^p x_{21}} & -Y \\ 0 & 0 & iZe^{-ik_f^p x_{21}} & -iZ \end{bmatrix} \quad \textbf{(B.10)}$$

$$M_2 = \begin{bmatrix} -1 & -e^{-k_f^p x_{21}} & 0 & 0 \\ X & -Xe^{-k_f^p x_{21}} & 0 & 0 \\ -Y & -Ye^{-k_f^p x_{21}} & 0 & 0 \\ Z & -Ze^{-k_f^p x_{21}} & 0 & 0 \\ e^{-k_f^p x_{21}} & 1 & -1 & -1 \\ -Xe^{-k_f^p x_{21}} & X & i & 1 \\ Ye^{-k_f^p x_{21}} & Y & 1 & -1 \\ -Ze^{-k_f^p x_{21}} & Z & -i & 1 \end{bmatrix} \quad \textbf{(B.11)}$$

B.2 Active Control System

Extensional Vibrations:

$$\begin{bmatrix} 1 & -1 & -e^{-ik_e x_{21}} & 0 \\ 1 & 1 & -e^{-ik_e x_{21}} & 0 \\ 0 & e^{-ik_e x_{21}} & 1 & -1 \\ 0 & -e^{-ik_e x_{21}} & 1 & 1 \end{bmatrix} \begin{bmatrix} F_1 \\ E_2 \\ F_2 \\ E_3 \end{bmatrix} = \begin{bmatrix} -E_1 e^{-ik_e x_1} \\ E_1 e^{-ik_e x_1} + \frac{i\alpha_e}{k_e} v_e \\ 0 \\ -\frac{i\alpha_e}{k_e} v_e \end{bmatrix} \qquad \textbf{(B.12)}$$

Flexural Vibrations:

$$\begin{bmatrix} M_1 & M_2 \end{bmatrix} \begin{bmatrix} B_1 \\ D_1 \\ A_2 \\ B_2 \\ C_2 \\ D_2 \\ A_3 \\ C_3 \end{bmatrix} = \begin{bmatrix} -A_1 e^{-ik_f x_1} - C_1 e^{-k_f x_1} \\ iA_1 e^{-ik_f x_1} + C_1 e^{-k_f x_1} \\ A_1 e^{-ik_f x_1} - C_1 e^{-k_f x_1} - \frac{\alpha_f}{k_f^2} v_f \\ -iA_1 e^{-ik_f x_1} + C_1 e^{-k_f x_1} \\ 0 \\ 0 \\ \frac{\alpha_f}{k_f^2} v_f \\ 0 \end{bmatrix} \qquad \textbf{(B.13)}$$

where M_1 and M_2 are eight by four matrices detailed on the following page.

$$M_1 = \begin{bmatrix} 1 & 1 & -1 & -e^{-ik_f x_{21}} \\ i & 1 & i & -ie^{-ik_f x_{21}} \\ -1 & 1 & 1 & e^{-ik_f x_{21}} \\ -i & 1 & -i & ie^{-ik_f x_{21}} \\ 0 & 0 & e^{-ik_f x_{21}} & 1 \\ 0 & 0 & -ie^{-ik_f x_{21}} & i \\ 0 & 0 & -e^{-ik_f x_{21}} & -1 \\ 0 & 0 & ie^{-ik_f x_{21}} & -i \end{bmatrix} \qquad \textbf{(B.14)}$$

$$M_2 = \begin{bmatrix} -1 & -e^{-k_f x_{21}} & 0 & 0 \\ 1 & -e^{-k_f x_{21}} & 0 & 0 \\ -1 & -e^{-k_f x_{21}} & 0 & 0 \\ 1 & -e^{-k_f x_{21}} & 0 & 0 \\ e^{-k_f x_{21}} & 1 & -1 & -1 \\ -e^{-k_f x_{21}} & 1 & i & 1 \\ e^{-k_f x_{21}} & 1 & 1 & -1 \\ -e^{-k_f x_{21}} & 1 & -i & 1 \end{bmatrix} \qquad \textbf{(B.15)}$$

B.3 Active/Passive Control System Configuration 1

Extensional Vibrations:

$$\begin{bmatrix} M_1 & M_2 \end{bmatrix} \begin{bmatrix} F_1 \\ E_2 \\ F_2 \\ E_3 \\ F_3 \\ E_4 \\ F_4 \\ v_e \end{bmatrix} = \begin{bmatrix} -E_1 e^{-ik_e x_1} \\ E_1 e^{-ik_e x_1} \\ 0 \\ 0 \\ 0 \\ 0 \\ 0 \\ 0 \end{bmatrix} \tag{B.16}$$

where M_1 and M_2 are eight by four matrices defined as follows:

$$M_1 = \begin{bmatrix} 1 & -1 & -e^{-ik_e^P x_{21}} & 0 \\ 1 & W & -We^{-ik_e^P x_{21}} & 0 \\ 0 & e^{-ik_e^P x_{21}} & 1 & -1 \\ 0 & -e^{-ik_e^P x_{21}} & 1 & 1 \\ 0 & 0 & 0 & e^{-ik_e^P x_{32}} \\ 0 & 0 & 0 & -e^{-ik_e^P x_{32}} \\ 0 & 0 & 0 & 0 \\ 0 & 0 & 0 & 0 \end{bmatrix} \tag{B.17}$$

$$
M_2 = \begin{bmatrix}
0 & 0 & 0 & 0 \\
0 & 0 & 0 & 0 \\
-e^{-ik_e^p x_{32}} & 0 & 0 & 0 \\
-e^{-ik_e^p x_{32}} & 0 & 0 & -\dfrac{i\alpha_e}{k_e^p} \\
1 & -1 & -e^{-ik_e^p x_{43}} & 0 \\
1 & 1 & -e^{-ik_e^p x_{43}} & \dfrac{i\alpha_e}{k_e^p} \\
0 & e^{-ik_e^p x_{43}} & 1 & 0 \\
0 & -We^{-ik_e^p x_{43}} & W & 0
\end{bmatrix} \qquad \textbf{(B.18)}
$$

Flexural Vibrations:

$$\begin{bmatrix} M_1 & M_2 \\ M_3 & M_4 \end{bmatrix} \begin{bmatrix} B_1 \\ D_1 \\ A_2 \\ B_2 \\ C_2 \\ D_2 \\ A_3 \\ B_3 \\ C_3 \\ D_3 \\ A_4 \\ B_4 \\ C_4 \\ D_4 \\ v_f \\ C_5 \end{bmatrix} = \begin{bmatrix} -A_1 e^{-ik_f x_1} - C_1 e^{-k_f x_1} \\ iA_1 e^{-ik_f x_1} + C_1 e^{-k_f x_1} \\ A_1 e^{-ik_f x_1} - C_1 e^{-k_f x_1} \\ -iA_1 e^{-ik_f x_1} + C_1 e^{-k_f x_1} \\ 0 \\ 0 \\ 0 \\ 0 \\ 0 \\ 0 \\ 0 \\ 0 \\ 0 \\ 0 \\ 0 \end{bmatrix} \qquad \textbf{(B.19)}$$

where M_1, M_2, M_3 and M_4 are square matrices of dimension eight detailed on the following pages.

Matrix M_1:

$$M_1 = \begin{bmatrix} 1 & 1 & -1 & -e^{-ik_f^p x_{21}} & -1 & -e^{-k_f^p x_{21}} & 0 & 0 \\ i & 1 & iX & -iXe^{-ik_f^p x_{21}} & X & -Xe^{-k_f^p x_{21}} & 0 & 0 \\ -1 & 1 & Y & Ye^{-ik_f^p x_{21}} & -Y & -Ye^{-k_f^p x_{21}} & 0 & 0 \\ -i & 1 & -iZ & iZe^{-ik_f^p x_{21}} & Z & -Ze^{-k_f^p x_{21}} & 0 & 0 \\ 0 & 0 & e^{-ik_f^p x_{21}} & 1 & e^{-k_f^p x_{21}} & 1 & -1 & -e^{-ik_f^p x_{32}} \\ 0 & 0 & -ie^{-ik_f^p x_{21}} & i & -e^{-k_f^p x_{21}} & 1 & i & -ie^{-ik_f^p x_{32}} \\ 0 & 0 & -e^{-ik_f^p x_{21}} & -1 & e^{-k_f^p x_{21}} & 1 & 1 & e^{-ik_f^p x_{32}} \\ 0 & 0 & ie^{-ik_f^p x_{21}} & -i & -e^{-k_f^p x_{21}} & 1 & -i & ie^{-ik_f^p x_{32}} \end{bmatrix} \quad \textbf{(B.20)}$$

Matrix M_2:

$$M_2 = \begin{bmatrix} 0 & 0 & 0 & 0 & 0 & 0 & 0 & 0 \\ 0 & 0 & 0 & 0 & 0 & 0 & 0 & 0 \\ 0 & 0 & 0 & 0 & 0 & 0 & 0 & 0 \\ 0 & 0 & 0 & 0 & 0 & 0 & 0 & 0 \\ -1 & -e^{-k_f^p x_{32}} & 0 & 0 & 0 & 0 & 0 & 0 \\ 1 & -e^{-k_f^p x_{32}} & 0 & 0 & 0 & 0 & 0 & 0 \\ -1 & -e^{-k_f^p x_{32}} & 0 & 0 & 0 & 0 & \frac{\alpha_f}{k_f^{p2}} & 0 \\ 1 & -e^{-k_f^p x_{32}} & 0 & 0 & 0 & 0 & 0 & 0 \end{bmatrix} \quad \textbf{(B.21)}$$

Matrix M_3:

$$M_3 = \begin{bmatrix} 0 & 0 & 0 & 0 & 0 & 0 & e^{-ik_f^p x_{32}} & 1 \\ 0 & 0 & 0 & 0 & 0 & 0 & -ie^{-ik_f^p x_{32}} & i \\ 0 & 0 & 0 & 0 & 0 & 0 & -e^{-ik_f^p x_{32}} & -1 \\ 0 & 0 & 0 & 0 & 0 & 0 & ie^{-ik_f^p x_{32}} & -i \\ 0 & 0 & 0 & 0 & 0 & 0 & 0 & 0 \\ 0 & 0 & 0 & 0 & 0 & 0 & 0 & 0 \\ 0 & 0 & 0 & 0 & 0 & 0 & 0 & 0 \\ 0 & 0 & 0 & 0 & 0 & 0 & 0 & 0 \end{bmatrix} \quad \textbf{(B.22)}$$

Matrix M_4:

$$M_4 = \begin{bmatrix} e^{-k_f^p x_{32}} & 1 & -1 & -e^{-ik_f^p x_{43}} & -1 & -e^{-k_f^p x_{43}} & 0 & 0 \\ -e^{-k_f^p x_{32}} & 1 & i & -ie^{-ik_f^p x_{43}} & 1 & -e^{-k_f^p x_{43}} & 0 & 0 \\ e^{-k_f^p x_{32}} & 1 & 1 & e^{-ik_f^p x_{43}} & -1 & -e^{-k_f^p x_{43}} & -\frac{\alpha_f}{k_f^{p2}} & 0 \\ -e^{-k_f^p x_{32}} & 1 & -i & ie^{-ik_f^p x_{43}} & 1 & -e^{k_f^p x_{43}} & 0 & 0 \\ 0 & 0 & e^{-ik_f^p x_{43}} & 1 & e^{-k_f^p x_{43}} & 1 & 0 & -1 \\ 0 & 0 & -iXe^{-ik_f^p x_{43}} & iX & -Xe^{-k_f^p x_{43}} & X & 0 & 1 \\ 0 & 0 & -Ye^{-ik_f^p x_{43}} & -Y & Ye^{-k_f^p x_{43}} & Y & 0 & -1 \\ 0 & 0 & iZe^{-ik_f^p x_{43}} & -iZ & -Ze^{-k_f^p x_{43}} & Z & 0 & 1 \end{bmatrix}$$

(B.23)

Appendix C

Derivation of the Minimum of the Cost Function

The purpose here is to determine the minimum of the cost function, which is the total power flow P_t in the farfield, and the associated optimal applied voltages v_1 and v_2. The method used to determine the minimum of P_t is identical to the one developed by Nelson et al. [64]. The extensional and flexural power flows in the farfield (third section of the beam) are expressed as functions of the primary and secondary fields as follows:

$$P_e^3 = \frac{ESk_e\omega}{2}\left|\frac{iF_e(1-\nu^2)}{2ESk_e}e^{-ik_e x_2}+\frac{iK^e d_{31}}{2k_e T_a}(e^{-ik_e(x_2-x_1)}-1)(v_1+v_2)\right|^2 \qquad \text{(C.1)}$$

$$P_f^3 = EIk_f^3\omega\left|\frac{-iF_f}{4EIk_f^3}e^{-ik_f x_2}+\frac{K^f d_{31}}{4k_f^2 T_a}(1-e^{-ik_f(x_2-x_1)})(v_1-v_2)\right|^2 \qquad \text{(C.2)}$$

In order to simplify the calculations and isolate the coefficients of v_1 and v_2, the following variables are defined:

$$\alpha_e = \frac{ESk_e\omega}{2} \qquad \text{(C.3)}$$

$$\beta_e = \frac{iF_e(1-\nu^2)}{2ESk_e}e^{-ik_e x_2} \qquad \text{(C.4)}$$

$$\gamma_e = \frac{iK^e d_{31}}{2k_e T_a}(e^{-ik_e(x_2-x_1)}-1) \qquad \text{(C.5)}$$

$$\alpha_f = EIk_f^3\omega \tag{C.6}$$

$$\beta_f = \frac{-iF_f}{4EIk_f^3} e^{-ik_f x_2} \tag{C.7}$$

$$\gamma_f = \frac{K^f d_{31}}{4T_a k_f^2} (1 - e^{-ik_f(x_2 - x_1)}) \tag{C.8}$$

which results in the following simple relations for the extensional and flexural power flows in the farfield:

$$P_e^3 = \alpha_e \, | \beta_e + \gamma_e(v_1 + v_2) |^2 \tag{C.9}$$

$$P_f^3 = \alpha_f \, | \beta_f + \gamma_f(v_1 - v_2) |^2 \tag{C.10}$$

Knowing that the norm squared of a complex expression is equivalent to the multiplication of this complex expression by its complex conjugate, equations (C.9) and (C.10) are decomposed into:

$$\begin{aligned} P_e^3 = {} & \alpha_e |\gamma_e|^2(|v_1|^2 + |v_2|^2) + \alpha_e |\gamma_e|^2(v_1 v_2^* + v_1^* v_2) + \alpha_e \beta_e^* \gamma_e(v_1) \\ & + \alpha_e \beta_e \gamma_e^*(v_1^*) + \alpha_e \beta_e^* \gamma_e(v_2) + \alpha_e \beta_e \gamma_e^*(v_2^*) + \alpha_e |\beta_e|^2 \end{aligned} \tag{C.11}$$

$$\begin{aligned} P_f^3 = {} & \alpha_f |\gamma_f|^2(|v_1|^2 + |v_2|^2) - \alpha_f |\gamma_f|^2(v_1 v_2^* + v_1^* v_2) + \alpha_f \beta_f^* \gamma_f(v_1) \\ & + \alpha_f \beta_f \gamma_f^*(v_1^*) - \alpha_f \beta_f^* \gamma_f(v_2) - \alpha_f \beta_f \gamma_f^*(v_2^*) + \alpha_f |\beta_f|^2 \end{aligned} \tag{C.12}$$

Then, the total power flow P_t is expressed in the form of a quadratic function, in terms of the applied voltages v_1 and v_2:

$$P_t = a|v_1|^2 + a|v_2|^2 + b\, v_1 v_2^* + b\, v_1^* v_2 + c\, v_1 + d\, v_1^* + e\, v_2 + f\, v_2^* + g \tag{C.13}$$

where:

$$a = \alpha_e |\gamma_e|^2 + \alpha_f |\gamma_f|^2 \quad \text{(C.14)}$$

$$b = \alpha_e |\gamma_e|^2 - \alpha_f |\gamma_f|^2 \quad \text{(C.15)}$$

$$c = \alpha_e \beta_e^* \gamma_e + \alpha_f \beta_f^* \gamma_f \quad \text{(C.16)}$$

$$d = \alpha_e \beta_e \gamma_e^* + \alpha_f \beta_f \gamma_f^* \quad \text{(C.17)}$$

$$e = \alpha_e \beta_e^* \gamma_e - \alpha_f \beta_f^* \gamma_f \quad \text{(C.18)}$$

$$f = \alpha_e \beta_e \gamma_e^* - \alpha_f \beta_f \gamma_f^* \quad \text{(C.19)}$$

$$g = \alpha_e |\beta_e|^2 + \alpha_f |\beta_f|^2 \quad \text{(C.20)}$$

The real and imaginary parts of the complex applied voltages v_1 and v_2 are defined to be:

$$v_1 = v_1^R + iv_1^I \quad \text{(C.21)}$$

$$v_2 = v_2^R + iv_2^I \quad \text{(C.22)}$$

and the quadratic power flow P_t given in equation (C.13) is now differentiated with respect to each of the real and imaginary components of both v_1 and v_2, which results in four equations. In order to determine the optimal applied voltages v_1 and v_2 associated with the unique minimum of the total power flow, these four equations are set equal to zero, which can be expressed as follows:

$$\frac{\partial P_t}{\partial v_1^R} = \frac{\partial P_t}{\partial v_2^R} = \frac{\partial P_t}{\partial v_1^I} = \frac{\partial P_t}{\partial v_2^I} = 0 \qquad \text{(C.23)}$$

After solving the set of equations defined by (C.23), the optimal applied voltages are found to be:

$$v_1 = \frac{b\,f - a\,d}{a^2 - b^2} \qquad \text{(C.24)}$$

$$v_2 = \frac{b\,d - a\,f}{a^2 - b^2} \qquad \text{(C.25)}$$

which can be rewritten after replacing each variable by its analytical expression and results in:

$$v_1 = \frac{(1-\nu^2)T_a F_e}{2ESK^e d_{31}} \frac{e^{-ik_e x_2}}{1-e^{-ik_e(x_2-x_1)}} + \frac{iT_a F_f}{2k_f EIK^f d_{31}} \frac{e^{-ik_f x_2}}{1-e^{-ik_f(x_2-x_1)}} \qquad \text{(C.26)}$$

$$v_2 = \frac{(1-\nu^2)T_a F_e}{2ESK^e d_{31}} \frac{e^{-ik_e x_2}}{1-e^{-ik_e(x_2-x_1)}} - \frac{iT_a F_f}{2k_f EIK^f d_{31}} \frac{e^{-ik_f x_2}}{1-e^{-ik_f(x_2-x_1)}} \qquad \text{(C.27)}$$

Substituting the expressions for v_1 and v_2 given in equations (C.24) and (C.25) respectively, into the general expression for P_t detailed in equation (C.13), the minimum value of P_t is found to be zero.

Vita

Florence Lydie Deneufve was born on August 17, 1970 in Enghien, France. After graduating from high school in 1988, she joined the Institute of Technology of Saint-Denis, France, where she received a technical degree in Engineering Sciences (DUT) in June, 1991. Then, she entered the Mechanical Engineering Department in the Acoustics and Vibrations section at the University of Technology of Compiègne (UTC), France. She obtained her degree in Mechanical Engineering from UTC in September 1994, while pursuing graduate studies at Virginia Polytechnic Institute and State University since August, 1993. She completed her M.S. degree in July, 1996 and worked on experimental investigations of active/passive control of beam vibrations at the same time during the spring and summer 1996. Her experimental research was sponsored by the Office of Naval Research (ONR).